QUANTIFICATION OF LAND COVER SURROUNDING PLANNED DISTURBANCES USING UAS IMAGERY

by

Zachary Miller

A Thesis

Submitted to the Faculty of Purdue University

In Partial Fulfillment of the Requirements for the degree of

Master of Science

School of Aviation and Transportation Technology

West Lafayette, Indiana

December 2021

THE PURDUE UNIVERSITY GRADUATE SCHOOL
STATEMENT OF COMMITTEE APPROVAL

Dr. Joseph Hupy, Chair

School of Aviation and Transportation Technology

Dr. Sarah Hubbard

School of Aviation and Transportation Technology

Dr. Guofan Shao

School of Aviation and Transportation Technology

Approved by:

Dr. Mary E. Johnson

Dedicated to my niece, Dallas, for whom I will ensure a brighter future through a lifelong pursuit of environmental stewardship.

ACKNOWLEDGMENTS

TABLE OF CONTENTS

LIST OF TABLES

LIST OF FIGURES

GLOSSARY

Aerial survey – the process of collecting and combining images from an airborne platform to produce a composite photograph with which volumes, areas, and counts of assets can be derived (Hupy & Kroening, 2018).

CHF – the central hardwood forest region describes an area throughout the east-central United States that predominantly consists of deciduous hardwood species such as Oak and Hickory, which display mesophytic elements, as well as mixed noncommercial conifer species (Fralish, 2003).

CORS – continuously operating reference stations are a network of ground GNSS receivers operated by the national geodetic survey which provide constant position correcting measurements to enhance precision of geographic measurements (CORS, 2021).

Disturbance – for the purposes of this study, a disturbance refers to a discrete fire or timber felling event that significantly and rapidly changes the vegetated composition of an area.

GCP – ground control points are physical markers, placed throughout the study area, to have their coordinates collected and referenced during photogrammetric processing in order to geospatially align aerial imagery (Zhang, Aldana-Jague, et al., 2019).

GEOBIA – geographic object-based image analysis involves the clustering of neighboring pixels in an aerial image based on similar spectral and spatial characteristics in order to classify out various objects for geospatial analysis (Kucharczyk et al., 2020).

Georeferencing – the act of associating "real-world coordinates" to an "ordinary image" for the purposes of scaling and querying an image relative to the physical space on earth it represents (GISGeography, 2021c).

GIS – geographic information systems are used to "store, analyze, and visualize" spatial relationships of geographic data through a network of "computer-based" tools, (GISGeography, 2021b).

GNSS – global navigation satellite system refers to the synonymous network of "positioning, navigation, and timing" satellites used in triangulation for determining an object's position on earth (GPS.gov, 2021a).

GPS – global positioning system is the United States owned network of satellites and correction stations which relates earth positioning information to receivers (GPS.gov, 2021b).

GSD – ground sample distance is the size of a given image pixel relative to its true ground measurement (Tomaštík et al., 2019).

Image segmentation – the first step in image classification, image segmentation is a semi-automated process of clustering multiple pixels together based on similar spectral and spatial characteristics through user-defined parameters (Nuijten et al., 2019).

Land classification – land classification refers to the development and use of vectorized GIS layers which display ground objects as generalized categorical land covers (LaGro Jr, 2005).

Land cover – land cover refers to the vegetation, materials, or surfaces that comprise the horizontal space in an aerial image (Gibril et al., 2020).

Orthomosaic – a geometrically oriented data product which is constructed by blending multiple aerial photographs into one composite image (Pix4D, 2021a).

Photogrammetry – calculating measurements from photographs by computing the distance away from an object, the focal length, and angle of capture (Walford, 2017).

PPK – post-processing kinematics refers to the corrective calculations of the UAS' camera position and orientation, relative to a known reference point (Zhang, Aldana-Jague, et al., 2019).

Prescribed burn – periodical fire events that are intentionally set and controlled for a variety of ecological management objectives (Newman, 2019).

RTK – real-time kinematics involves a dual-frequency GNSS station, emitting reference positioning data in real-time to the receivers on the UAS (Zhang, Aldana Jague, et al., 2019).

Selective timber harvest – the deliberate removal of timber from a forest stand, where the stems selected are based on temporal, spatial, and phenological characteristics (Newman, 2019).

SfM – structure from motion photogrammetry relies on keypoint matching of similar pixels from multiple aerial images to reconstruct a single composite image and 3D model (Tomaštík et al., 2019).

Treatment – for the purposes of this study, a treatment refers to an intentional act conducted by land managers in an attempt to restore native vegetation and facilitate sustainable regeneration.

UAS – an unmanned aerial system or 'drone' is "an aircraft and its associated elements which are operated with no pilot on board," (ICAO, 2011).

WGS 84 / UTM Zone 16 North – the World Geodetic Datum is a vertical coordinate system that is used in conjunction with a projected coordinate system, Universal Transverse Mercator (UTM), to determine positions within localized zones, for instance Zone 16 North (GISGeography, 2021d).

LIST OF ABBREVIATIONS

AA accuracy assessment

AFC above forest canopy (referring to flight altitude)

AGL above ground level (referring to flight altitude)

DSM digital surface model

ESR equal stratified random (sampling)

GEOBIA geographic object-based image analysis

GNSS Global Navigation Satellite System

GSD ground sample distance

KPIS key point image scale (Pix4D processing parameter for feature scaling)

LC land cover

LULC land use land cover

ML maximum likelihood

NDBM natural disturbance-based management

NPS National park service

OA overall accuracy

OBC object-based classification

PBC pixel-based classification

RF random forests (classification algorithm)

RGB red, green, and blue (visible light spectrum)

RTK real time kinematics

SS shutter speed

SVM support vector machines

TDF temperate deciduous forest

VTOL vertical take-off and landing (in reference to an aircraft)

UAS unmanned aerial system

USDA United States Department of Agriculture

USFS United States Forest Service

WFI wildfire intensity (WFI = fuel load x rate of spread)

WFP wilderness fire policy

ABSTRACT

Three prescribed burn sites and seven selective timber harvest sites were surveyed using a UAS equipped with a PPK-triggered RGB sensor to determine optimal image collection parameters surrounding each type of disturbance and land cover. The image coordinates were corrected with a third-party base station network (CORS) after the flight, and photogrammetrically processed to produce high-resolution georeferenced orthomosaics. This addressed the first objective of this study, which was to *establish effective data procurement methods from both before and after planned* disturbances.

Orthomosaic datasets surrounding both a prescribed burn and a selective timber harvest, were used to classify land covers through geographic image-based analysis (GEOBIA). The orthomosaic datasets were segmented into image objects, before classification with a machine-learning algorithm. Land covers for the prescribed prairie burn were 1) bare ground, 2) litter, 3) green vegetation, and 4) burned vegetation. Land covers for the selective timber harvest were 1) mature canopy, 2) understory vegetation, and 3) bare ground. 65 samples per class were collected for prairie burn datasets, and 80 samples per class were collected for timber harvest datasets to train the classifier. A supported vector machines (SVM) algorithm was used to produce four land cover classifications for each site surrounding their respective planned disturbance. Pixel counts for each class were multiplied by the ground sampled distance (GSD) to obtain area calculations for land covers. Accuracy assessments were conducted by projecting 250 equalized stratified random (ESR) reference points onto the georeferenced orthomosaic datasets to compare the classification to the imagery through visual interpretation. This addressed the second objective of this study, which was to *establish effective data classification methods from both before and after planned* disturbances.

Finally, a two-tailed t-Test was conducted with the overall accuracies for each disturbance type and land cover. Results showed no significant difference in the overall accuracy between land covers. This was done to address the third objective of this study which was to *determine if a significant difference exists between the classification accuracies between planned disturbance types*. Overall, effective data procurement and classification parameters were established for both *before* and *after* two common types of *planned* disturbances within the CHF region, with slightly better results for prescribed burns than for selective timber harvests.

CHAPTER 1 - INTRODUCTION

In 2019, record-breaking wildfires across the globe incinerated millions of acres of forest, reduced thousands of structures to ash, nearly extirpated some wildlife species, and killed hundreds of people (CRS, 2020). Since then, the number and intensity of wildfires have only increased; degrading natural forest resources and wildland/urban interfaces in a negative reinforcing loop (CRS, 2021). To combat these destructive disturbance events, land managers are increasingly implementing frequent low-intensity *planned* disturbances such as selective timber harvest and prescribed burn "treatments" to remove overgrown and/or non-native vegetation fuel loads in a controlled setting. Planned disturbance treatments like these belong to a methodology of forest management known in the industry as *natural disturbance-based management* or "NDBM". NDBM treatments can significantly reduce damage from *unplanned* disturbances, as well as produce healthy, diverse, and resilient forest ecosystems (Kuppinger et al., 2010; O'Hara, 2016).

Despite decades of research demonstrating promising benefits for both prescribed burning and selective cutting, these treatments are inherently risky and can unintentionally accelerate forest degradation if done incorrectly (Kuppinger et al., 2010). Therefore, it is necessary when applying NDBM to repeatedly monitor changes to the physical environment of the treated area, to determine if the desired outcome was achieved and adjust practices accordingly (Fernandes & Botelho, 2003). To do this, land managers must properly inventory the treated area both *prior to* and *repeatedly after* the *planned* disturbance event (Rousselet, 2019). While there are is a lengthy repository of treatment efficacy and vegetation health indices, land cover is a commonly used example and is known for being a good indicator of a variety of forest health metrics (Anderson, 1976; Lister et al., 2020).

Traditionally, collecting inventories involved manual ground-based methods, which were time-intensive, laborious, and even dangerous in some areas (Frayer & Furnival, 1999). More recently, land managers have relied upon conventional aerial imaging platforms, such as manned aircraft or satellite networks to conduct inventories (King, 2000). However, manned aircraft operations can also be dangerous and are often too expensive to be worthwhile (Anderson & Gaston, 2013). Furthermore, satellite imagery often lacks the temporal (return rate) and spatial (pixel size) resolution needed for this scale of disturbance (Ruwaimana et al., 2018). For example, while many image-collecting satellites only return to an area every few weeks and are legally

limited to pixel sizes of ≥30cm, they can cover large areas such as multiple watersheds to produce landscape-level land cover classification (Sakumara, 2019). While this resolution is useful for disastrous *unplanned* disturbances, many *planned* disturbances are conducted at plot-level scales, where coarse spatial and temporal resolutions of traditional remote sensing platforms cannot provide the detail needed to derive useful land cover assessments (Asenova, 2018). Fortunately, drones are now a ubiquitous data collection tool across many industries, coveted for their ability to collect high-spatial resolution imagery nearly on-demand (Merkert & Bushell, 2020).

Drones are known in the industry as "unmanned aerial systems"—hereafter referred to as "UAS"— and have the potential to serve as flexible, inexpensive, and efficient aerial surveying platforms for land managers to conduct inventories *before* and *after* planned disturbance events (Hassler & Baysal-Gurel, 2019; Mayes et al., 2016). Despite their demonstrated capability as an effective geospatial data collection tool, the integration of UAS in the forestry community has, until recently, been limited. For example, the vast size of many forests could not be covered effectively with the short-endurance UAS of the past. Today, advancements to UAS design, battery technology, and mission planning software make it easier than ever to survey relatively large areas precisely and efficiently. Additionally, dense forest canopy made it difficult in the past to obtain an accurate survey of ground control tie-in points (GCPs)—a time and labor-intensive task, but necessary to obtain useful inventory measurements. Furthermore, real-time kinematics (RTK) technology, which relays positional data to the UAS during flight via a fixed dual-frequency ground station, has also demonstrated precision deficiencies in dense forest environments (Tomaštík et al., 2019). Now, with post-processing kinematic (PPK) technology, an on-board GPS sensor is used to simultaneously trigger the camera and capture the bounding coordinates of each image at sub-decimeter positional accuracies (Miller et al., 2021). This combination of precision and rapid deployment capabilities has the potential to produce robust datasets for analyzing the efficacy of planned disturbance treatments.

While UAS technology presents strong potential for this application, it also raises several important research questions: 1) Can the precise spatial and temporal resolutions offered by UAS be leveraged to effectively inventory land covers *prior to* and *repeatedly after* planned disturbance events? 2) Can the UAS imagery be effectively processed and classified to accurately quantify land cover both *before* and *after* planned disturbance events? And 3) Can this combination of

technological methods produce similar results across different disturbance treatments and land covers? The following research objectives were developed to address these research questions.

1.1 Research Objectives

Image acquisition parameters and processing methods vary significantly between other similar studies. Subsequently the difference in UAS image quality and resulting land cover classifications between these studies is vast. However, to better understand the factors influencing the quality of UAS imagery, diligent testing of data collection parameters and associated results are needed to integrate UAS into forestry applications effectively (Buters et al., 2019). Therefore, my **first research objective** is to establish effective data procurement methods with UAS for both *before* and *after* planned disturbances. In this first objective, I also intend to optimize processing parameters for this application, and examine to what extent the parameters can be modified to enhance data collected with poor quality. While collecting and processing quality data are important to any forest inventory, equally as important is the quality and usefulness of the resulting data products (Cromwell et al., 2021).

Data classification parameters and results also vary significantly across other pertinent studies, yet are crucial to the replicability and effective implementation of this method (Buters et al., 2019). Therefore, my **second research objective** is to establish effective data classification methods with UAS imagery to quantify land cover from both *before* and *after* planned disturbances. By developing sequential maps of land cover at every stage surrounding the disturbance treatment, quantifiable areas of vegetation loss, retention, and regeneration can be determined (Fernandes & Botelho, 2003).

Because this part of the study will also involve validating the resulting classifications through visual interpretation, these results can be used to compare output quality between land cover types (Husson et al., 2016). Therefore, my **third research objective** is to determine *if* there was a significant difference in output classification quality between the prescribed burn and the selective harvest treatment land covers. By comparing the quality of classified map series between the two disturbance types, the reliability of this inventory method between open and closed canopy land covers can be examined. Completing these objectives promises to establish an effective

methodology for the efficient inventorying of land cover change both *before* and *after planned* disturbance treatments.

CHAPTER 2 – REVIEW OF THE LITERATURE

For centuries, scientists have studied disturbance by quantifying damage to and recovery of forests following the event (Fernandes & Botelho, 2003; Frayer & Furnival, 1999). This is due to disturbances being viewed as mainly *unplanned* events such as wildfires, tornadoes, and floods for example (Samiappan et al., 2019). However, many land managers are increasingly implementing frequent low-intensity disturbances to not only reduce damage caused by naturally occurring disturbances, but also to develop healthy, diverse, and resilient ecosystems (Hobbs et al., 2006; Kuppinger et al., 2010). Due to the nature of conducting a *planned* disturbance, such as a prescribed burn or selective timber harvest, land managers now have an opportunity to inventory management areas *before* the disturbance *as well as* after (Anderson, 2019). Despite this potential, traditional methods of forest inventory fall short in terms of providing the necessary temporal and spatial granularity needed for such a discrete timeframe and event (Asenova, 2018). As a result, land managers are looking for new and efficient methods to conduct *pre* and *post* disturbance inventories with greater temporal and spatial detail than traditional means. While UAS have demonstrated their capability as an efficient and precise data collection tool, their use for inventorying *planned* disturbances, until now, has been limited.

In this review, I will begin by providing a brief overview of disturbance ecology and management, to highlight the importance of maintaining proper inventories and adjusting management actions accordingly. Then, traditional forest inventory and remote sensing methods will be reviewed to explain both the benefits and shortcomings of these methods. Finally, exemplary use-cases of UAS in disturbance ecology will be examined to gain a better understanding of how to best apply relevant methods from the literature to prescribed burns and selective timber harvest treatments.

2.1 Disturbance Ecology and Management Overview

This section of the literature review first defines what disturbances are within the context of forest ecology, then describes disturbances from post-European settlement through the present. This then leads into the development of wilderness fire policy, prescribed burning management, and selective timber harvesting management.

2.1.1 Defining Forest Disturbances

Disturbances are any event that cause significant change in the composition of forests (Aplet, 2006; Hobbs et al., 2006; Kuppinger et al., 2010; O'Hara, 2016). Typically, these include a variety of naturally occurring and/or anthropogenic-caused damage such as: fire, windthrow, disease, pests, non-native plant invasion, agriculture, and timber harvests (Alvarez-Taboada et al., 2017; Asenova, 2018; Fernandes & Botelho, 2003; Garcia Millan et al., 2020; Hesseln, 2000; Lehmann et al., 2017; Martin et al., 2018; Sandino et al., 2018). Changes caused by disturbances can introduce or propagate problems to the ecological sustainability and economic benefit of forests, such as: wildlife habitat degradation; soil erosion; and introduction or propagation of pests, disease, or non-native vegetation—all of which produce compounding effects to biodiversity and productivity of forest ecosystems (Kuppinger et al., 2010). For over a century, land managers have studied how the size, frequency, and intensity of disturbances affect the composition, health, and value of forests to directly address these challenges through continually advancing silvicultural management (Alberdi, 2021; Beheler, 2020; Frayer & Furnival, 1999; Hobbs et al., 2006; HTIRC, 2017; Nordén et al., 2019; Powell, 1996).

2.1.2 Post-Settlement Disturbance in the United States

After decades of intense logging during early European settlement of the US, most of the forests throughout the country were cleared for agricultural development (Evans et al., 2001). The sudden and vast change in land cover from settlement has led to novel ecosystem development at a variety of spatial and temporal scales. Novel ecosystems are characterized by Hobbs, et al (2006):

> "Novel ecosystems have species compositions and relative abundances that have not occurred previously within a given biome" and "ecosystems that are the result of deliberate or inadvertent human action, but do not depend on continued human intervention for their maintenance," (Hobbs et al., 2006, p. 2).

The combination of globalized markets, land degradation, and manipulation of sites for crop cultivation have contributed to the creation of novel ecosystems. Globalization has led to species propagation spanning vast distances that would be otherwise nearly impossible to happen naturally. Land degradation comes in the form of urbanization, intensive grazing/ agricultural practices, and extraction of resources, all of which have caused significant soil erosion, low biodiversity, and resource depletion (Hobbs et al., 2006). As a result, one of the most degraded

landscapes in the world today are temperate deciduous forests (TDF) (Nordén et al., 2019); an exemplary case of which exists in the state of Indiana, which makes up part of the central hardwood forested (CHF) region of the US (HTIRC, 2017).

In the early 1800's prior to European settlement, meso/pyrophytic forests covered an estimated 87% of Indiana, with the remainder consisting of prairie (5%) and wetland (10%) in the northwestern corner. By 1920, just 6% of the state's pre-settlement forested area remained after intensive clear-cutting for crop cultivation. In 2001, less than 1% of pre-settlement old growth remained in Indiana, with just 17% of the state's land use/ land cover (LULC) comprising forest (Evans et al., 2001). Today, forests comprise 19.4% of Indiana's land cover with 85% under private ownership, and are commonly divided into 10-60 acre plots managed for hardwood lumber and veneer production but also provide critical wildlife habitat (Brown et al., 2018; Grimm, 2017; NCRS, 2021). While profitable wood products can be extracted from these areas, which benefits the local economy, it must be done carefully and with objective reasoning to sustain healthy native ecosystems, as there is little margin for error. Without repetitive monitoring and precise record-keeping, these ecosystems could rapidly disappear through non-native invasion, habitat reduction, or destructive unplanned disturbances (Kuppinger, et al., 2010).

2.1.3 Wilderness Fire Policy

Since the inauguration of the US Department of Agriculture (USDA) – Forest Service (FS) and the National Park Service (NPS) during the early 1900's, research on silvicultural systems has played a vital role in shaping the nation's forest resources and how those resources are managed (Frayer & Furnival, 1999). As Aplet (2006) discusses, these programs were established after wildfires destroyed millions of acres in Idaho and Montana, killing 86 in 1910. This led to the development of wilderness fire policy (WFP) and initially was made to suppress all wilderness fires. Between 1968-78, following scientific review, the USDA-FS and NPS adopted the "let it burn" policy, which allowed some naturally occurring fires in federally protected lands to burn under controlled circumstances. Then, in 1988, a series of fires in Yellowstone, combined with abundant fuel load, drought, and wind destroyed much of the park's ecological infrastructure—again fires were immediately suppressed. It wasn't until 1995 that WFP was adapted to "endorse wildland fire use for resource benefit," to fight against destructive wildfires ((Aplet, 2006)p. 10). In 2002, the policy's goal was amended to "restore, rehabilitate, and maintain fire-adapted

ecosystems," ((Aplet, 2006)p. 10). Now, WFP requires measurable performance via inventories to determine when and where the use of fire is appropriate for their goal (Aplet, 2006). From then on, the use of fire through prescribed burning, and the consequential effects on ecological processes and economic value of forests, have been studied extensively.

2.1.4 Prescribed Burning Management

Hesseln (2000) reviewed the economic consequences of wildfire suppression and prescribed burning of forest ecosystems:

> "It is widely acknowledged that in the absence of wildfire, vegetative changes have resulted in fuel loads far exceeding historic levels, which would pose a serious threat to forest and cultural resources if ignited" (p. 322).

While federal and local policy and perception of prescribed burning is based on economic incentive and risk aversion, many factors influence how risk and cost benefits can be calculated. These include: Site preparation (line building, partial cuts, etc), ignition type (manual ground torch, aerial, etc), post-fire clean-up (ash, coarse woody debris, equipment, etc), size of site (number of acres and volume of fuel burned), potential damage from escape (private, public, and cultural assets), and social costs (smoke intrusion, air quality, safety, and aesthetics). Due to the complex nature of this calculation, Hesseln found that determining acceptable levels of risk as well as proof of econo-ecological benefit must be studied further in order to implement this practice on a larger scale. To address these findings, Fernandes & Botehlo (2003) explained how wildfire intensity (WFI) is a function of 'fuel load' times the 'rate of spread' and performed a computer simulation with historical wildfire data to test the potential efficacy of various management actions (including prescribed burning) for reducing WFI. They found that reduction of fuel loads through frequent low-intensity prescribed fire disturbance worked best, showing reduction of "average fireline intensity of wildfires by 76% and total burned area by 37%" (Fernandes & Botelho, 2003, p.119).

While prescribed burning shows promise in restoring native fire regimes to heavily degraded landscapes, scrutinized by invasive-dominated regions for example, this practice poses risky management conditions where a combination of fire and poor post-fire maintenance could unintentionally propagate invasive populations. Kuppinger, et al., (2010) discuss how fire suppression in the southern Appalachian Mountains has led to the foreign invasion of princess tree (*Paulownia tomentosa*) establishment in areas where native species (Virginia Pine, Pitch Pine,

Table-Mountain Pine, Eastern White Pine, Scarlet Oak, Chestnut Oak, and White Oak) are disturbance-dependent. They found that prescribed burning led to 67% reduction of predicted habitat for princess tree after 4 years following fires, and 73% after 6 years following fires. However, the authors warn of perpetuating invasive dominance following burns in xeric regions where biodiversity is already low. Because of this risk, but also because some species/regions do not require fire to reproduce, another common NDBM practice for wildlife habitat maintenance and often sustainable timber production comes in the form of selective timber harvesting.

2.1.5 Selective Timber Harvesting Management

O'Hara (2016) investigated how forest managers are increasingly implementing frequent and low-intensity controlled disturbances, such as selective timber harvests (and prescribed burns), as a means to simulate native disturbance regimes. Selective cutting assists in restoring native compositions and/or producing profitable vegetation species, while simultaneously preventing destructive wildfires through fuel reduction, patch dynamics, and removal of invasive species. Selective cutting has been shown to contribute to healthier biodiversity, wildlife habitats, and natural species regeneration (O'Hara, 2016). An exemplary study on this was conducted by Halpern, et al., (2012).

The research team assessed long-term (>10yr) responses of understory vegetation to various harvest experiments of mature conifer forests in the Pacific Northwest. Selective harvesting has been recognized as a practical way to enhance econo-ecological value and species continuity, but only if enough late-seral species (a.k.a "bio-legacies") remain. Five 13ha sites were used to perform various harvest experiments where two variables were tested: Size (40% or 15%) of retention, and dispersal (uniformly dispersed or aggregated) of 1ha harvest patches. They found that while species composition didn't change much, larger and more uniform harvests did have more pronounced changes on some understory bushes and bryophytes. Clear-cuts retained the lowest species richness of the harvest types, but all sites recovered well, with some species even exceeding their pre-harvest heights. This was likely due to the recruitment of early-seral species as well as the recovery and expansion of more disturbance-tolerant forest herbs (Halpern et al., 2012).

Additionally, Nordén, et al., (2019) studied the econo-ecological effects of converting low-longitude boreal forests to temperate deciduous forests (TDF) along the Norway/Sweden border

through selective harvest regeneration. After a 2016 harvest, net lumber revenue from the sites averaged -€1,668 (~$1,980). Despite this, mean basal area increased from 79% to 89% between 2003 and 2018, and coarse woody debris (CWD) increased by 78% between 2001-2018, both of which are useful indicators of forest health and wildlife habitat. An additional benefit of converting to TDF is that minimal ungulate browsing, due to lack of preferred species, will benefit more natural regeneration without the need for planting or fencing. Spruce regeneration in these environments will contribute to greater economic revenue than non-transitioned stands. Furthermore, the authors suggest that converting abandoned farmlands to TDF will better prepare them for climate change. For example, these converted TDF areas would likely benefit from reduced WFI with greater diversity of more fire-resistant/dependent species spaced further apart than a typical boreal forest setting. In order to continue examining the objective and tangential benefits of select timber harvest and prescribed burn management, researchers must have a way to obtain inventories both *before* and *after* the *planned* disturbance event, however most of the literature to date focuses solely on the *after*-event inventory without having a temporally relevant or spatially detailed enough dataset from *before* the event.

2.2 Post-Disturbance Inventories

Clearly, much effort has been put into studying the effects of NDBM treatments, however these efforts have largely focused on studying regrowth solely *after* disturbance events. Alvarez-Taboada, et al., (2017) mapped invasive bushy needlewood (*Hakea sericea*) species *after* establishment. Fernández-Guisuraga, et al., (2018) classified land cover (LC) of heterogenous forest *after* a 2016 wildfire in Spain. Garcia Millan, Rankine, Sanchez-Azofeifa, (2020) calculated crop loss *following* various disturbances to develop a general applicability model. Knoth, et al., (2013) performed object-based classification (OBC) of vegetation cover in *previously* cut-over peat bogs. Larrinaga and Brotons, (2019) computed greenness indices for *post*-wildfire succession of scots and black pine (*Pinus sylvestris* and *P. nigra*) in coastal Spain. Lehmann, et al., (2017) identified invasive black wattle (*Acacia mangium*) in a savannah-type Brazilian Atlantic Forest *following* establishment. Martin, et al., (2018) developed LC assessments of knotweed (*Fallopia japonica* and *F. bohemica*) presence *after* invasion in eastern France. Pádua, et al., (2019; 2020) created 3-class burn severity assessment *following* a 2017 wildfire in Portugal. Pérez-Rodríguez, et al., (2020) examined efficacy of two prescribed burns in Spain exclusively from *after* the

disturbance took place. Rousselet (2019) classified burn severity from *post*-wildfire aerial imagery of the 2019 fires in Paradise, California. Samiappan, et al., (2019) generated a *post*-wildfire damage analysis and vegetation recovery for Grand Bay along the Mississippi/Alabama border. Sandino, et al., (2018) conducted invasive plant detection of desert vegetation in Australia *post*-establishment. White et al (2018) observed stone pine (*P. banksiana*) regeneration *following* a wildfire in the upper peninsula of Michigan.

The reason for this focus on *post*-disturbance inventories comes back to the historical view of disturbances as typically *unplanned* events and therefore researchers could not obtain inventories *prior* to the event (Aplet, 2006; Fernandes & Botelho, 2003; Garcia Millan et al., 2020; Larrinaga & Brotons, 2019; O'Hara, 2016; Pádua et al., 2019; Pádua et al., 2020; Rousselet, 2019; Samiappan et al., 2019; Simpson et al., 2016; White et al., 2018). Now, with increasing implementation of frequent but low-intensity *planned* disturbances, such as prescribed burns and selective timber harvests, various silvicultural management goals can be achieved ("Forest Inventory and Analysis Strategic Plan," 2016). Examples of these include: diverse species compositions, invasive species removal, wildfire fuel mitigation, and wildlife habitat maintenance (Alvarez-Taboada et al., 2017; Bagaram et al., 2018; Beheler, 2020; Getzin et al., 2014; Getzin et al., 2012; Hobbs et al., 2006; HTIRC, 2017; Kuppinger et al., 2010; Lehmann et al., 2017; Lister et al., 2020; Martin et al., 2018; Ollero et al., 2006; Powell, 1996; Pérez-Rodríguez et al., 2020; Restas, 2006; Ruwaimana et al., 2018; Sandino et al., 2018; Sill, 2020). An objective determination of phenomena like species diversity, amount of invasives/fuel removed, and percentage of suitable wildlife habitat in a given area following a NDBM treatment is needed for determining whether that action was effective at achieving its intended purpose. Without determining *what* was removed or how that area changed from *before* the event, land managers cannot effectively determine a *cause-and-effect* relationship needed for future applications of NDBM treatments.

2.2.1 Traditional Forest Inventory and Remote Sensing Techniques

In order to determine if a particular management action was effective, land managers must have a way to quantify the efficacy of the disturbance from both *before* and *after* the event (Anderson, 2019; Fernandes & Botelho, 2003; Ollero et al., 2006; Pérez-Rodríguez et al., 2020; Rousselet, 2019; Samiappan et al., 2019). Fernandes & Botehlo (2003) stress the importance of systematic data collection surrounding prescribed fires to assess management efficacy. The authors

suggest quantifying vegetated land cover categories and percentages of charred severity, from both *before* and *after* the event as indicators of fire efficacy, should be documented with a photograph series. In a similar study, Rousselet (2019) reiterated the importance of obtaining both *pre* and *post*-disturbance imagery for determining percentage of land cover change, but acknowledges that in order to be effective, the images must have:

"1. Precise spatial registration of multi-temporal images

2. Precise radiometric/atmospheric calibration of multi-temporal images

3. Similar phenological states between images

4. As similar as possible spatial and spectral resolution of images" (p. 4).

Aerial imagery provides an efficient way to cover areas which have been affected by a disturbance (Anderson & Gaston, 2013; Asenova, 2018; Berie & Burud, 2018; Boon et al., 2017; Dainelli et al., 2021; Goodbody et al., 2018; Lehmann et al., 2017; Li et al., 2019; Manfreda et al., 2018; Mayes et al., 2016; Ruwaimana et al., 2018; Sandino et al., 2018; Singh & Frazier, 2018). Traditionally, land managers have relied on satellite or manned aerial imagery to assess land covers (Al-Ali et al., 2020; Alvarez-Taboada et al., 2017; Boardman, 2020; Evans et al., 2001; Frayer & Furnival, 1999; Gibril et al., 2020; King, 2000; Kucharczyk et al., 2020; Latifi et al., 2014; Lister et al., 2020; Mao et al., 2020; Matasci et al., 2018; Matese et al., 2015; Pádua et al., 2020; Tang & Shao, 2015). However, obtaining a *pre*-disturbance dataset becomes challenging with traditional methods due to inherent limitations. For example, while satellites can cover large areas, they have fixed return periods which can limit the temporal resolution needed to obtain accurate pre-disturbance vegetation covers for planned events (Anderson, 2019; Boardman, 2020; Buters et al., 2019; Fernandes & Botelho, 2003; Pérez-Rodríguez et al., 2020; Samiappan et al., 2019). Additionally, many satellite images have too coarse of a spatial resolution—legally limited to 30cm per pixel in the US (Sakumara, 2019)—making them less than ideal for precise land cover quantification of discrete (often <20ha) planned disturbances (Manfreda et al., 2018; Matese et al., 2015; Ristorto et al., 2015) that are typical within the CHFR (Beheler, 2020; Evans et al., 2001; HTIRC, 2017). Furthermore, manned aircraft are capable of providing more appropriate spatial resolutions, but are often cost prohibitive to do so for discrete planned disturbances (Anderson & Gaston, 2013; Berie & Burud, 2018; Ruwaimana et al., 2018). Unmanned aerial systems (UAS) have been recognized as a cost-effective and efficient means to collect precise aerial imagery for

repeated analysis of disturbances (Anderson & Gaston, 2013; Berie & Burud, 2018; Buters et al., 2019; Getzin et al., 2014; Guerra-Hernández et al., 2017; Pádua et al., 2020; Rousselet, 2019; Ruwaimana et al., 2018; White et al., 2018).

2.3 UAS in Disturbance Ecology

While UAS is nothing new to the remote sensing (RS) and geographic information systems (GIS) communities, their popularity is growing in the field of forestry due to their rapid deployment, low-cost, and flexible mission-planning capabilities (Anderson & Gaston, 2013; Buters et al., 2019; Dainelli et al., 2021; Guimarães et al., 2020; Lister et al., 2020; Manfreda et al., 2018; Miller et al., 2021; Ruwaimana et al., 2018; Singh & Frazier, 2018). The versatility of UAS RS to collect vital forest inventory attributes has been demonstrated throughout numerous studies. For example, Getzin et al. (2014; 2012) showed how small canopy gaps (<1ha) are good indicators of biodiversity/forest health, but were only distinguishable with UAS imagery as opposed to coarse spatial resolutions of traditional RS platforms. Similarly, Baragam et al. (2018) were able to quantify the density, diversity, and development over time of understory vegetation within canopy gaps, again made possible by the high spatial and temporal resolution of UAS. Another study used UAS imagery for inventorying pest-infested and abiotically damaged trees in Bulgaria to carry out precise and efficient phytosanitary removal (Asenova, 2018). Due to the high spatial and temporal resolution of UAS as well as improvements to georeferencing capabilities, UAS can collect highly precise geometrically corrected images, making them even more rigorous of an inventory method. They have been used in combination with the 30+ year old RS technique (Kucharczyk et al., 2020) of geographic object-based image analysis (GEOBIA) to objectively classify various phenological conditions of discrete forests for damage and regeneration assessments *following* disturbances.

2.3.1 UAS with GEOBIA

Al-Ali et al. (2020) and Sandino et al. (2018) used UAS with GEOBIA to inventory non-native plant invasion in deserts with 93% overall accuracy (OA). Boardman (2020) leveraged the duo for inventorying woody plant encroachment in southern rangelands, and was able to classify 6 land covers with 84.4%-92.7% OA. Lehmann et al. (2017) compared different types of GEOBIA

(object-based classification [OBC] vs pixel-based classification [PBC]) for invasive plant identification, and found that both methods achieved similar accuracies (82.7%-85.4%). Most importantly, these methods have also been used for timber felling and fire related events. Two examples of timber felling events which were inventoried through UAS-derived OBC are Knoth (2013) and Goodbody (2018). They both examined previously cut sites which were under restoration. Knoth (2013) was able to inventory 4 peatbog species (waterlogged bare peat, tussocks, peat moss, and European white birch) with 91% OA and individual class accuracies ranging between 84%-95%. Goodbody et al. (2018) were able to inventory several conifer species such as Douglas-fir, western larch, western white pine, lodgepole pine, Engelmann spruce, and white spruce at various ages (5, 10, and 15 years since planting). 3 LCs were classified to assess seral succession performance: Conifer, deciduous, and bare ground. They achieved OAs of 86%-95% between age groups. Both of these studies exemplify the versatility of timber management applications this combination of tools can provide, and furthermore, mostly do so within the guidelines of today's remote sensing standard of ≥85% OA and ≥80% individual class accuracies for land cover assessment (Anderson, 1976).

For fire events, UAS-derived OBC has also been studied extensively. Larrinaga (2019) employed OBC for post-fire inventory of two successional pine species (black and scots pine) within an oak-dominant Mediterranean forest. Similarly, White et al. (2018) leveraged OBC for inventorying jack pine succession following a wildfire in northern Michigan with OAs of 98%. Both Pádua et al. (2019) and Anderson (2019) performed *manual* OBC for inventorying phenological condition of forests following fire events. Pádua (2019) digitized three classes of post-fire damage severity, in addition to target species tree identification using image segmentation. Anderson (2019) constructed a three-class vegetation height map and pine regeneration stand map through visual interpretation and digitization of image objects. Pérez-Rodríguez et al. (2020) achieved an 84.3% OA for a three-class vegetation burn severity inventory. Rousselet (2019) performed image differencing of burn classes *following* Paradise, CA wildfires with multiple OBC maps. Samiappan et al. (2019) also performed three-class OBC of burn severity following wildfires in the southern plains. And Simpson et al. (2016) assessed tropical peatland burn with OBC of LC and achieved 96% OA when compared to verified high resolution manned imagery.

2.3.2 Literature Shortcomings

While a range of OA and individual class accuracies have been demonstrated, much of the research that has been done in this area is concerned with assessing damage (burn severity, or gap size/frequency) and inventory of land covers (heights, species, and percent coverage) again from solely *after* burn events, with some studies using satellite or manned aircraft imagery for *pre*-disturbance datasets (Pádua et al., 2020; Samiappan et al., 2019; Sill, 2020; Simpson et al., 2016). However, these are typically at different spatial and temporal scales and require downsampling of the high spatial and temporal resolution of *post*-disturbance UAS imagery (Samiappan et al., 2019), which effectively negates the inherent advantages of using UAS in the first place. With increasing implementation of *planned* disturbances and the forest industry's desire to learn more about their associated econo-ecological effects efficiently, presents an opportunity to leverage the rapid, precise, and efficient data collection methods provided by UAS. Moreover, due to the *planned* nature of prescribed burns and selective timber harvests, as well as advancements to on-board post-survey georeferencing methods (which eliminate the need for time-consuming terrestrial-based surveys) (Miller et al., 2021), exists the opportunity to not only repeatedly inventory land cover *following* a disturbance, but also *before* to develop a comprehensive disturbance analysis which would advance the silvicultural management of local forests (Fernandes & Botelho, 2003; "Forest Inventory and Analysis Strategic Plan," 2016 ; HTIRC, 2017).

CHAPTER 3 – METHODS

This chapter describes the approach used to address the research questions and objectives of this study.

3.1 Study Area

Temperate deciduous forest (TDF) biomes are currently regarded as one of the most degraded in the world (Nordén et al., 2019), but make up crucial land covers for important ecosystems around the globe (Hoff et al., 2017). These biomes exist at mid-latitudes, and are dominated by mixed broadleaf deciduous trees, such as oak, maple, beech, and hickory, as well as a variety of shrubs, perennial vegetation, and mosses. Species in these biomes are resilient, facing temperature fluctuations between -22ºF (-30ºC) to 86ºF (30ºC) and receiving anywhere from 30 – 60 inches of rain in an average year (NASA, 2021). Furthermore, many ecosystems that comprise this biome are adapted to withstand frequent low-intensity disturbances and often require such events to sustain establishment (Kuppinger et al., 2010). One such example of a severely degraded TDF biome is the central hardwood forest (CHF) region (Figure 1) within the eastern interior of the United States (Evans et al., 2001).

The CHF region is home to a variety of deciduous hardwood species that exist in a segmented mosaic of savannahs and prairies between private plantings of agricultural crops and hardwood forests (Evans et al., 2001). Many prairies and hardwood forest plots in this region are protected areas that are privately owned and managed, ranging in size from 10-60 acres. To maintain native species in these areas, land managers often engage in controlled burns and selective timber harvests throughout the spring, fall, and winter. The goal of these planned disturbances is to mimic the frequency and intensity of natural fire and windthrow events, but in a controlled setting as to facilitate native species regeneration (Fernandes & Botelho, 2003). This way, both the ecosystem and the land manager can benefit by reducing biomass accumulation, increasing favorable conditions for native species regeneration and wildlife habitat, and producing valuable forestry goods (Hesseln, 2000).

However, in order to know if a particular natural disturbance-based management (NDBM) treatment was effective, land managers must be able to quantify what the land cover was *before* the disturbance, as well as *after*, to determine whether the disturbance was helpful or harmful to the affected area (Fernandes & Botelho, 2003). This is especially true in heavily degraded landscapes, such as the CHF, where novel monoculture ecosystems dominate and non-native invasions, like Asian bush honeysuckle, have established (Beheler, 2020). Instances like the CHF require diligent management plans, so that planned disturbances do not unintentionally advance degradation and extirpate native species (Kuppinger et al., 2010). Despite this, few studies exist where land cover change surrounding *planned* disturbances is quantified, let alone at such discrete management scales as those within the CHF region. In order to enhance the NDBM of natural resources within the CHF, quantitative measurements of planned disturbance efficacy must be conducted through precise and efficient means (HTIRC, 2017). Historically, this has been challenging to do as disturbances were—and still are—often thought of as solely *unplanned* events. Furthermore, traditional remote sensing methods cannot provide the temporal or spatial detail needed for assessing changes in land cover from *planned* disturbances in this region.

Fortunately, many recent studies on land cover assessments of disturbance have increased the temporal and spatial resolutions of aerial image collection by leveraging UAS, but failed to analyze the land cover from *before* the disturbance. Therefore, the many disturbance-treated plots within the CHF region presented a unique opportunity to apply UAS surveys for land cover assessments both *before* and *after* the event. This way, local stakeholders would have a precise and efficient means to objectively determine the efficacy of their NDBM treatments and adjust their management actions accordingly. With the help of local stakeholders, namely members of the Hardwood Tree Improvement and Regeneration Center (HTIRC) and Purdue's Forestry and Natural Resources (FNR) department, several suitable study areas within the CHF were identified, particularly throughout the state of Indiana and just over its Michigan and Ohio borders (Figure 1).
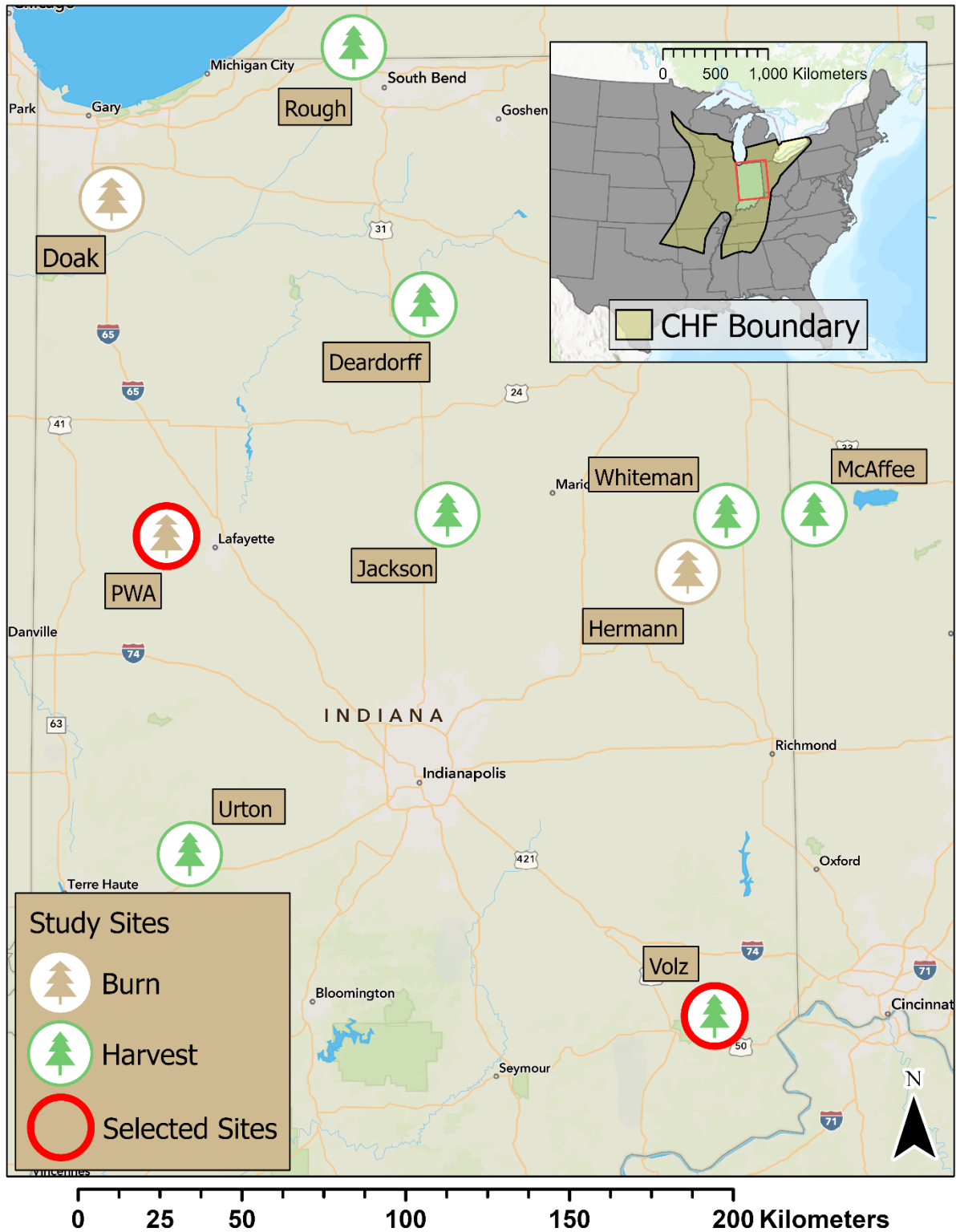
Figure 1. Study area and site map for prescribed burn and selective timber harvest plots throughout the state of Indiana. Sites selected for final analysis are outlined in red. The 'CHF Boundary' locator map was adapted from *The Central Hardwood Forest: Its Boundaries and Physiographic Provinces (Fralish, 2003).*

3.1.1 Prescribed Burn Sites

Data collection for prescribed burn treatments was conducted first at three different prairie properties. These prairies, symbolized as beige trees in Figure 1, are owned and maintained by Purdue's FNR department for local ecological resources. Each of these properties contains between 8 and 60 acres of native prairie land over relatively flat terrain. The properties are segmented into multiple 1-acre plantings of native grass and forb seed mixtures, which include Big/Little Blue Stem, Black/Bown-eyed Susan, Stiff Goldenrod, Indian Grass, White/Purple Prairie Clover, Wild Rye, Side Oats Grama, Prairie Dropseed, and many others (Brooke, 2021). With 10-15 ft fire line paths separating the plantings, the structure of these properties allows ecology researchers to conduct prescribed fire seasonality studies, where individual plots are burned at bi-annual, annual, or 2-year intervals so that correlations between fire frequency and species regeneration can be determined (Miller & Brooke, 2019).

Doak and Hermann properties (Figure 2) were used for preliminary flight testing with the UAS, and were burned on September 19th, 2019 and October 8th, 2019 respectively. Each of these sites were surveyed both immediately *before* and *after* the prescribed burn treatment to gather preliminary datasets with the UAS. Then, PWA (Figure 2) was burned on April 2nd, 2020, and was flown multiple times; one day before the burn, one day after the burn, and multiple times thereafter (Table 1).

Table 1. Prescribed burn information for each prairie site surveyed.

Property	Prairie Coverage	Number of Plots Burned	Total Burned Area (in acres)	Burn Date	UAS Survey Dates
Doak (49.2 acres)	15 acres	5 plots	~5	9/19/19	Pre and Post Burn: 9/19/19
Hermann (38.4 acres)	8.9 acres	4 plots	~4	10/8/19	Pre and Post Burn: 10/8/19
PWA (290 acres)	60 acres	9 plots	~14.7	4/2/20	Pre-burn: 4/1/20 Post-burn: 4/3/20 4/11/20, 4/22/20, 4/28/20, 5/1/20, 5/9/20, 5/13/20, 6/21/20, 6/26/20, 7/17/20
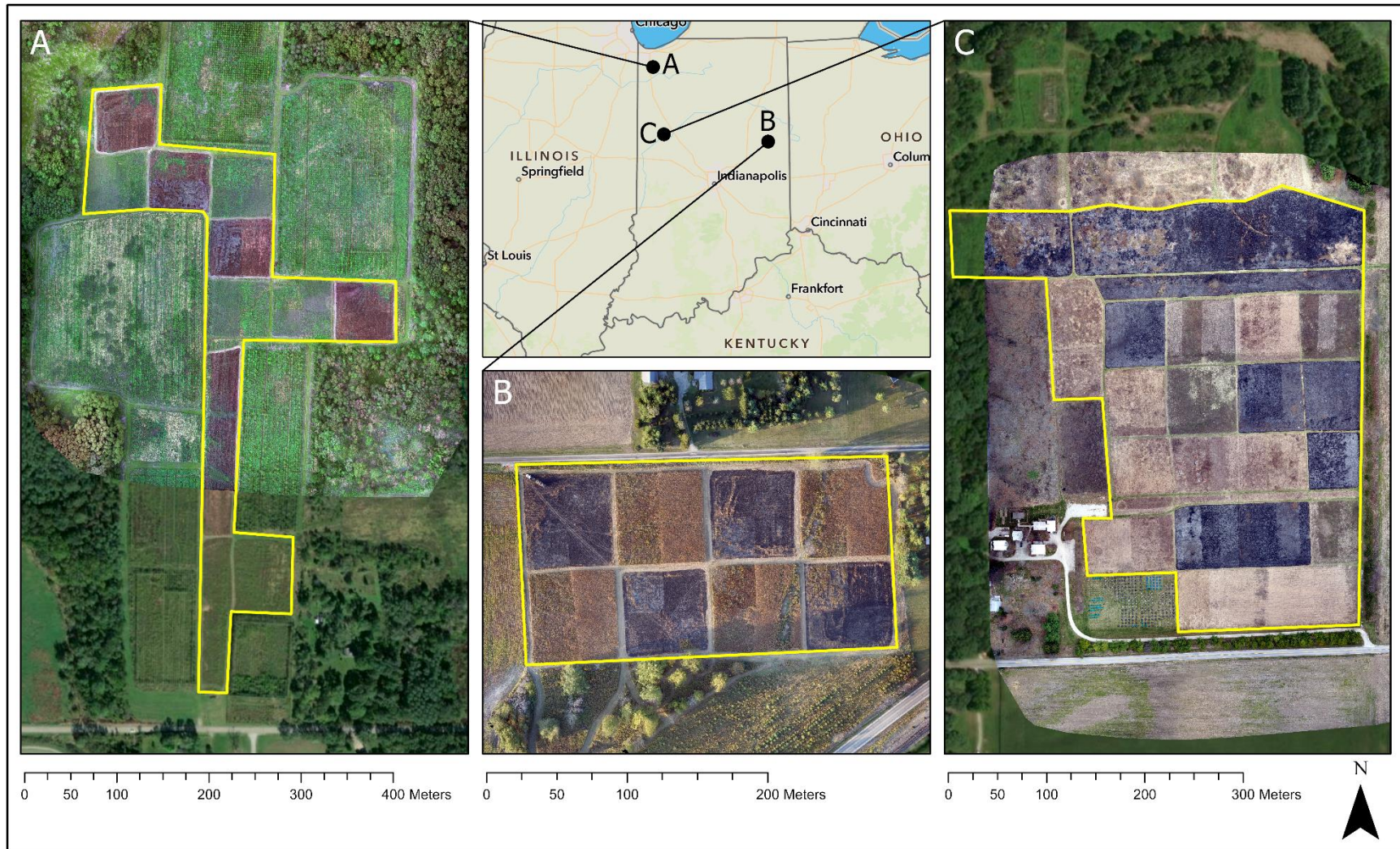
Figure 2. Purdue FNR prairie plots for prescribed fire seasonality research (outlined in yellow). (A) = Doak, (B) = Hermann, (C) = PWA. PWA was selected for final land cover analysis of prescribed burns.

The proximity of PWA made it possible to gather many datasets following the disturbance, achieving the best temporal resolution of the three sites. Therefore, this site was used in the final land cover assessment for prescribed burns in this project. By assessing land cover change surrounding the prescribed burn at PWA, FNR land managers can leverage this information in conjunction with their current management procedures to assess the efficacy and ecological response of their burn treatment (Fernandes & Botelho, 2003).

3.1.2 Selective Timber Harvest Sites

Data collection for selective timber harvests was conducted after prescribed burns at seven different hardwood timber plantings (Figure 3). These plantings, symbolized as green trees in Figure 1, are owned and maintained by Pike Lumber Company for valuable hardwood lumber and veneer production (Pike, 2017). Each of these properties is between 10 and 60 acres (Table 2), harboring species such as Oak, Maple, Hickory, Beech, Poplar, Basswood, Walnut, and many others (Table 3). These discrete plantings are surrounded by private agricultural fields and/or unmanaged forests, often with easement corridors that allowed for sufficient vertical take-off and landing (VTOL) clearance with the UAS. However, some sites were more accessible than others and this determined which were revisited (Table 2). Every site was flown once *before* harvest, five sites were flown more than once, and just one site was chosen for the resulting land cover classification analysis; Volz (Figure 3). Although Volz was farthest away, it was chosen for three primary reasons: 1) Open space surrounding the plot provided a safe environment for VTOL with the UAS; 2) Volz was the smallest site and therefore most efficient for testing various data collection parameters; and 3) Pike recently assumed management of Volz in February of 2010, making this harvest their first management action on the site (Tables 2 & 3). By assessing the land cover change surrounding the first harvest of Volz, Pike's land managers can leverage this information in conjunction with their current management procedures to assess the efficacy and ecological response as a result of their harvest actions (Halpern et al., 2012).
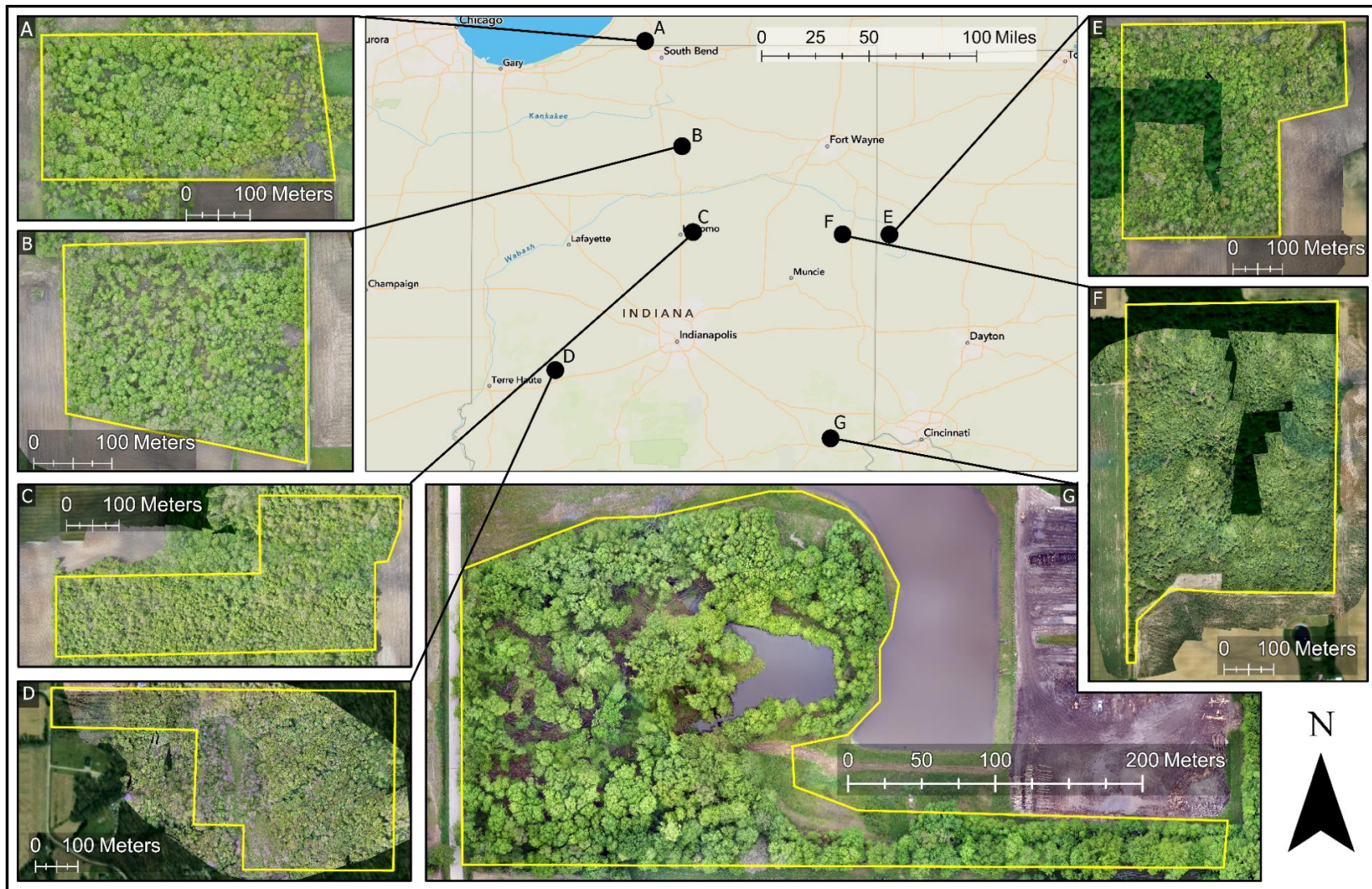
Figure 3. Pike Lumber Company forest plots for timber production (outlined in yellow). (A) = Rough, (B) = Deardorff, (C) = Jackson, (D) = Urton, (E) = McAffee, (F) = Whiteman, (G) = Volz*. Volz was selected for the final land cover analysis.

Table 2. Selective timber harvest information for each forest site surveyed.

Property	# of Trees Harvested	Amount Harvested (in Board feet')	Harvest Duration	UAS Survey Dates
Deardorff (17.3 acres)	127	35,824'	5/8/20 -5/13/20	Pre-cut: 5/7/20, 5/18/20 Post-cut: 7/2/20, 10/9/20
Jackson (23.6 acres)	126	58,702'	6/11/20 - 8/20/20	Pre-cut: 5/16/20
McAffee (27 acres)	217 selected*	*Not yet harvested	NA	Pre-cut: 5/16/20
Rough (20.7 acres)	199	11,268'	6/1/20 -6/10/21	Pre-cut: 5/18/20, 10/9/20
Urton (51.9 acres)	311	109,209'	5/30/20 - 6/20/20	Pre-cut: 5/22/20
Whiteman (56.2 acres)	166	74,956'	5/13/20 - 6/25/20	Mid-cut: 5/16/20 Post-cut: 7/9/20
Volz (10 acres)	65	39,515'	5/7/20 -6/25/20	Pre-cut: 5/7/20 Mid-cut: 5/21/20 Post-cut: 7/2/20, 8/26/20

Table 3. Harvest sites information.

Site	Dominant Species	Minor Species	Soils	Topography
Deardorff *Akron, IN* **(1968)**	Hackberry Hard Maple Hickory Beech Soft Maple Basswood Red Oak	Cottonwood Walnut Sycamore Bur Oak Blue Ash Red Elm Poplar Coffeenut	*Crosier* Loam (75 SI—Red/White Oak) *Barry* Loam (75 SI—White Oak, 78 SI—Red Oak)	Flat with depressions that hold standing water much of the year
Jackson *Kokomo, IN* **(1982)**	Hard Maple Basswood Soft Maple Hickory	Hackberry Poplar Bur Oak Elm Walnut Cottonwood Swamp White Oak Red Oak Beech Buckeye	58% *Crosby* Silt Loam (75 SI—Red/White Oak) 42% *Brookston* Silty Clay Loam (75 SI—White Oak)	Flat with depressions that tend to pond
McAffee *Coldwater, OH* **(1965)**	Red Oak Soft Maple Bur Oak Hard Maple Hickory Basswood White Oak	Miscellaneous	No Soil Information	Flat with depressions that hold standing water much of the year

Table 3. continued

Rough *Buchanan, MI* **(1985)**	**Hard Maple** **Tulip Poplar** **Beech** **Red Oak** **Hickory** **Basswood**	**Soft Maple** **Bitternut Hickory** **Shagbark Hickory** **Butternut** **Cherry** **Sassafras** **Ironwood** **Red Elm** **Grey Elm**	**67% *Martinsville* fine sandy loam** **(98 SI—Tulip Poplar)** **15% Selfridge loamy sand** **10% *Metea* loamy sand** **(68 SI—Red Oak)** **6% *Oshtemo* loamy sand** **(61 SI—Sugar Maple)**	**Flat to slightly rolling with eastern and southern parts wet, perennial ponds during wet periods**
Urton *Reelsville, IN* **(1997)**	Poplar White Oak Bitternut Hickory Shagbark Hickory Mockernut Hickory Red Oak Hard Maple	Beech Cherry Red Maple Sycamore Walnut	43% *Hickory* loam (85 SI—White/Red Oak) 30% *Ava* silt loam (75 SI—White Oak)	Flat to steep
Whiteman *Kitt, IN* **(1986)**	Hard Maple Red Oak White Oak Hickory Swamp White Oak Bur Oak Soft Maple	Miscellaneous	36% Blount-Glynwood (65 SI—White/Red Oak) 20% Pewamo silty clay (90 SI—Pin Oak)	Very slight slope to the north (wetter)
Volz *Milan, IN* **(2010)**	Pin Oak Soft Maple Shagbark Hickory Sweet Gum Black Gum	White Oak Poplar Beech Bitternut Hickory Pignut Hickory Black Locust Eastern Red Cedar	On 0-2% slopes, 81% Avonburg silt loam (75 SI--Northern Red Oak) On 2-6% slopes, 16% Nabb silt loam (eroded, no SI available)	Flat, slightly higher in southern part, manmade horseshoe pond on eastern side of plot

Note: SI = Site Index, which "is the height in feet a tree reaches in 50 years and is a measurement for the productivity of a forest soil," (Grimm, 2017).

Once the sites for both NDBM treatments were established, the next step was to engage in data collection testing. This was done in order to optimize the atmospheric, sensor, and mission planning parameters for quality imagery surrounding burn and harvest events. Data collection was performed with an industry-grade UAS and sensor combination.

3.2 Materials

This section describes the UAS and image collection systems employed for data collection.

3.2.1 UAS and Sensors Combination

To test various data collection parameters and gather image datasets for each planned disturbance, a multi-rotor UAS was equipped with a mirrorless interchangeable lens (MIL) digital camera and post-processing kinematic (PPK) sensor (Figure 4, Table 4, Table 5, and Table 6). The UAS used was a DJI Matrice 600 Pro (M600) and was selected for its well-balanced combination of payload capacity, rapid deployment, and endurance. With six propeller motors affixed to a full carbon frame, this UAS was powered by six lithium polymer (LiPo) batteries and capable of a relatively long flight time (Max. ~26 min) while remaining steady in strong winds (up to 20 mph) (DJI, 2021).

Table 4. UAS specifications (DJI, 2021).

UAS	Type	Rotors	Dimensions (mm)	Dry Weight	Takeoff Weight	Max Flight Time
DJI M600 Pro	Multi-rotor	6	1668 x 1518 x 727	9.6kg (21.2lbs)	11kg (~24.2lbs)	~26 min

Note: Dry weight is weight of platform with all TB48S batteries installed but no sensor payload. Takeoff weight is weight of platform including batteries and all payload used for data collection. Max flight time is for takeoff weight of UAS.

This particular UAS and sensor combination was selected for its ability to rapidly gather multiple datasets, sometimes up to three flights in one day, with precise and accurately geolocated images in a variety of field settings. This allowed for efficient testing of multiple data collection parameters between flights until quality imagery was consistent. Because the sites were relatively discrete, and high temporal datasets were necessary, a multi-rotor was chosen over a fixed wing, which often require more time in the field and larger deployment areas to be safe and worthwhile (Berie & Burud, 2018). Furthermore, the VTOL capability of a multi-rotor allowed the aircraft to launch and land in tight areas, such as road ditches, easement corridors, or small canopy openings, in addition to open areas (Boon et al., 2017)—all of which were present in this study. Additionally, the M600 was light weight and had ample surface area that allowed for mounting external payloads such as the camera and georeferencing system used to capture and geolocate imagery.

Figure 4. The UAS platform used in this study was a DJI M600 Pro (DJI, 2021) and was equipped with a Geosnap PPK (Field of View, 2021) which triggered a Sony A6000 Mirrorless Interchangeable Lens Camera (Sony, 2018).

Table 5. The UAS platform used in this study was a DJI M600 Pro (DJI, 2021) and was equipped with a Geosnap PPK (Field of View, 2021) which triggered a Sony A6000 Mirrorless Interchangable Lens Camera (Sony, 2018).

Image Sensor	Weight	Lens	Focal Length	Megapixels	Ground Sample Distance (GSD)	DJI Sensor	Weight
Sony A6000	~0.5kg (~1lb)	Voigtländer Color Skopar Aspherical	21mm	24.3 MP	2-3cm per pixel	**Zenmuse XT2 (13mm)**	~0.6kg (~1.3lbs)

The camera used in this study was chosen because of its interchangeable lens, which was able to fit a short (21mm) lens with a wide field of view (91.2°), and had a 24.3-megapixel (MP) resolution. This allowed the camera to capture many overlapping pixels between images, thus providing the photogrammetric software with many tie-points when producing orthomosaic composites (Cromwell et al., 2021; Pix4D, 2021b). With a manual shutter speed, ISO, aperture, and zoom, the settings on this camera could be adjusted for the given atmospheric conditions in order to capture intense detail (2.3cm/pixel GSD) while suspended from a moving platform with

a frequently changing depth of field. The detailed resolution of this camera is important, because according to Seifert, et al. (2019) the greatest contributing factors to producing quality aerial image products are the camera's resolution and heavy overlap between images. The authors also suggest georeferencing with on-board PPK, which requires a compatible image sensor. Fortunately, the Sony A6000 was compatible with the PPK system selected for this study. Lastly, while vegetated land covers were the focus of this study, and therefore could benefit from using a multi-spectral sensor, the goal was to determine the effectiveness of UAS-based GEOBIA with technology that has a low barrier to entry. In this case, a 'normal-colored' (RGB) camera was used to demonstrate the feasibility of this practice with relatively inexpensive and easy-to-use equipment.

Table 6. Georeferencing payload specifications (DJI, 2018; Field of View, 2021). The UAS positioning system was fixed to the aircraft and controlled the position of UAS during flight. The image georeferencing system was the GeoSnap PPK and was independently operational from the UAS.

Georeferencing System	Uncorrected PPK Accuracy	Max Corrected PPK Accuracy	Weight	Dimensions (mm)	UAS Positioning	GPS Accuracy
Field of View GeoSnap PPK	30 cm Vertical/Horizontal	2 cm Vertical/Horizontal	206g (~0.5lb)	90 x 50 x 28	A3 GPS Compass Pro	50cm Vertical, 150cm Horizontal

The georeferencing system used for this study was a GeoSnap PPK (Field of View, 2021). This system was designed to mount on most any mapping-grade UAS and contains its own GPS receiver, internal metric unit (IMU), and central processing unit (CPU) to gather its own position (externally from the UAS) and trigger the camera based on predefined user settings. By adjusting the PPK configuration file settings, the PPK was responsible for triggering the Sony A6000 to capture 80% overlap and sidelap between consecutive images in a gridded mapping mission. This system of georeferencing was not only more efficient than traditional ground control point (GCP) surveys, but also produced inherently more precise resulting datasets (Miller et al., 2021). This is because each image taken from the camera is triggered by the PPK—which has its own set of coordinates that can be corrected with third-party base stations to cm-level precision. Whereas GCPs require the manual identification of ground control points in the imagery, for which some images might not contain a visible GCP marker. Furthermore, placing GCP markers and collecting

coordinates for them is a time-intensive task that is prone to refraction of multi-path satellite signals in dense forest canopies (Miller et al., 2021; Tomaštík et al., 2019).

With this combination of UAS and sensors, each of the identified burn and harvest sites were surveyed (Figure 1), testing the various data collection parameters that affect image quality before processing the imagery and engaging in land cover assessments (Figure 5).
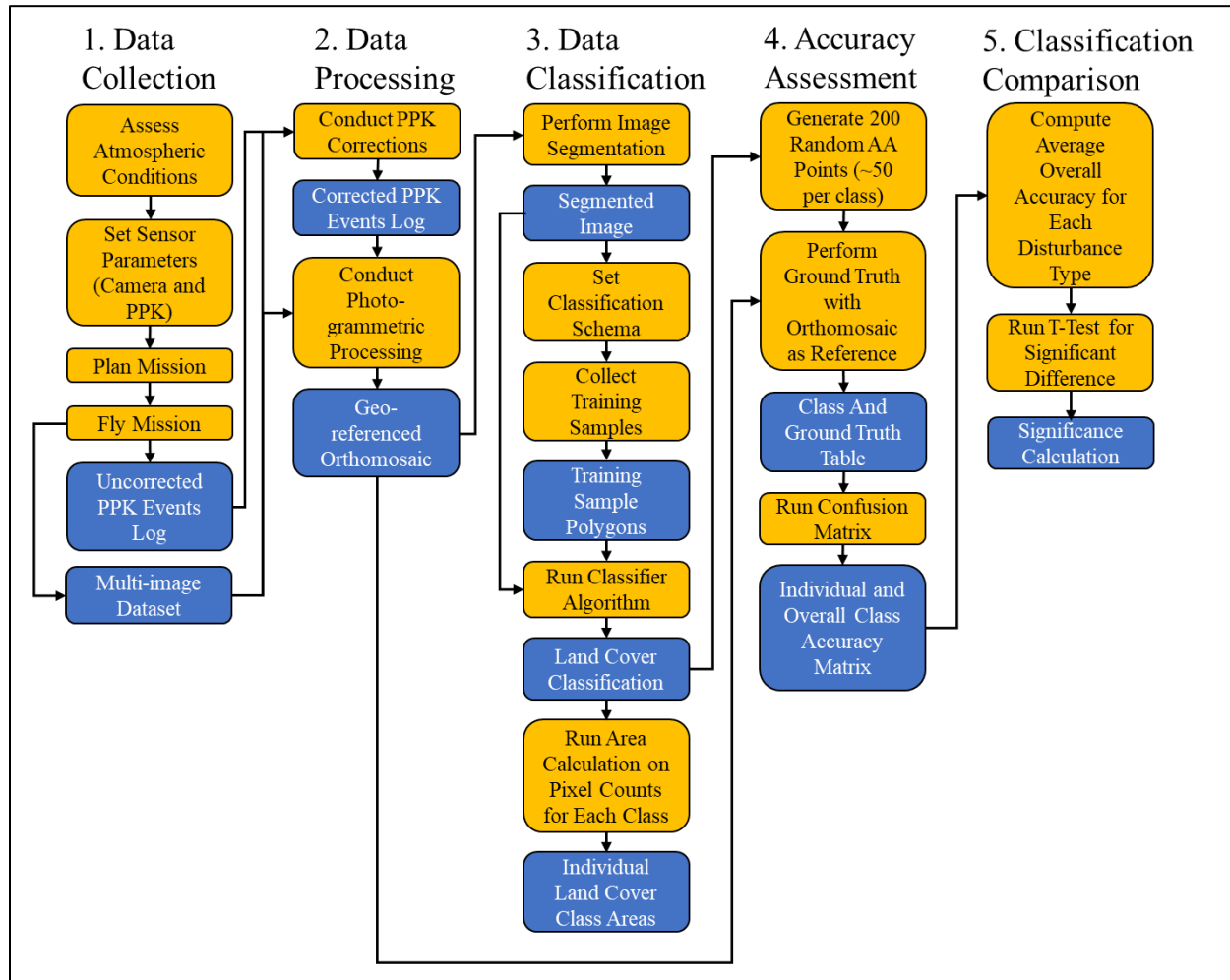
Figure 5. Workflow diagram of methods. Yellow squares = user actions/processes, and blue circles = outputs (and inputs).

3.3 Data Collection

This section describes the procedure used for collecting images surrounding each planned disturbance event.

3.3.1 Objective 1 – Part I

To address the **first objective** of this study, which was to: *Establish effective data procurement methods for both before and after planned disturbances*, the many factors contributing to quality image collection with UAS needed to be identified and tested to ensure quality aerial image products before engaging in land cover analyses (Buters et al., 2019). Before conducting any flights with the UAS, the main data collection variables affecting image quality were identified through the literature and previous UAS survey experience. These variables were divided into three main categories: 1) atmospheric conditions, 2) sensor settings, and 3) mission planning (Table 7).

Table 7. Data collection parameters affecting image quality that were tested throughout the data collection phase.

Category	Data Collection Parameters
Atmospheric Conditions	Sun angle, brightness (cloud cover), and wind
Sensor Settings	Shutter speed, aperture, ISO, and zoom
Mission Planning	Flight altitude, overlap/sidelap, and number of images collected outside study area

Atmospheric conditions are often only considered for how they might affect the safe operation of the UAS, but also should be considered for quality image collection especially in forested environments (Cromwell et al., 2021; Seifert et al., 2019). Conditions such as wind, sun illumination, and sun angle can all have an effect on the quality of images captured by the UAS and therefore, the quality of output image products (Dandois et al., 2015; Getzin et al., 2014). Similarly, sensor settings affecting the quality of imagery were defined as shutter speed, aperture, ISO, and zoom (Bagaram et al., 2018; Díaz-Varela et al., 2015; Frey et al., 2018; Guerra-Hernández et al., 2017; Larrinaga & Brotons, 2019; Lehmann et al., 2017; Seifert et al., 2019; Simpson et al., 2016). Finally, mission planning settings that affect image quality included flight altitude, overlap/sidelap between images, and number of images collected outside the study area (Fraser & Congalton, 2018; Seifert et al., 2019; Shahbazi et al., 2014). Once these settings were identified, the next step was to test them in the field, first at Doak and Hermann prairie burn sites (Figures 1 and 2).

Preliminary flights were conducted at Doak and Hermann prairie burn sites in 2019 to test these data collection parameters. The first dataset was collected at the Doak burn with 'default' collection parameters (Table 8), such as flying at 400 ft above ground level (AGL) and using the preset shutter speed of 1/1600 sec, to determine the quality of outputs with these settings. Then, these settings were revised and tested at the Hermann burn (Table 9), before conducting the series of UAS surveys surrounding the PWA prairie burn in 2020 for the final land cover analysis (Table 10).

3.3.1.1 Prairie Site Testing

Prairie sites were tested first due to the openness of these areas which provided safe operational practice with the UAS and reduced risk for tree, bird, and aircraft collisions (Hubbard et al., 2017). Here, 'default' data collection variables were tested both *before* and *after* a prescribed burn was conducted at the Doak site (Table 8).

Table 8. Preliminary data collection parameters tested for first two flights at Doak prairie burn site.

Consideration	Subject	Parameter Tested	Notes
Atmospheric Conditions	Sun Angle° (Takeoff time)	48.6° (1130) & 39.9° (1500)	Shadows present in both datasets, slightly longer shadows present in second flight
	Brightness	Clear, sunny	Shadows present from tall objects in both datasets, high reflectance of exposed vegetation
	Wind	Variable, around 5 MPH	No issues with motion blur
Sensor Parameters	Shutter Speed	1/1600	Slightly overexposed, difficult to see shaded areas
	Aperture and Focal Length	Wide (f/3.5) and short (21mm)	Wide field of view, no warping present on outer edges, all objects in focus
	ISO and Zoom	ISO 'Auto' and '∞' zoom	Well-balanced ambiance, all objects in focus
Mission Planning	Flight Altitude	120m (400ft) AGL	Quality detail (~2 GSD), wide field of view, no motion blur present
	Overlap / Sidelap	80% x 80%	321 images (for each flight) collected, strong overlap present between consecutive images
	Number of Boundary Images	At least 1 image pass outside of study area	Ground exposure present along study area border, complex ground objects not present

Fortunately, the Doak burn started at 1200 noon and was completed by 1500, which allowed for data collection to occur at two different times of the day (1130 and 1500) and at two different sun angles (48.6° and 39.9°). The sky was clear and sunny, which meant shadows were present in both sets of images, however those present in the second dataset were slightly longer as the sun angle had decreased later in the day. Winds were variable but calm, hovering around five miles per hour, and producing little to no movement of prairie vegetation. The default shutter speed of 1/1600 was used, which slightly overexposed the images, making vegetation in shaded areas undistinguishable in both datasets from the burned areas in the second dataset (Figure 6). Despite this, the field of view and clarity of image objects were superb. This was likely because the relatively short (21mm) focal length and wide (f/3.5) aperture captured a 91.2° field of view, while the ISO (set to 'auto') balanced the gain, and the ∞ zoom setting ensured consistent detail in all image objects. Additionally, at 400 ft AGL with an 80 x 80 overlap/sidelap percentage, these preliminary images achieved a ground sampled distance (GSD) of 2cm per pixel—which is finer than many resolutions achieved by similar studies at lower altitudes and with higher overlap percentages (Fernández-Guisuraga et al., 2018; Fraser & Congalton, 2018; Fraser & Congalton, 2019; Frey et al., 2018; Larrinaga & Brotons, 2019; Lehmann et al., 2017; Li et al., 2019; Martin et al., 2018; Mayes et al., 2016; Simpson et al., 2016).
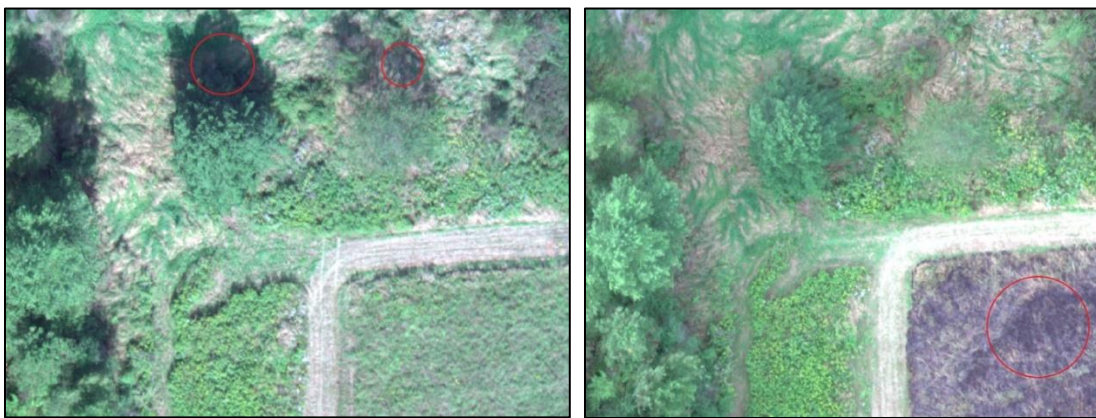
Figure 6. Shaded areas in pre-burn present similar spectral profile to burned areas in post-burn dataset.

For the second data collection test at Hermann, much of the same settings were used with the exception of sun angles, wind, and shutter speed (Table 9). Because the Hermann burn (10/8/19) was performed almost a month after the Doak burn (9/19/19), the burn was conducted later in the

day (between 1500 and 1730). Given that the total sun exposure and sun angles were reduced at this time of year, this allowed the treated vegetation to be as dry as possible in order to produce a 'complete burn' (Miller & Brooke, 2019). This later start time also provided an opportunity to test data collection with the UAS at later times of the day and with lower sun angles (43.2° and 2.5°). Flights were conducted on 10/8/19 both *before* (1315) and *after* (1800) the prescribed burn, and the shutter speed was increased from the default (1/1600) to 1/2500 (Table 9).

Table 9. Data collection parameters tested for two flights at Hermann prairie burn site.

Consideration	Subject	Parameter Tested	Notes
Atmospheric Conditions	Sun Angle° (Takeoff time)	43.2° (1315) & 2.5° (1750)	Shadows present in both datasets, longer shadows present in second flight
	Brightness	Clear, sunny	Shadows present from tall objects in both datasets, moderate reflectance of exposed vegetation
	Wind	Low, > 5 MPH	No issues with motion blur
Sensor Parameters	Shutter Speed	1/2500	Better exposure and view into shaded areas than 1/1600
	Aperture and Focal Length	Wide (f/3.5) and short (21mm)	Wide field of view, no warping present on outer edges, all objects in focus
	ISO and Zoom	ISO 'Auto' and '∞' zoom	Well-balanced ambiance, all objects in focus
Mission Planning	Flight Altitude	120m (400ft) AGL	Quality detail (~2 GSD), wide field of view, no motion blur present
	Overlap / Sidelap	80% x 80%	140 images (for each flight) collected, strong overlap present between consecutive images
	Number of Boundary Images	At least 1 image pass outside of study area	Ground exposure present along study area border, complex ground objects minimal

Upon examining the preliminary image datasets from both burn sites, it was determined that the sensor parameters and mission plan settings used for the Hermann burn flights produced higher quality images than those collected from the Doak burn flights. Despite lower sun angles producing longer shadows, the shutter speed increase (1/2500) balanced the exposure and view into shaded areas. Therefore, the sensor parameters and mission plan settings for the Hermann burn were used for data collection surrounding the PWA burn (Table 8). Atmospheric conditions of the repeat PWA flights varied slightly, but were mostly conducted during peak sun angle times (1100 – 1600), with clear skies, and low wind (Table 10).

48

3.3.1.2 PWA Burn Data Collection

In order to capture the vegetation coverage from *before* the prescribed burn at PWA, a pre-burn image dataset was successfully collected on April 1st, 2020—a day before the prescribed burn took place. The next day, on April 2nd, 2020, the prescribed burn was conducted by intentionally setting 4 x 1-acre interior plots and 2 x 5-acre border plots ablaze until most if not all vegetation within each plot was consumed by the fire. Then, on April 3rd, 2020 a post-burn image dataset was successfully collected covering the same area in order to capture the vegetation immediately *after* the burn while affected plots were still heavily charred. Then, to monitor the recovery and regeneration of the prairie plots, the same mission was flown as close to weekly as possible for three months *following* the burn (Table 10).

Table 10. Flight information for each UAS survey surrounding PWA prescribed burn.

Date	Takeoff	Landing	Total Duration	Number of Images	Clouds / Brightness[1]	Wind[1]
4/01/20*	1500	1520	20 min	303	Scattered, sunny	Variable ~8 MPH
4/03/20	1113	1130	17 min	378	Overcast, diffuse	Calm <3 MPH
4/11/20	1409	1428	19 min	389	Clear, sunny	Low <5 MPH
4/22/20	1008	1023	15 min	374	Clear, sunny	Calm <3 MPH
4/28/20	1251	1313	22 min	388	Scattered, sunny	Calm <3 MPH
5/01/20	1332	1347	15 min	310	Clear, sunny	Variable ~5 MPH
5/09/20	1500	1518	18 min	399	Scattered, sunny	Low <5 MPH
5/13/20	1347	1406	19 min	399	Overcast, diffuse	Variable ~6 MPH
6/21/20	1520	1540	20 min	399	Overcast, diffuse	Variable ~8 MPH
6/26/20	1434	1457	23 min	327	Broken, diffuse	Calm <3 MPH
7/17/20	1303	1328	25 min	249	Clear, sunny	Low <5 MPH

*NOTE: * = pre-burn, 1= unstandardized data collection parameters.*

Every repeat flight at the PWA site was flown using the same mission plan which was constructed before conducting the first flight at PWA. This was possible because the mission planning software used in this study has a feature that allows users to save and re-use mission plans. Therefore, each UAS flight covered the same 26-acre area in roughly 15 minutes (not including manual launch and landing time), by flying a north-to-south "snake" pattern at a height of 400 ft AGL and a maximum ground speed of 20 MPH during image passes. While the mission was set to capture 80% overlap between consecutive images, and 80% sidelap between image passes, the mission planning software based this parameter on the dimensions of the DJI sensor,

which was required to operate the UAS, but has different dimensions than the external PPK-triggered Sony A6000 sensor. While the PPK was also configured to trigger images with 80% overlap, the actual sidelap of the images was likely higher because neighboring image passes were based on a narrower field of view than the Sony A6000.

3.3.1.3 Forest Site Testing

During the *post*-burn data collection phase of PWA, preliminary testing for data collection parameters at timber harvest sites began. Each forest site was flown to test the data collection parameters established for the PWA burn site (* in Table 9). With these settings, some of the initial images contained motion blur, were overexposed, and had low depth of field (Figure 7 and Table 11). On the next iteration of data collection parameter test flights (** in Table 11), the flight altitude was increased to 500ft (150m) AGL to broaden depth of field and field of view, as well as reduce motion blur and overall number of images (Fraser & Congalton, 2018). Since the canopy heights were around 100ft (30m) tall, this increase in flight altitude was permittable by 14 CFR Part 107 regulations, which allows for the operation of UAS no more than 400ft above the ground *or* above the tallest object in open airspaces (FAA, 2021).

Figure 7. Examples of poor-quality image over forest site with initial data collection settings. (Left) high contrast from intermittent cloud cover, overexposed canopy, and dark canopy gaps, (right) motion blur from high wind, overexposed canopy and dark canopy gaps.

Table 11. UAS data collection parameters tested for preliminary imaging of forest sites.

Site	Date	Sun Angle° (Takeoff Time)	Cloud Cover & Brightness	Wind (MPH)	Shutter Speed	Flight Altitude (AGL)	Notes
Volz*	5/7/20	(0900)	Clear, sunny	Med ~9	1/2500	400 ft	Slightly overexposed
Deardorff*	5/7/20	(1230)	Clear, sunny	High ~11.5	1/2500	400 ft	Motion blur, overexposed
McAffee*	5/16/20	(1115)	Broken, variable	Med ~7	1/2500	400 ft	Motion blur, inconsistent lighting
Whiteman*	5/16/20	(1230)	Scattered, sunny	Low ~4.5	1/2500	400 ft	Motion blur, inconsistent lighting
Jackson*	5/16/20	(1545)	Scattered, variable	High ~10	1/2500	400 ft	Motion blur, good exposure
Rough**	5/18/20	(1330)	Overcast, diffuse	VRB ~3, gusting 10	1/2500	500 ft	Some blur, slightly overexposed
Deardorff**	5/18/20	(1615)	Overcast, diffuse	High ~10	1/2500	500 ft	Some blur, slightly overexposed
Volz***	5/21/20	(1130)	Overcast, diffuse	Med ~8	1/4000	500 ft	Good detail, slightly underexposed
Urton****	5/22/20	(1445)	Scattered, sunny	Med ~9	1/4000	500 ft	Good detail, good exposure

Note: number of '*' denotes change to iteration of data collection parameter tests. *= various atmospheric conditions, 1/2500 ss, and 400 ft AGL; **= low and high wind, 1/4000 ss, 500 ft AGL; ***= diffuse and overcast lighting, 1/4000 ss, 500 ft AGL; ****= bright lighting, 1/4000 ss, 500 ft AGL.

After reviewing the preliminary image datasets from the second round of flights (** in Table 11), many images were still overexposed and blurry even with little wind present. It was then determined that increasing the shutter speed as well as avoiding particularly clear/sunny skies whenever possible would likely correct these issues (Getzin et al., 2014). A faster shutter speed was set (1/4000) and tested with overcast lighting (*** in Table 11), which appeared to resolve motion blur, but produced underexposed images. This meant that if overcast lighting was present, shutter speed could be reduced to 1/3200 in the next flights, and left at 1/4000 if brighter conditions were present (****= in Table 11). Additionally, after the first iteration of harvest site tests it was determined that 1 image outside the study area was not adequate for preventing outer image distortion at forested sites. To compensate for this, the number of 'buffer' images was increased to ≥ 2 images outside the study area at plots with borders containing visible ground, and ≥ 3 images

in areas with dense canopy surrounding borders. All remaining flights were then conducted at 500 ft AGL and switching between 1/3200 (for overcast lighting) and 1/4000 (for bright lighting).

3.3.1.4 Volz Selective Harvest Data Collection

In order to capture the vegetation coverage from *before* the selective harvest at Volz, a pre-cut image dataset was successfully collected on May 7th, 2020—a day before the selective harvest began. Then, between May 8th, 2020 and June 25th, 2020, the selective timber harvest was conducted, removing 65 select trees totaling 39,515 board feet of hardwood lumber. During that time, a mid-cut flight was conducted (5/21/2020) as a pseudo post-cut test with the data collection parameters being tested at the time (Table 11). Following the completion of the harvest, a post-cut image dataset was successfully collected (7/2/20) in order to capture the vegetation coverage immediately *after* the cut while the forest floor in canopy gaps was still bare. Then, to monitor the recovery and regeneration within the understory, the plot was flown again two-months *following* the harvest (Table 12).

Table 12. Flight information for each UAS survey surrounding Volz selective timber harvest.

Date	Takeoff	Landing	Total Duration	Number of Images	Clouds / Brightness	Wind (MPH)
5/07/20*	0901	0916	15 min	256	Clear, sunny	Med ~9
5/21/20	1128	1143	15 min	159	Overcast, diffuse	Med ~8
7/2/20	1140	1158	18 min	157	Clear, sunny	Med ~6
8/26/20	1127	1140	13 min	176	Clear, sunny	High ~10

NOTE: * = pre-cut

Every repeat flight at the Volz site was flown using the same mission plan which was constructed before conducting the first flight at Volz. Therefore, each UAS flight covered the same 10-acre area in 15 to 20 minutes, by flying an east-to-west "snake" pattern. Since the flight height changed between the first and last three flights (400 ft AGL to 500 ft AGL) the number of images was reduced, but also captured a wider field of view and greater depth of field.

Once all flights for the prescribed burn at PWA and the selective timber harvest at Volz were completed, the next step was to correct the image coordinates that were collected by the PPK and engage in photogrammetric processing (see Figure 5 for workflow).

3.4 Data Processing

This section describes the procedure used for processing imagery surrounding each planned disturbance event.

3.4.1 Objective 1 – Part II

The next step in *establishing effective data procurement methods for both before and after planned disturbances*, was to produce quality output products; specifically, georeferenced orthomosaics. Georeferencing is the process of pairing each image with their associated coordinates. This can be achieved in many different ways, such as with GCPs, RTK, or PPK, or a combination of these methodologies (Jurjević et al., 2020; Tomaštík et al., 2019; Zhang, Aldana Jague, et al., 2019; Zhang, Aldana-Jague, et al., 2019). Once the images have been georeferenced, their orientation and true-earth locations upon capture are known. This way, the images can be mosaicked together to create a composite photograph of the entire surveyed area with precise proportions and dimensions in a GIS. A composite aerial photograph from numerous images is called an orthomosaic dataset. Georeferenced orthomosaics were produced for each image dataset, while those surrounding the PWA and Volz disturbances were used in the final land cover classification assessments. When testing processing methods for prairie and forested sites, the procedures were mostly the same, however some forested datasets performed better after adjusting two specific parameters in Pix4D (Table 14).

3.4.1.1 Georeferencing

PPK was used in this study to both capture images and georeference the imagery. A Geosnap PPK (Field of View, 2021) was attached to the UAS platform and connected to the Sony A6000 camera via a 5-pin data cable (Figure 4). The PPK device has its own system of location sensors, such as GPS and GLONASS communications, IMU, and CPU (Table 13). These systems are used to determine the position of the PPK and trigger the camera at user-defined overlap

settings (Figure 8). Trigger command settings are stored in a configuration file on a microSD card that is inserted into the PPK. The microSD card also stores the trigger event data; documenting the UTC time, altitude, and 2D coordinates for each picture taken. This information was synchronized to each image in the dataset for georeferencing.
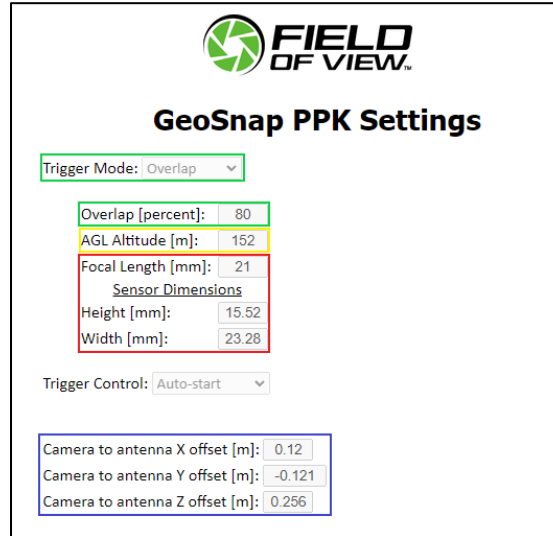
Table 13. GeoSnap PPK positioning and collection information.

Accessible Constellations	Estimated XYZ Accuracy	Trigger Configuration Options	Data Files Collected	Storage Capacity
GPS, GNSS, Galileo	2 cm	2-D distance, time interval, overlap %	RINEX, trigger events, configuration snapshot, geotags tool	microSD card capacity (32 GBs)

Amazingly, PPK is capable of georeferencing individual images with centimeter-level precision and does not require additional georeferencing methods, such as GCPs or RTK (Field of View, 2021; Miller et al., 2021). GCP surveys are a time-intensive process that involves placing physical ground markers within the survey area and collecting their position either with a dual-frequency survey-grade GPS ground station or on-board GPS sensors embedded within the physical marker (Harwin & Lucieer, 2012). Positions collected for each GCP marker are then brought into the photogrammetric processing software and used to orient images that show GCPs. This is done by manually clicking on the center point of each marker within every image that contains one, then reprocessing the dataset.

While generally quite accurate in open areas, GCP surveys have been shown to increase time-in-field and induce positional errors in dense forested environments. This is due to the refraction of GPS signals and/or the inability to view GCP markers because of canopy coverage, making them both imprecise and inefficient when conducting aerial surveys of forests (Miller et al., 2021). Real-time kinematics (RTK) on the other hand, relay positioning data to the UAS in real time via a dual-frequency survey-grade base station (Bakuła et al., 2009). This can be done with a base station set up in the field or a third-party network of base stations such as the National Oceanic and Atmospheric Authority (NOAA) Continuously Operating Reference Stations (CORS). Again, this georeferencing technology is quite accurate in open areas, but in densely forested environments, trees can disrupt either the signal between the base station and UAS or the signal

between the base station and satellites, making RTK less than reliable for forest surveys (Tomaštík et al., 2017). With PPK, positional coordinates of the UAS and sensor are captured above the canopy and can be corrected and processed with the imagery in a matter of minutes upon returning from the field, as opposed to GCPs and RTK which can greatly extend time in the field and in processing.

Figure 8. PPK configuration settings. Trigger mode was set to 'overlap' and the percentage was set to '80' (in green), altitude of flight was set to match the mission plan at '152 m AGL' (in yellow), focal length and sensor dimensions were set to match the Sony A6000 camera (in red), and X, Y, Z offsets between camera and PPK antenna were entered (in blue).

3.4.1.1.1 PPK Corrections

Following each flight, the microSD card in the PPK contained a .html file of the configuration settings for the flight (shown in Figure 8), a .bin file with RINEX data, and a .txt file with the raw coordinates of trigger events. Receiver INdependent EXchange, or 'RINEX' data files "contain raw satellite navigation system data relative to a specified interval of time," (Souliman, 2021). Data included in these files are: the name of base station, the day of the year (out of 365), the hour when recording started, the year, and connected satellite networks (GPS & GLONASS) (Souliman, 2021). Next is the .txt file, which contains raw coordinate positions for trigger events including: the event number; latitude (x), longitude (y), and altitude (z) of the PPK antenna; 3D orientation uncertainties (O, P, K); GPS date and time; and much more (Figure 9).

```
#FieldofView,GeoSnapPPK,SerialNumber:,19180131,Firmware:,1.7.21,CarrierBoard:,389323-0066,Bootloader:,3.1,GNSSreceiver:,5.9Aa06,AtlasExpiry:,N/A,Xo
#Event,Lat[deg],Lon[deg],Alt[WGS84-m],Omega[deg],Phi[deg],Kappa[deg],LatAccy[m],LonAccy[m],AltAccy[m],GPSdate,GPStime,SystemT[s],GPSweek,GPStow[s],
event_00001,41.790933748,-86.361803239,224.0814,0,0,-230.240,1.459,1.459,2.425,2020-10-09,16:24:46.163489980,80.204,2126,491086.163489980,0.824,0.7
event_00002,41.790966764,-86.362115774,374.0420,0,0,-276.891,0.207,0.207,0.290,2020-10-09,16:30:48.759230009,442.799,2126,491448.759230009,0.644,0.
event_00003,41.791014486,-86.362648201,374.2028,0,0,-279.165,0.207,0.207,0.290,2020-10-09,16:30:53.700000022,447.739,2126,491453.700000022,0.644,0.
event_00004,41.791078432,-86.363189389,374.2604,0,0,-277.930,0.207,0.207,0.290,2020-10-09,16:30:58.869170016,452.909,2126,491458.869170016,0.644,0.
event_00005,41.791137985,-86.363719016,374.2782,0,0,-279.509,0.207,0.207,0.290,2020-10-09,16:31:03.874850017,457.914,2126,491463.874850017,0.644,0.
event_00006,41.791194379,-86.364248843,373.8369,0,0,-276.965,0.207,0.207,0.290,2020-10-09,16:31:08.846860024,462.886,2126,491468.846860024,0.643,0.
event_00007,41.791251198,-86.364788054,373.7623,0,0,-279.268,0.207,0.207,0.290,2020-10-09,16:31:13.951419982,467.991,2126,491473.951419982,0.643,0.
event_00008,41.791312868,-86.365328188,373.8163,0,0,-279.166,0.207,0.207,0.290,2020-10-09,16:31:19.023429979,473.063,2126,491479.023429979,0.643,0.
```

Figure 9. Screenshot of text file containing raw trigger event coordinates and other pertinent positioning data within time and space.

Upon returning from the field, the trigger event coordinates were validated with a PPK correction software, which in this case was EZSurv. PPK correction software works by determining the time and position of data collection relative to the nearest third-party base station service to compensate for any atmospheric anomalies that could have affected satellite signals during the flight. In the US, the NOAA CORS network serves as a federal survey-grade system of ground stations for correcting positioning data; which was accessible through EZSurv PPK correction software. While EZSurv is one among many PPK correction software packages, it was selected for its compatibility with the data products derived from the GeoSnap PPK—outputting a corrected position table, that was readable by the photogrammetric processing software selected for this study, quickly and easily (Miller et al., 2021).

Table 14. Datum and projected coordinate system used for georeferencing. NOTE: Estimated error obtained from World Geodetic System - 'WGS84' (GISGeography, 2021d).

Datum	Projected Coordinate System	Zone	Orthometric Surface	Estimated Error
World Geodetic System – 1984 revision (WGS 84)	Universal Transverse Mercator (UTM)	16 North	Ellipsoidal	2 cm

The first step in using EZSurv was to set the spatial reference by selecting a datum and projected coordinate system in order to preserve the true proportions of the survey area when producing orthomosaics. A regional datum and coordinate system were established so that the corrected image coordinates were projected into an appropriate spatial reference (Table 14). The datum chosen for this project was the World Geodetic System (WGS 84). WGS 84 was selected because it is the datum referenced by the GPS satellites used in flights to determine the position of the PPK and trigger the camera. Furthermore, this datum is compatible with the chosen projected

coordinate system in this project, which was UTM Zone 16 N. Universal Transverse Mercator (UTM) is a system of projected coordinate system zones that are optimal for mapping local areas in detail (GISGeography, 2021a). The calculated error of this datum and coordinate system is less than 2cm (GISGeography, 2021d), making them highly accurate and compatible with the level of precision achieved by the UAS imagery, which has a GSD of 2-3cm/pixel.

Next, the .bin file containing RINEX data was uploaded to the EZSurv project. The software then automatically obtained the flight information and identified the nearest CORS location to perform corrections (Table 13). For the PWA prescribed burn site, the CORS referenced was "P775" which was located about 6km away. For the Volz timber harvest site, the CORS referenced was "KYBO" which was located about 35km away. While still effective at correcting positions from the flight, the accuracy can diminish as the distance between the CORS location and study site increases. Generally, sub-centimeter levels of accuracy can be expected when a site is 7km or less away from the CORS referenced. However, sites up to 41km away are still capable of producing positional accuracies within a few centimeters (Miller et al., 2021). Once the nearest CORS location was identified, the positional data from that station during the time of flight was referenced and used to calibrate any periods of uncertainty as well as remove outliers (float epochs in Table 15) from the PPK-collected positions.

Table 15. NOAA CORS locations used for correcting PWA prairie burn (P775) and Volz timber harvest (KYBO) sites.

CORS Site	Distance from Site	Mean Fixed Epochs	Mean Float Epochs	Constellations Used	Mean Position Uncertainty (X)	Mean Position Uncertainty (Y)	Mean Position Uncertainty (Z)
P775	6 km (3.7 mi)	30,086 (99.9%)	3.2 (0.012%)	GPS	2.15 cm	2.18 cm	2.43 cm
KYBO	35 km (21.4 mi)	23,302 (89.9%)	4,869 (10.1%)	GPS + GLONASS	2.7 cm	2.65 cm	2.73 cm

Finally, an events interpolator tool in EZSurv was used to link the images to each trigger event coordinate captured by the PPK. This was done by locating the events file and image folder, entering in the offset between the camera and PPK, and selecting the data columns desired in the corrected output file (Figure 10).
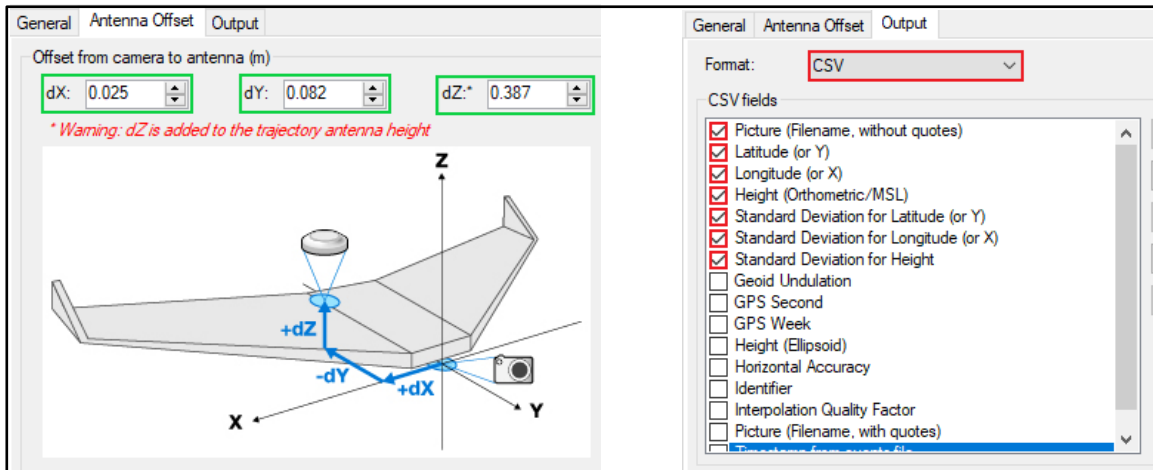
Figure 10. (Left) X, Y, Z offset between camera and PPK antenna in meters. (Right) Corrected output data columns, set to be readable by photogrammetric processing software.

An output .csv file was produced with the corrected coordinates for each image. Because photogrammetric processing was to be done in Pix4D, the columns in this file needed to match the exact formatting that was required of the software during georeferencing. Three columns for the 3D camera position uncertainties of each image were entered into the data table as 'O, P, K' and given '0' values (Figure 11). Omega, phi, and kappa are position uncertainties in geodesy where O is yaw (Z axis), P is pitch (X axis), and K is roll (Y axis). Pix4D looks for these values in georeferencing files to orient the images, but since these were corrected for in EZSurv, they were given '0' values throughout (Field of View, 2019). After completing PPK corrections, the images and georeference file were tied together in Pix4D photogrammetric processing software.

Picture	Y	X	EllHgt	O	P	K	StdDevY	StdDevX	StdDevHgt
DSC00001.JPG	4477348.842	495462.208	302.502	0	0	0	0.008	0.006	0.016
DSC00002.JPG	4477338.525	495481.952	302.358	0	0	0	0.008	0.007	0.017
DSC00003.JPG	4477328.397	495501.162	302.252	0	0	0	0.008	0.006	0.016
DSC00004.JPG	4477317.664	495520.468	302.142	0	0	0	0.008	0.006	0.016
DSC00005.JPG	4477306.717	495539.822	301.924	0	0	0	0.008	0.007	0.017
DSC00006.JPG	4477295.836	495559.183	301.76	0	0	0	0.008	0.006	0.017
DSC00007.JPG	4477285.413	495577.919	301.744	0	0	0	0.008	0.006	0.016
DSC00008.JPG	4477275.205	495597.13	301.698	0	0	0	0.007	0.006	0.016
DSC00009.JPG	4477264.633	495616.296	301.691	0	0	0	0.008	0.006	0.016
DSC00010.JPG	4477254.154	495635.484	301.483	0	0	0	0.008	0.007	0.018

Figure 11. Screenshot of PPK-corrected image coordinate output file from EZSurv.

3.4.1.2 Photogrammetric Processing

Once the corrected image coordinates were in a proper data table, this information was brought in to Pix4D along with the associated image dataset to produce a georeferenced orthomosaic. Pix4D is a photogrammetric processing software, and was chosen for this project due to the user-friendly interface and value for price, as opposed to other conventional software (Fraser & Congalton, 2018; Manfreda et al., 2018), in addition to the inherent compatibility with the EZSurv PPK corrections output (Figure 11). From there, the input and output coordinate system were selected to align with those from the corrected PPK file (Table 14). Then, the '3D Maps' template was used to produce a georeferenced orthomosaic, as well as a 3D point cloud and digital surface model (DSM). Every site was processed at least once, using Doak and Hermann burns as test datasets before processing PWA, while Deardorff and Rough datasets served as test sites before processing Volz. Burn datasets were processed first, using the default parameters in the 3D Maps template. Then, harvest datasets were processed; at first with default parameters, then with adjusted parameters as needed to correct for blurry images and/or the visually complex land cover present in densely forested areas. The two main parameters that Pix4D recommended to correct difficult datasets were: 1) keypoint image scale, and 2) calibration method.

3.4.1.2.1 Keypoint Image Scale (KPIS)

When using the 3D Maps template in Pix4D, the user can adjust several parameters that affect the processing speed, output quality, and reconstruction detail. One such parameter is the Keypoint Image Scale (KPIS) in the "initial processing" step. KPIS defines the scale at which the processing algorithm looks for similar pixels of identifying objects between multiple images in order to properly position each image within the orthomosaic (Pix4D, 2021b). For example, setting the KPIS to 1, means that the algorithm will search the entire image for similar pixel objects relative to the other images in the dataset. Generally, accepting the default of "1" for KPIS will provide the most thorough and detailed reconstruction of image objects in the resulting orthomosaic, however Pix4D recommends reducing the KPIS if there are images within the dataset that are blurry or the survey area contains homogenous land covers, such as snow, or visually complex land covers, such as dense forest canopy (Pix4D, 2021b). For prescribed burn prairie sites, the default KPIS of "1" was used almost exclusively, while some selective harvest sites performed

better with a reduced KPIS of "½" or "¼", especially when some of the images contained motion blur (Table 14). In some instances, adjusting the KPIS still wasn't enough to produce a quality georeferenced orthomosaic, and for those cases, Pix4D recommends adjusting the calibration method from "standard" to "alternative" (Pix4D, 2021c).

3.4.1.2.2 Calibration Method

Because Pix4D is a proprietary software, many of the background algorithms are not described in detail—the calibration method is one such algorithm. Although the difference between the "standard" and "alternative" calibration methods is not known, Pix4D recommends using the "alternative" option when the number of calibrated images upon initial processing is low, or again, when the survey area contains homogenous or complex land covers (Pix4D, 2021c). Because the burn sites performed well with the default "standard" calibration method, "alternative" was not tested for PWA. However, after discovering issues within some of the orthomosaics for harvest sites, Volz datasets were processed with both "standard" and "alternative" calibration methods for each KPIS to determine the best combination.

3.4.1.2.3 Photogrammetric Parameter Testing

When testing harvest sites with these parameter adjustments, the number of calibrated images and the overall visual quality of the resulting orthomosaic varied widely. Therefore, to determine which parameters were optimal for Volz datasets, each was processed with every combination of KPIS and calibration method parameters in order to both validate these methods and use the best iteration from each flight in the final land cover assessments. Then, in order to be thorough, the pre-burn PWA dataset was processed with each KPIS to see if any improvement in number of calibrated images could be made despite the already impressive performance of 'default' parameters. Table 16 contains the photogrammetric processing parameters tested for PWA prairie burn and Volz timber harvest datasets.

As a result of photogrammetric processing, orthomosaic composites, as well as 3D Point Clouds and DSMs, were produced. From there, four orthomosaics were selected from the entire PWA dataset for classification, which included the pre-burn (4/1/20), post-burn (4/3/20), post-

Table 16. Photogrammetric processing parameters tested for georeferenced orthomosaic generation at PWA prescribed burn and Volz selective timber harvest sites.

Dataset	Keypoint Image Scale	Calibration Method	Number of Calibrated Images
PWA pre-burn (4/1/20)	1	Standard	615/621 (99%)
	1/2	**Standard**	**618/621 (99%)**
	1/4	Standard	615/621 (99%)
PWA post-burn (4/3/20)	1	Standard	377/378 (99%)
PWA post-burn 2 (4/11/20)	1	Standard	388/389 (99%)
PWA post-burn 3 (4/22/20)	1	Standard	372/374 (99%)
PWA post-burn 4 (4/28/20)	1	Standard	387/388 (99%)
PWA post-burn 5 (5/1/20)	1	Standard	309/310 (99%)
PWA post-burn 6 (5/9/20)	1	Standard	399/399 (100%)
PWA post-burn 7 (5/13/20)	1	Standard	398/398 (100%)
PWA post-burn 8 (6/21/20)	1	Standard	398/399 (99%)
PWA post-burn 9 (6/26/20)	1	Standard	324/327 (99%)
PWA post-burn 10 (7/17/20)	1	Standard	248/249 (99%)
Volz pre-cut (5/7/20)	1	Standard	241/256 (94%)
	1/2	Standard	241/256 (94%)
	1/4	Standard	239/256 (93%)
	1/2	**Alternative**	**243/256 (94%)**
	1/4	Alternative	239/256 (93%)
Volz mid-cut (5/21/20)	1	Standard	149/159 (94%)
	1/2	Standard	151/159 (95%)
	1/4	Standard	146/159 (92%)
	1	Alternative	148/159 (93%)
	1/2	**Alternative**	**154/159 (97%)**
	1/4	Alternative	149/159 (94%)
Volz post-cut (7/2/20)	1	Standard	155/157 (99%)
	1/2	Standard	156/157 (99%)
	1/4	Standard	154/157 (98%)
	1/2	**Alternative**	**157/157 (100%)**
	1/4	Alternative	156/157 (99%)
Volz post-cut 2 (8/26/20)	1	Standard	166/174 (95%)
	1/2	Standard	168/174 (96%)
	1/4	Standard	163/174 (93%)
	1/2	**Alternative**	**169/174 (97%)**
	1/4	Alternative	163/174 (93%)

burn 2 (4/11/20), and post-burn '5' (5/1/20). These datasets were selected to show what the vegetation was before the burn, immediately after the burn, one week after the burn, and one month after the burn. Later datasets were ultimately not used in the resulting classification as the vegetation did not display noticeable changes in land cover following the post-burn '5' dataset. Furthermore, in order to compare the accuracies of land cover between both disturbance types, an equal number of datasets was needed for each NDBM treatment. Thus, four surveys surrounding the PWA burn were selected to match the number of datasets collected for the Volz timber harvest. These georeferenced orthomosaics were then used as the basis for land cover classifications.

3.4.2 Data Classification

This section describes the procedure used for producing land cover classifications with the UAS imagery surrounding each planned disturbance.

3.4.2.1 Objective 2

To directly address the **second objective** in this study, which was to: *Establish effective data classification methods to quantify land cover from both before and after planned disturbances*, the georeferenced orthomosaics produced in the previous step were brought into a GIS software to engage in geographic object-based image analysis (GEOBIA). When using GEOBIA for land cover classification, there are two types: supervised and unsupervised. The difference between these has to do with the level of user input (Domadia & Zaveri, 2011). As the name implies, 'unsupervised' algorithms classify pixels within an image dataset based on pre-defined settings and do not require supervision from the user during that process. These types of algorithms are useful when the number or types of land covers are unknown and/or when working with large datasets covering vast areas, such as high-resolution satellite images. On the other hand, 'supervised' algorithms are less autonomous and do require supervision from the user during classification, which bases the classification on user-identified samples for each class. Supervised algorithms are useful when the number, types, or distribution of land covers are known.

Within these methods, there are two sub-divisions: pixel-based classification (PBC) and object-based classification (OBC). PBC classifies individual pixels within an image based on spectral characteristics, either through pre-defined parameters (unsupervised) or user-selected

samples (supervised). Conversely, OBC groups multiple pixels into objects based on similar spectral, textural, and proximate characteristics, again either through pre-defined parameters (unsupervised) or user-selected samples (supervised). PBC is useful when pixels are larger than objects within the image, such as low-resolution photos covering large areas, while OBC is useful when image objects are comprised of many pixels such as with high-resolution imagery covering relatively smaller areas (White et al., 2018). In the case of high-resolution UAS imagery, Kucharczyk, et al. (2020) highlight how object-based classification (OBC) enhances pixel-based classification (PBC) for aerial imagery with geographic applications:

> "(i) the partitioning of images into image-objects mimics human visual interpretation; (ii) analyzing image-objects provides additional related information (e.g., texture, geometry, and contextual relations); (iii) image-objects can more easily be integrated into a GIS; and (iv) using image-objects as the basic units of analysis helps mitigate the modifiable areal unit problem (MAUP) in remote sensing," where MAUP refers to varying pixel-sizes from inconsistencies during data collection (p. 4).

Furthermore, OBC relies on image segmentation prior to classifying land covers (Figure 12). The process of segmentation groups pixels into objects with similar spectral and spatial characteristics, to simplify texture and color variances, before sample collection, making the process easier on the user and classification easier on the algorithm (Li & Shao, 2012). Segmentation requires user-set parameters for spectral, spatial, and minimum segment size sensitivities, that are typically optimized through trial-and-error and vary based on pixel resolution (Kucharczyk et al., 2020).

Once the image has been segmented, the types of land cover classes are defined in a classification schema, and are typically based on those developed by James R. Anderson (1976). Next, the user collects samples for each land cover type within the classification schema by drawing polygons of exemplary objects over the segmented image (Figure 13). These sample polygons are then used to train the classification algorithm, which looks for objects of similar spectral and spatial characteristics as the samples collected for each class within the orthomosaic. Kucharczyk, et al. (2020) state while the optimal number of samples per class is subjective, it is generally agreed upon that "as the number of high-quality training samples increases, overall
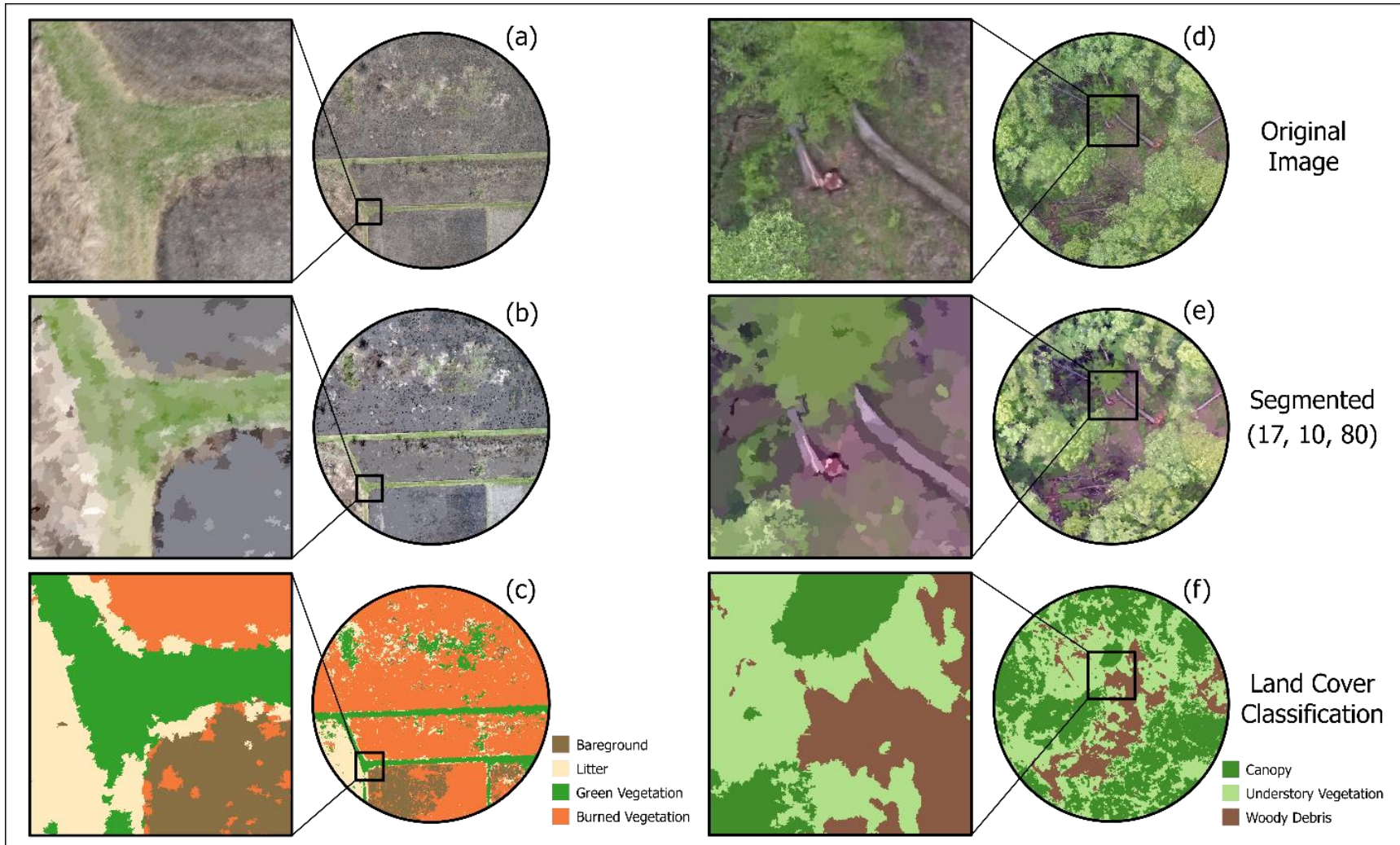
Figure 12. Geographic object-based image analysis (GEOBIA) process. (a) PWA original image, (b) PWA segmented image, (c) PWA classified image, (d) Volz original image, (e) Volz segmented image, (f) Volz classified image.

accuracy increases," (p. 14) and that each class should contain an equal number of samples with a minimum of 50 per class. However, there is a trade-off between number of samples collected and the inherent efficiency of using semi-automated classification algorithms in the first place. After collecting training samples, another consideration for producing land cover assessments is the classification algorithm.

While there are many software packages for performing land cover classification from aerial imagery, and therefore, many classification algorithms, numerous studies suggested using supported vector machines (SVM) over other popular algorithms, such as random forests, maximum likelihood, and ISO clusters to name a few (Al-Ali et al., 2020; Belgiu & Drăguţ, 2016; Boardman, 2020; Gibril et al., 2020; Liu et al., 2018; Mountrakis et al., 2011; Pande-Chhetri et al., 2017; White et al., 2018). Additionally, few studies have examined the efficacy of a SVM classification algorithm in ArcGIS Pro for land cover change surrounding disturbances, and instead have focused on software packages such as eCognition, AgiSoft, and others (Al-Ali et al., 2020; Bagaram et al., 2018; Díaz-Varela et al., 2015; Fraser & Congalton, 2019; Manfreda et al., 2018; Martin et al., 2018). Fortunately, ArcGIS Pro was available for use in this study, and therefore could be tested for this purpose.

Lastly, determining the accuracy of the resulting land cover classification can be done by plotting points randomly on top of the classified image and comparing what class each point falls within to what the actual land cover of each point is. Husson, Ecke, and Reese (2016) validated this procedure by comparing the proportions of land covers in their classified dataset to proportions collected through field samples. After achieving an overall classification accuracy of 95% when compared to field measurements, the authors determined that standalone visual interpretation of their high spatial resolution orthomosaic image was sufficient for performing an accuracy assessment of land cover classifications produced with that imagery. While these findings provided a good foundation for performing geographic object-based image analysis (GEOBIA), the specific parameters for this application required further experimentation to produce quality land cover classifications for image datasets surrounding both prescribed burn and selective timber harvest NDBM treatments.
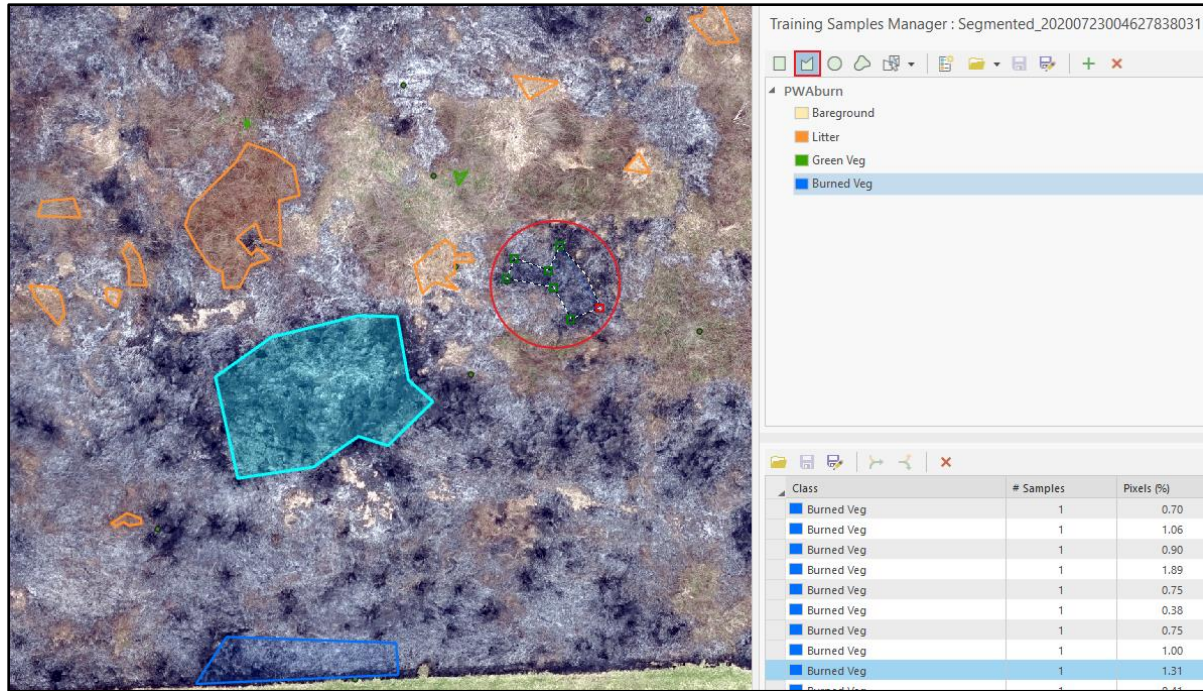
Figure 13. Screenshot of training sample polygon collection from PWA post-burn dataset.

Supervised OBC was chosen for this study because the high-resolution imagery obtained by the UAS contained objects that were comprised of many pixels and the types of land covers were known. Preliminary testing was done using the Doak post-burn and Volz mid-cut datasets to optimize the many factors that contribute to quality land cover classifications, before applying them to PWA and remaining Volz datasets.

3.4.2.1.1 Image Segmentation

The first step when engaging in object-based classification (OBC) is to reduce the complexity of the high-resolution imagery by grouping pixels of similar color and textures into objects containing many pixels. This process is known as image segmentation, and involves setting three main parameters that effect the range of colors and size of objects in the resulting segmented image. These parameters are defined by ArcGIS Pro documentation (ESRI, 2021):

"There are three parameters that control how your imagery is segmented. Spectral Detail: Set the level of importance given to the spectral differences of features in your imagery. Valid values range from 1.0 to 20.0. A higher value is appropriate when you have features you want to classify separately but have somewhat similar spectral characteristics. Smaller values result in more smoothing and longer

processing times. For example, a higher spectral detail value in a forested scene will result in greater discrimination between the different tree species.

Spatial Detail: Set the level of importance given to the proximity between features in your imagery. Valid values range from 1 to 20. A higher value is appropriate for a scene where your features of interest are small and clustered together. Smaller values create spatially smoother outputs. For example, in an urban scene, you could classify impervious surface features using a smaller spatial detail value, or you could classify buildings and roads as separate classes using a higher spatial detail value.

Minimum Segment Size: This parameter is directly related to your minimum mapping unit. Segments smaller than this size are merged with their best fitting neighbor segment. Units are in pixels," (lines 10-27).

However, defining segmentation parameters is no small task. As declared by Kuckarczyk, et al. (2020),"in the GEOBIA literature the consensus is that determining an optimal segmentation parameter value is a heuristic, subjective, challenging, and time-intensive trial-and-error process" (p. 7). In ArcGIS Pro, the 'default' segmentation parameters are 15.5 (spectral), 15 (spatial), and 20 (min. segment size). For the first test, the post-burn dataset from Doak was segmented using these default parameters, and then adjusted until image objects were comprised of as few segments as possible, without grouping multiple objects into one segment (Husson et al., 2016). This was done by increasing the spectral detail, decreasing the spatial detail, and increasing the minimum segment size. Figure 14 shows the progression of segmentation parameters tested, using the Doak post-burn dataset.

Upon optimizing the segmentation parameters, orthomosaics for the PWA and remaining Volz sites were segmented using the 'Segment Mean Shift' tool in ArcGIS. The parameters used were: 17 spectral detail, 10 spatial detail, and 80 minimum segment size. After this was completed, the next step was to define a classification schema for each type of NDBM treatment.

3.4.2.1.2 Classification Schema

One advantage of supervised OBC is that the classification schema is defined by the user. This allows for assessing land covers that are pertinent to the study. In this case two classification schemas were developed; one for each disturbance type (Table 17). For the PWA datasets, four classes were used to assess land covers surrounding the prescribed burn: 1) bare ground, 2) litter, 3) burned vegetation, and 4) green vegetation. For the Volz datasets, four classes

were used to assess land covers surrounding the selective timber harvest: 1) bare ground, 2) woody debris, 3) understory vegetation, and 4) mature canopy.
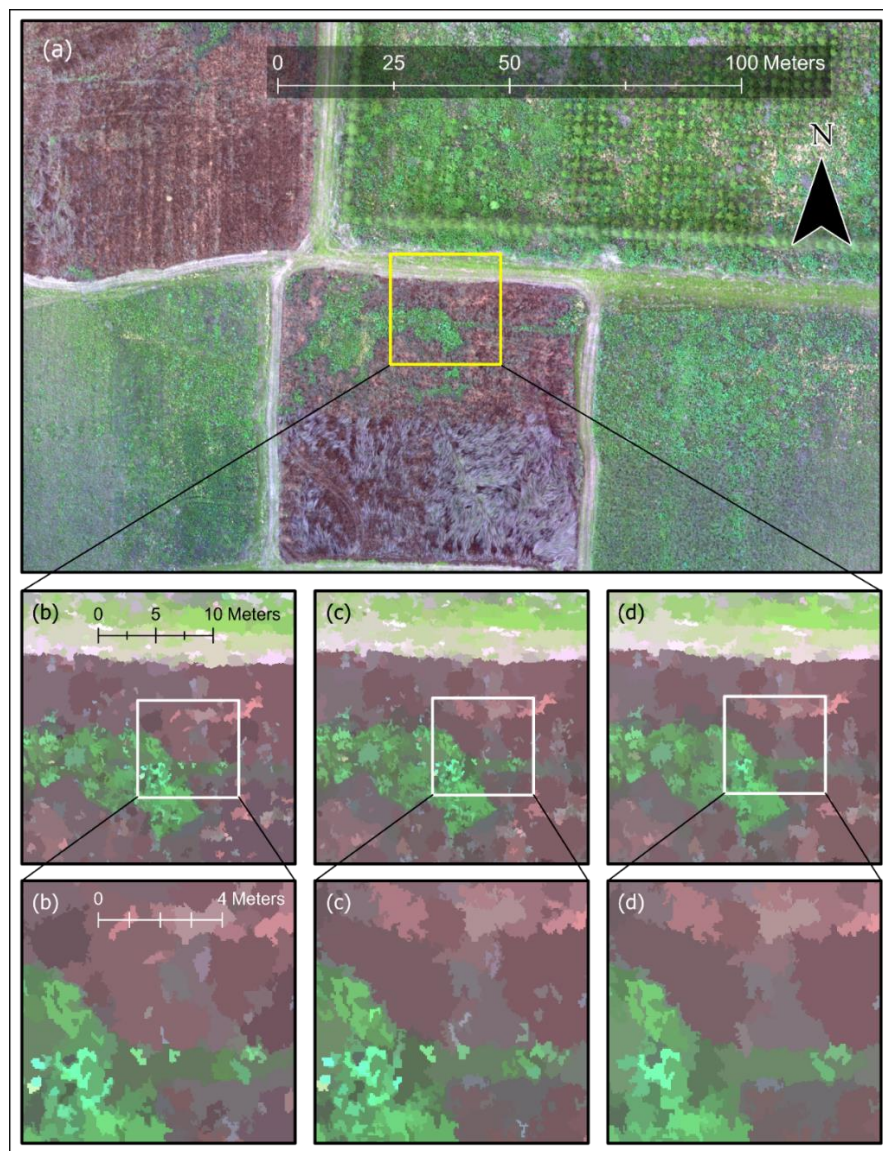
Figure 14. Segmented image parameters tested. (a) original image; (b) 'default' segmentation parameters 15.5 spectral, 15 spatial, 20 minimum segment size (MSS); (c) 17 spectral, 10 spatial, 20 MSS; (d) 17 spectral, 10 spatial, 80 MSS.

The 'bare ground' class was based on Anderson's land use / land cover (LULC) schema (Anderson, 1976) and applied to both disturbance types. Because both burning and cutting treatments remove vegetation from the surface and leave soil exposed, 'bare ground' was a suitable land cover for either disturbance type. Bare ground land covers were visually interpreted in the imagery as exposed soil that was beige-to-brown in color, and when in direct sunlight, had high

reflectance. Because healthy vegetation reflects green light, any areas with high and non-selective reflectance could be collected as bare ground with high confidence. From there, the schemas deviate to include land covers more relevant to each type of NDBM treatment.

Table 17. Land cover classification schemas for PWA burn and Volz harvest datasets.

PWA Burn Classes	Volz Harvest Classes	Final Volz Harvest Classes*
Bare Ground	Bare Ground	Bare Ground
Litter	Woody Debris	
Burned Vegetation	Understory Vegetation	Understory Vegetation
Green Vegetation	Mature Canopy	Mature Canopy

NOTE: Woody debris* samples were collected and used to produce land cover classifications, but were later grouped in with the 'bare ground' class for the final harvest classification maps (Figures 30 - 36 in Results section).

For prescribed burn datasets, the next class was 'litter'. Litter was defined as dry and/or dead prairie grasses within burn plots, which act as the primary fuel source when conducting prescribed burns (Brooke, 2021; Miller & Brooke, 2019). Litter was visually interpreted in the imagery as beige-colored areas with grassy texture. The third class was 'burned vegetation' and was defined as severely discolored vegetation, ash, and visibly charred soil. These areas ranged in color from grey/black to dark maroon/brown and were not considered 'bare ground' until: 1) the charring and ash was no longer present, and 2) the soil had reverted back to its natural color. The last class was 'green vegetation' and was defined as areas of living grass and forbs. Green vegetation was identified in the imagery in order to classify unburned plots as well as areas within burn plots that were unsuccessfully consumed by the fire.

For the selective timber harvest sites, 'woody debris' was defined as felled trees lying on the forest floor. Woody debris was visually interpreted as grey-to-brown tree trunks perpendicular to standing stems visible through canopy gaps. Next, 'understory vegetation' was defined as shrubs, forbs, grasses, and tree seedlings below the canopy. Understory vegetation was visually interpreted in the dataset as shaded areas of green vegetation displayed underneath the crowns of mature trees that make up the canopy layer. Lastly, the 'mature canopy' class was defined as tree crowns within the top layer, or 'canopy', of the property. Mature canopy was visually interpreted as green areas within the dataset that were often noticeably brighter than understory vegetation and displayed well-developed crown structures.

After determining the classification schemas for each NDBM treatment type, the Doak post-burn and Volz mid-cut datasets were used first to test how the number of samples affected the performance of land cover classifications.

3.4.2.1.3 Sample Collection

Within the GEOBIA literature, the number of samples collected for each class is still widely debated (Buters et al., 2019). However, the ideal number can change based on the size and complexity of the dataset, as well as the level of accuracy desired in the final land cover classification. For example, Ghosh and Joshi (2014) were able to achieve 94% overall accuracy (OA) in their resulting classification from 10 samples per class, whereas Gibril, et al., (2020) required 21-32 samples per class to achieve similar OAs (90.5% - 94.5%) in their classification. Furthermore, Kucharczyk, et al., (2020) suggest collecting an equal number of samples per class with a minimum of 50 to properly train the classification algorithm. In order to determine the ideal number of samples needed to produce quality land cover classifications in this study, various sampling sizes were tested using the Doak post-burn and Volz mid-cut imagery.

At first, 65 samples were collected for each class within the Doak post-burn dataset to train a supported vector machines (SVM) classification algorithm (Table 18). After observing the resulting classification accuracy (see *Accuracy Assessment* section), this sample size and classifier was then applied to the selected PWA burn datasets. Then, the Volz datasets were also initially processed with a sample size of 65 per class, but achieved mediocre outputs with the SVM classification algorithm. To determine if a better output could be achieved, the Volz mid-cut dataset was tested with the other three algorithms available (RF, ML, and ISO), using the same 65 samples per class. The initial outputs revealed that SVM and RF generated visibly better results than the ML or ISO algorithms. Therefore, SVM and RF were tested again with 80 samples per class. From there, the remaining Volz datasets were classified with SVM from 80 samples per class (Table 18).

Table 18. Sample size and machine-learning classification algorithms examined for both burn and harvest treatment datasets.

Dataset	Iteration Number	Sample Size (per class)	Classification Algorithm
Doak post-burn (9/19/19)	1	65	SVM
PWA pre-burn (4/1/20) and post-burns (4/3/20, 4/11/20, & 5/1/20)	1	65	SVM
Volz mid-cut (5/21/20)	1	65	SVM
	2	65	ML
	2	65	RF
	2	65	ISO
	3	80	SVM
	3	80	RF
Volz pre-cut (5/7/20) and post-cuts (7/2/20 & 8/26/20)	1	65	SVM
	2	80	SVM

3.4.2.1.4 Classification Algorithm

The 'Image Analyst' module within ArcGIS Pro contains the 'Classify Raster' tool which offers four different classification algorithms for OBC. These classifiers include: Random forests (RF), supported vector machines (SVM), ISO clusters (ISO), and Maximum likelihood (ML). Each of these machine-learning algorithms are trained by the samples collected in the previous step to interpolate land covers within the rest of the segmented image. Of course, many other classification algorithms exist, but three of the four offered in ArcGIS Pro (RF, SVM, and ML) were commonly used in previous studies.

When researching the effectiveness of various machine-learning classifiers, RF and SVM were both highly regarded for their reliability and usability, and were often compared to each other. One such example was the review by Belgiu and Drăguţ's (2016) who noted that both algorithms were equally reliable with RF performing better in multi-sourced and/or hyperspectral imagery with known compositions, and SVM performing better in smaller datasets with unknown compositions when vegetated features are made of many object segments. Since the latter was more applicable to this study, further investigation revealed that SVM often outperformed RF and other classifiers when high-resolution UAS imagery was used in particular. For instance, Boardman (2020) found that SVM outperformed RF and ML classifiers with UAS imagery, achieving OAs of 84.4% - 92.7%. Furthermore, Gibril, et al. (2020) found that SVM performed most consistently, achieving OAs between 90.5%-94.5%, when compared to 'decision trees' and

RF algorithms. This finding was confirmed by Liu, et al. (2018), which revealed that SVM consistently outperformed the RF classifier regardless of sample size.

Based on these findings, SVM was used to classify the selected PWA burn datasets after visually interpreting its effectiveness with the Doak post-burn dataset. However, when attempting to classify the Volz datasets with the same parameters (65 samples per class and SVM classifier), the outputs were not as good as expected and further investigation into both sample size and algorithm type was conducted. The mid-cut dataset was then classified with all four algorithms available through ArcGIS Pro to compare the performance of sample size and classifier. This led to using 80 samples per class and the SVM classifier for the remaining Volz datasets (Table 18).

The iterative process of optimizing the classification methods for Volz was based on trial-and-error (Kucharczyk et al., 2020), using visual interpretation of the outputs to eliminate ML and ISO classifiers, then verifying RF and SVM performance objectively through accuracy assessments.

3.4.2.1.5 Area Calculations
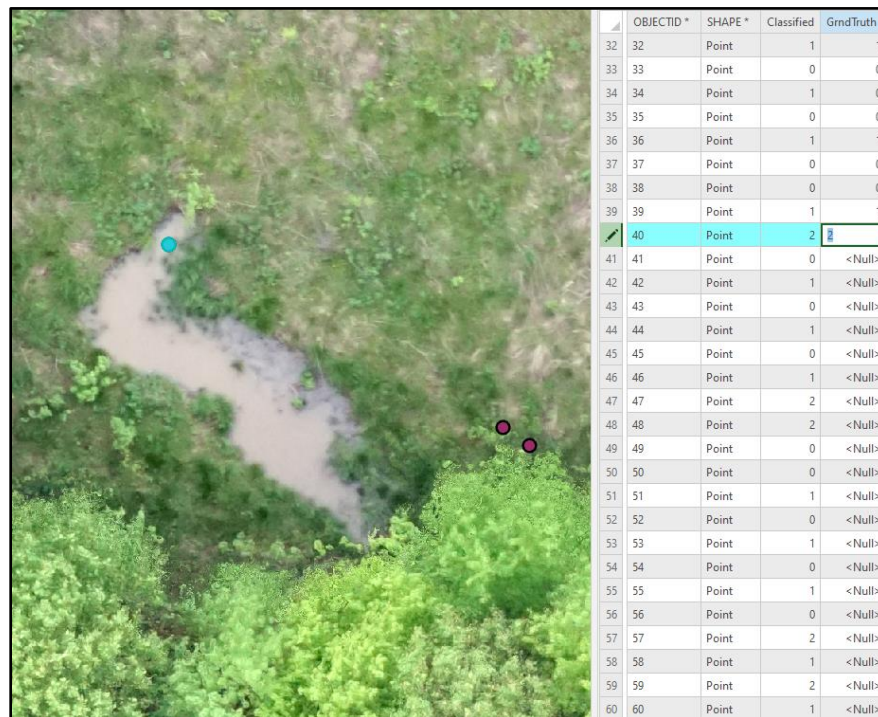
Following each classification, a count of pixels within each land cover class was included in the resulting attribute table. Areas for each land cover were calculated by multiplying the number of pixels for each classification by the ground sampled distance (GSD). GSD is the size that one pixel in the image represents on the earth, which in this case was between 2-3cm. Area calculations were conducted for each PWA (Tables 25 – 28) and three-class Volz datasets (Tables 35 – 38).

3.4.2.1.6 Accuracy Assessment and Confusion Matrix

Accuracy assessments were conducted for two classification outcomes: 1) to determine the performance of RF and SVM classifications with the initial four-class Volz datasets, and 2) to obtain the resulting classification accuracies for the final PWA and Volz (three-class) datasets. The former used an equalized stratified random (ESR) sample of 100 points to examine both the overall and individual class accuracies between each classification method (80 samples per class, RF and SVM) for Volz datasets. Then, the 'woody debris' class was grouped into the 'bare ground' class and each Volz dataset was reprocessed with 80 samples per class and SVM. From there, final

classification accuracies were examined for each three-class Volz dataset and each PWA dataset, both produced with 80 samples per class and the SVM algorithm. This was also done with an ESR sample, but with 250 points to get a better representation of the sample population (Al-Ali et al., 2020; Knoth et al., 2013; Pande-Chhetri et al., 2017). Accuracy assessments were performed using the "create accuracy assessment points" and "compute confusion matrix" tools in ArcGIS Pro.

The accuracy assessment points tool projected an equal number of points for each class (ESR) onto the classified output, which generated a table with columns for: a) point ID, b) classified as, and c) ground truth (Figure 15). Each point was then examined using the georeferenced orthomosaic as a reference (Husson et al., 2016) to determine its true land cover for which the corresponding class value was entered into the 'ground truth' column. Once the table was filled with both the 'classified as' and 'ground truth' values, the "compute confusion matrix" tool was used to generate a table with individual class accuracies and overall classification accuracy (see *Results* section).

Figure 15. Screenshot of ground truth referencing during accuracy assessment.

The individual class accuracies describe both errors of omission (type I error) and errors of commission (type II error) (ESRI, 2021). Type I errors are reference points that were omitted from

73

the correct class. For example, a segment that was actually bare ground in the reference image, but was misclassified as mature canopy would represent a type I error (omission) and affect the producer's accuracy. This describes the reliability of the classification method. Conversely, type II errors are reference points that were added (commissioned) to the wrong class. For example, a segment that was classified as 'bare ground' in the map, but was actually 'mature canopy' in the reference image would represent a type II error (commission) and affect the user's accuracy. This describes the reliability of the classified map. Another way to think about this is the probability that a given land cover is accurately classified in the resulting map is the producer's accuracy, while the probability that the classified map accurately depicts what the true land cover is represents the user's accuracy ("Accuracy Metrics," 2019).

Producer's accuracy is calculated through dividing the number of reference points classified accurately by the total number of reference points within that column for a given class. User's accuracy is calculated through dividing the number of correct classifications by the total number of reference points within that row for a given class. Finally, overall accuracy (OA) is calculated by taking the sum of correctly classified reference points for all classes and dividing it by the total number of reference points in the accuracy assessment ("Accuracy Metrics," 2019).

3.5 Significant Difference Testing

To compare the overall classification performance between both types of NDBM treatment and their respective land covers, a two-tailed t-test was conducted with the overall accuracies from each resulting classification.

3.5.1 Objective 3

To directly address the third objective in this study, which was to *determine if there was a significant difference in final classification quality between the prescribed burn and selective harvest treatment land covers*, a two-tailed t-test assuming equal variances was performed. This was conducted in order to determine if, 1) the variance within disturbance types/land covers, and 2) the variance between disturbance types/land covers, was significant at a 95% confidence level. By calculating this statistic, the reliability of the classification method for either type of disturbance and land cover could be determined. Excel was used for the calculation by first putting the overall

classification accuracies (OA) for each disturbance/land cover type into their own columns. Then, the "t-Test Two-Sample: Assuming Equal Variances" data analysis tool was used. The range of OA values for each disturbance/land cover type were put into the model as well as the "hypothesized mean difference", which in this case was "0" because the variances were assumed to be equal. The data analysis tool generated an output with the mean, variance, and observation size (or sample) for each disturbance/land cover type; a pooled variance between both ranges of OAs; the hypothesized mean difference ("0"); degrees of freedom; then the t Stat, the P-value, and the t Critical values (see Table 43 in *Results* section).

CHAPTER 4 – RESULTS

This chapter describes the findings for the research questions and objectives of this study.

4.1 Objective 1

Objective 1 was to *establish effective data procurement methods for both before and after planned disturbances*, and was achieved by testing various data collection and processing parameters with UAS imagery at multiple prescribed burn and selective timber harvest sites in the Central Hardwood Forest (CHF) region. Key UAS data collection variables were tested for two types of land cover (prairie and forest) surrounding their respective natural disturbance-based management (NDBM) treatments (Tables 19 and 22). Three main categories of data collection variables were identified as: 1) atmospheric conditions, 2) image sensor settings, and 3) mission planning parameters. Atmospheric conditions included: i) sun angle/time of collection, ii) brightness/cloud cover, and iii) wind. Image sensor settings considered were: iv) shutter speed, v) aperture and focal length, and vi) ISO and zoom. Mission planning parameters involved: vii) flight altitude, viii) overlap/sidelap, and ix) number of boundary images. An on-board independent post-processing kinematic (PPK) sensor was responsible for triggering the camera at a predefined overlap setting, and recording the position and time of each image captured.

4.1.1 Optimized Data Procurement Methods for Prescribed Prairie Burns

This section shows the results of data collection and processing methods used for producing georeferenced orthomosaics from the UAS imagery surrounding the prescribed burn at PWA.

4.1.1.1 UAS Data Collection Parameters for Prairie Burn Sites

Quality image datasets were collected at Purdue Wildlife Area (PWA) both *before* and repeatedly *after* the prescribed prairie burn, which was conducted on April 2nd, 2020. Following preliminary data collection tests at Doak and Hermann prescribed prairie burn sites, the atmospheric, sensor, and mission planning parameters were optimized and implemented for PWA burn surveys (Table 19).

Table 19. Optimal data collection parameters for surveying prescribed prairie burn sites.

Consideration	Subject	Recommendation	Justification
Atmospheric Conditions	Sun Angle/ Time of Collection	Mid-morning to mid-evening	Little to no tall objects that would cause long shadows. Wider range of collection times than forested sites.
	Brightness/ Cloud Cover	Bright to Diffuse/ Clear to Overcast	Low vegetation height was less sensitive to overexposure from bright light.
	Wind	0-10 mph (med)	Motion blur less common with low vegetation height.
Sensor Parameters	Shutter Speed	1/2500 – 1/3200	Properly exposed image with sharp detail for given lighting conditions.
	Aperture and Focal Length	f/3.5 and 21mm	Wide field of view for high image overlap.
	ISO and Zoom	Auto and ∞	Auto-balanced gain and focused images.
Mission Planning	Flight Altitude	121m AGL (400ft)	Sufficient depth of field for sharp detail.
	Overlap/ Sidelap	80% x 80%	Ensured thorough coverage of study area
	Number of Boundary Images	≥ 1 image	Inherently more visible ground cover than forested sites allowed for smaller outside image buffer.

4.1.1.2 Georeferencing and Photogrammetric Processing Parameters for Prairie Burns

The optimal data collection parameters listed in Table 19, produced quality imagery for a total of 12 survey dates surrounding the prescribed burn. Images from each UAS survey were synchronized with their respective coordinate positions at the time of capture, and photogrammetrically processed to produce georeferenced orthomosaics that would serve as the foundation for conducting land cover assessments. Image coordinates were collected by the independent on-board post-processing kinematic (PPK) sensor and corrected with the continually operational reference station (CORS) network to achieve centimeter-level precision (Table 20). Corrected coordinates were then used to geolocate the imagery and produce precise aerial composites for each dataset. Key variables for photogrammetric processing were identified as keypoint image scale (KPIS) and calibration method. Multiple iterations of these variables were tested for harvest datasets to determine which combination was most effective at producing quality orthomosaics for either type of NDBM treatment and land cover (Table 21).

Table 20. PPK correction and coordinate system information for PWA prescribed prairie burn site.

Study Site	CORS Site	Distance	Mean Horizontal Accuracy	Mean Vertical Accuracy	Constellations Used
PWA	P775	6km (3.7mi)	2.17 cm	2.43 cm	GPS

Table 21. Optimal photogrammetric processing parameters for prescribed prairie burn datasets.

Site	Keypoint Image Scale (KPIS)	Calibration Method
PWA	1	Standard

4.1.1.3 Resulting Georeferenced Orthomosaics Surrounding PWA Prescribed Burn

Upon georeferenced orthomosaic production, four datasets were selected for engaging in land cover classification. These datasets included: 1) pre-burn, collected on 4/1/20 (Figure 16); 2) post-burn, collected on 4/3/20 (Figure 17); post-burn 2, collected on 4/11/20 (Figure 18); and post-burn "3", which was actually the fifth dataset collected on 5/9/20 (Figure 19).

Figure 16. PWA pre-burn orthomosaic. UAS flight area shown in yellow, study area for land cover classification shown in green.

Figure 17. PWA post-burn orthomosaic. UAS flight area shown in yellow, study area for land cover classification shown in green.

Figure 18. PWA post-burn 2 orthomosaic. UAS flight area shown in yellow, study area for land cover classification shown in green.

Figure 19. PWA post-burn 3 orthomosaic. UAS flight area shown in yellow, study area for land cover classification shown in green.

4.1.2 Optimized Data Procurement Parameters Surrounding Selective Timber Harvests

This section shows the results of data collection and processing methods used for producing georeferenced orthomosaics from the UAS imagery surrounding the selective timber harvest at Volz.

4.1.2.1 UAS Data Collection Parameters for Timber Harvest Sites

Optimal data collection parameters for harvest sites differed slightly from prairie burn sites due to the height of vegetation and sometimes minimal ground visibility. Quality imagery was collected for harvest sites with the parameters shown in Table 22.

Table 22. Optimal data collection parameters for surveying Volz selective timber harvest site.

Consideration	Subject	Recommendation	Justification
Atmospheric Conditions	Sun Angle/ Time of Collection	Mid-day	Tall objects and dense canopy restricted times of collection to highest sun angle possible.
	Brightness/ Cloud Cover	Diffuse/ Overcast	Tall vegetation height was more sensitive to overexposure if too bright and view into canopy gaps was better with diffuse overcast lighting.
	Wind	$\leq$ 5 mph (low)	Motion blur more common with tall vegetation, wind needed to be minimal.
Sensor Parameters	Shutter Speed	1/3200 – 1/4000	Properly exposed image with sharp detail for given lighting conditions.
	Aperture and Focal Length	f/3.5 and 21mm	Wide field of view for high image overlap.
	ISO and Zoom	Auto and ∞	Auto-balanced gain and focused images.
Mission Planning	Flight Altitude	152m AGL (500ft)	Sufficient depth of field for sharp detail.
	Overlap/ Sidelap	80% x 80%	Ensured thorough coverage of study area.
	Number of Boundary Images	$\geq$ 2 images	Commonly less visible ground cover than prairie sites necessitated larger outside image buffer.

4.1.2.2 Georeferencing and Photogrammetric Processing Parameters for Timber Harvests

Following a similar procedure as prairie burn sites, Volz image datasets and their associated coordinates were gathered by the on-board PPK during flight, and corrected with the nearest CORS in EZSurv (Table 23). The images and coordinates were then synchronized in Pix4D photogrammetric processing software with slightly different parameters (Table 24) to produce four quality georeferenced orthomosaics for land cover classification surrounding the selective timber harvest (Figures 20 – 23).

Table 23. PPK correction and coordinate system information for Volz selective timber harvest site.

Study Site	CORS Site	Distance	Mean Horizontal Accuracy	Mean Vertical Accuracy	Constellations Used
Volz	KYBO	35km (21.4mi)	2.68 cm	2.73 cm	GPS + GLONASS

Table 24. Optimal photogrammetric processing parameters for Volz selective timber harvest datasets.

Site	Keypoint Image Scale (KPIS)	Calibration Method
Volz	1/2	Alternative

Georeferenced orthomosaics for both NDBM treatments were then brought into a GIS software to engage in geographic object-based image analysis (GEOBIA) for producing land cover assessments surrounding either NDBM treatment.

4.1.1.3 Resulting Georeferenced Orthomosaics Surrounding Volz Timber Harvest

Upon georeferenced orthomosaic production, four datasets were produced for engaging in land cover classification. These datasets included: 1) pre-cut, collected on 5/7/20 (Figure 20); 2) mid-cut, collected on 5/21/20 (Figure 21); post-cut, collected on 7/2/20 (Figure 22); and post-cut 2, collected on 8/26/20 (Figure 23).

Figure 20. Volz pre-cut orthomosaic. Study area for land cover classification shown in yellow.

Figure 21. Volz mid-cut orthomosaic. Study area for land cover classification shown in yellow.

Figure 22. Volz post-cut orthomosaic. Study area for land cover classification shown in yellow.

Figure 23. Volz post-cut 2 orthomosaic. Study area for land cover classification shown in yellow.

4.2 Objective 2

Objective 2 was to *establish effective data classification methods to quantify land cover from both before and after planned disturbances*, and was achieved by testing the various segmentation, sampling, and classification algorithms for the chosen prescribed prairie burn (PWA) and selective timber harvest (Volz) datasets. The same segmentation parameters were used for both PWA and Volz datasets, after testing the preliminary Doak post-burn survey. 17 spectral detail, 10 spatial detail, and 80 minimum segment size were used. Once each orthomosaic was segmented with these parameters, classification schemas were established for either NDBM treatment and land cover type. For the PWA prescribed burn, a four-class schema was used and included: 1) bare ground, 2) litter, 3) green vegetation, and 4) burned vegetation. For the Volz selective timber harvest, a four-class schema was also used initially, which included: 1) mature canopy, 2) understory vegetation, 3) woody debris, and 4) bare ground. However, after achieving poor outputs with this initial classification schema, particularly with the 'woody debris' class, the schema was adjusted to group 'woody debris' into the 'bare ground' class.

60 samples were collected for each class in the PWA prescribed prairie burn datasets, and in the initial four-class testing phase for Volz selective timber harvest datasets. A supported vector machines (SVM) classification algorithm was used to classify the PWA datasets (Figures 24 – 27 and Tables 25 – 28), using an accuracy assessment of 250 equalized stratified random (ESR) points to produce confusion matrices for resulting classifications (Tables 29 – 32). Within each of the final land cover classifications, a new set of accuracy assessment points were generated, thus providing an objective determination of accuracy for individual maps. Volz was tested with all available algorithms because of the complexity of the image objects. This involved testing SVM, maximum likelihood (ML), random forests (RF), and ISO clusters (ISO) algorithms with 60 samples per class (Figures 28 – 31). The initial outputs of these classifications revealed that SVM and RF performed best with the Volz mid-cut dataset and was classified again with each algorithm, using 80 samples per class (Figures 32 – 33 and Tables 33 – 34).

Then, the accuracy of these output classifications was determined by an accuracy assessment of 100 equalized stratified random points, which showed SVM performed better in both overall accuracy (OA) and individual class accuracy. From there, the 'woody debris' class was combined with the 'bare ground' class, and SVM was used to produce a three-class land cover assessment for the remaining Volz datasets with 80 samples per class (Figures 34 – 37 and Tables

35 – 38). The accuracy of the resulting three-class land covers for Volz were examined with a 250 ESR accuracy assessment to produce confusion matrices for all four datasets surrounding the harvest (Tables 39 – 42). Again, a new set of accuracy assessment points were generated for each of the final land cover classifications.

4.2.1 Resulting Land Cover Classifications Surrounding PWA Prescribed Prairie Burn

The four selected georeferenced orthomosaics surrounding the prescribed prairie burn at PWA were used for producing land cover classifications (Figures 24-27 and Tables 25-28).

Figure 24. PWA pre-burn land cover classification. Burn plots shown in red outline.

Table 25. PWA pre-burn land cover quantification.

Pre Burn - (04/01/20)	Square Meters	Percentage
Bare Ground	888	1.1%
Litter	58,093	70.0%
Green Vegetation	9,275	11.2%
Burned Vegetation*	14,773	17.8%
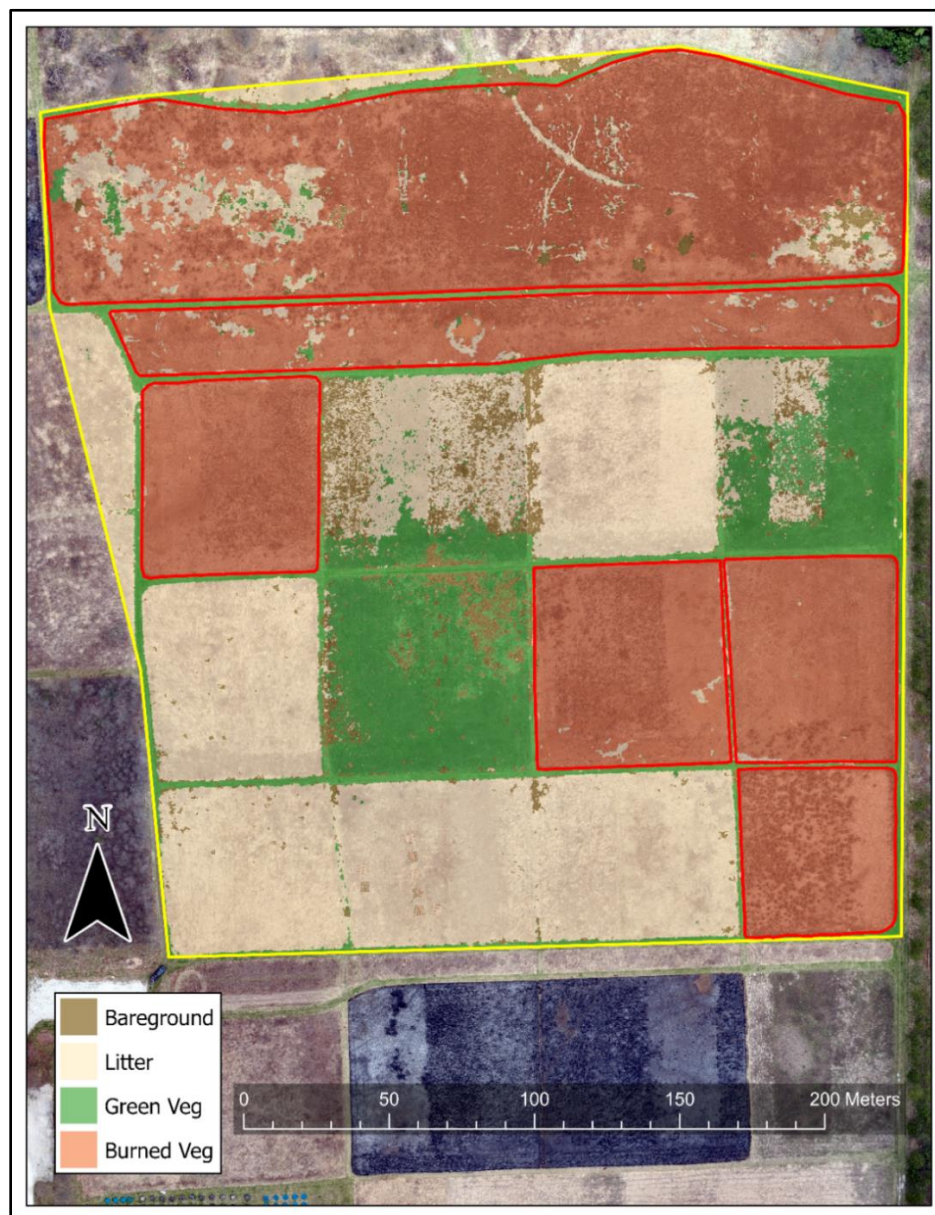
Figure 25. PWA post-burn land cover classification. Burn plots shown in red outline.

Table 26. PWA post-burn land cover quantification.

Post Burn - (04/03/20)	Square Meters	Percentage
Bare Ground	3,947	4.8%
Litter	27,766	33.4%
Green Vegetation	13,563	16.3%
Burned Vegetation	37,751	45.5%

Figure 26. PWA post-burn 2 land cover classification. Burn plots shown in red outline.

Table 27. PWA post-burn 2 land cover quantification.

Post Burn 2 - (04/11/20)	Square Meters	Percentage
Bare Ground	13,278	16.0%
Litter	21,177	25.5%
Green Vegetation	16,775	20.2%
Burned Vegetation	31,801	38.3%
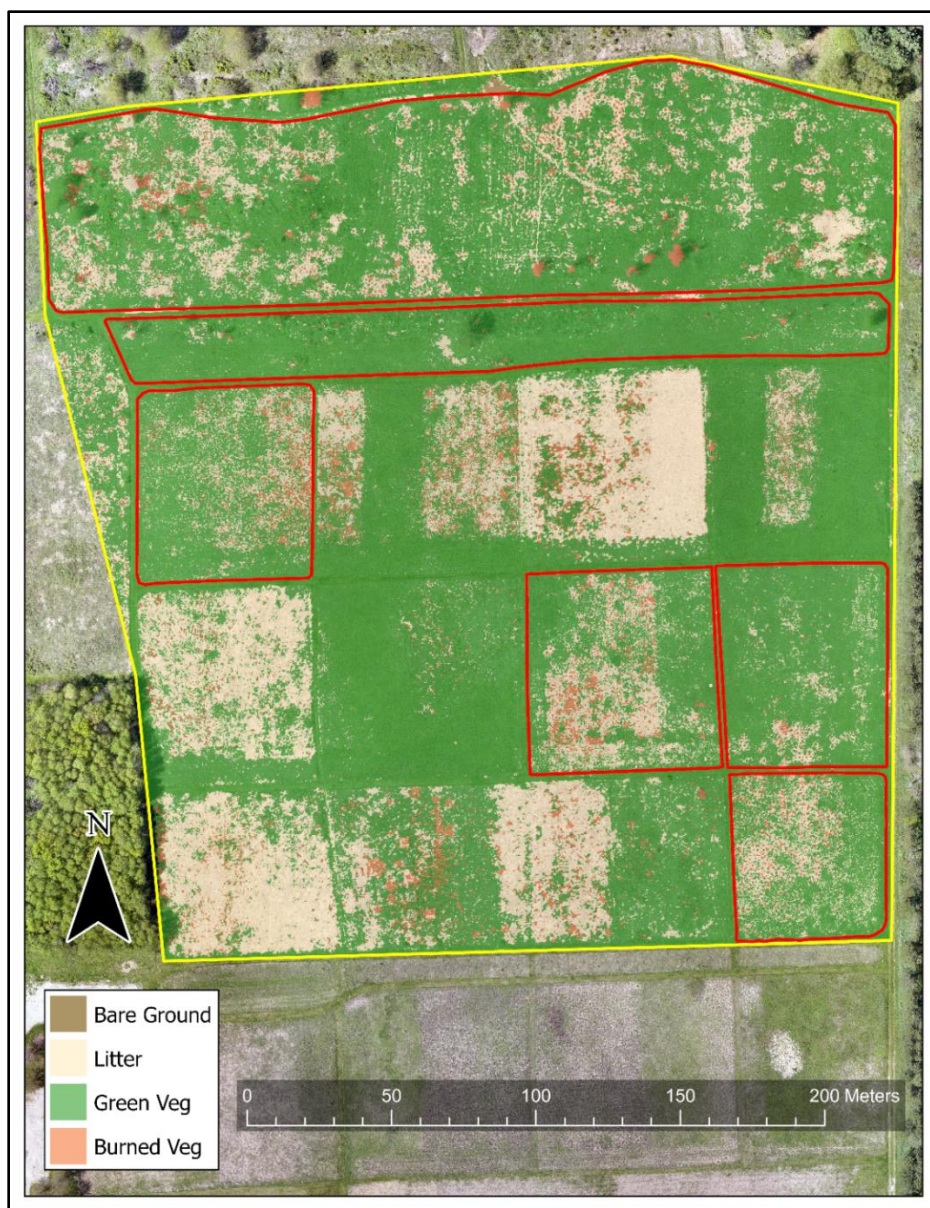
Figure 27. PWA post-burn 3 land cover classification. Burn plots shown in red outline.

Table 28. PWA post-burn 3 land cover quantification.

Post Burn 3 - (05/09/20)	Square Meters	Percentage
Bare Ground	881	1.1%
Litter	19,882	24.0%
Green Vegetation	58,591	70.6%
Burned Vegetation	3,636	4.4%

4.2.1.1 Resulting PWA Prescribed Prairie Burn Confusion Matrices

Each land cover classification surrounding the prescribed burn at PWA were assessed for accuracy with 250 ESR reference points, the results of wich were used to produce confusion matrices (Tables 29-32).

Table 29. PWA pre-burn confusion matrix.

Pre-Burn	Bare Ground	Litter	Green Vegetation	Burned Vegetation	Total	*User's Accuracy*
Bare Ground	**54**	9	0	0	63	85.7%
Litter	0	**63**	0	0	63	100%
Green Veg	0	2	**57**	4	63	90.5%
Burned Veg	1	3	2	**57**	63	90.5%
Total	55	77	59	61	**252**	
Producer's Accuracy	98.2%	81.8%	96.6%	93.4%	**OA=**	**91.7%**

Table 30. PWA post-burn confusion matrix.

Post-Burn	Bare Ground	Litter	Green Vegetation	Burned Vegetation	Total	*User's Accuracy*
Bare Ground	**48**	14	1	0	63	76.2%
Litter	2	**59**	2	0	63	93.7%
Green Veg	8	1	**53**	1	63	84.1%
Burned Veg	0	0	0	**63**	63	100%
Total	58	74	56	64	**252**	
Producer's Accuracy	82.8%	79.7%	94.6%	98.4%	**OA=**	**88.5%**

Table 31. PWA post-burn 2 confusion matrix.

Post-Burn 2	Bare Ground	Litter	Green Vegetation	Burned Vegetation	Total	*User's Accuracy*
Bare Ground	**51**	5	3	4	63	81%
Litter	3	**60**	0	0	63	95.2%
Green Veg	4	3	**55**	1	63	87.3%
Burned Veg	9	7	2	**45**	63	71.4%
Total	67	75	60	50	**252**	
Producer's Accuracy	76.1%	80%	91.7%	90%	**OA=**	**83.7%**

Table 32. PWA post-burn 3 confusion matrix.

Post-Burn 3	Bare Ground	Litter	Green Vegetation	Burned Vegetation	Total	*User's Accuracy*
Bare Ground	**47**	15	1	0	63	74.6%
Litter	4	**58**	1	0	63	92.1%
Green Veg	0	0	**62**	1	63	98.4%
Burned Veg	10	1	1	**51**	63	81%
Total	61	74	65	52	**252**	
Producer's Accuracy	77%	78.4%	95.4%	98.1%	**OA=**	**86.5%**

4.2.2 Volz Selective Timber Harvest Classification Algorithm Testing (Mid-Cut)

The mid-cut Volz dataset was tested with four different OBC algorithms and 60 samples per class to determine which classifier preformed the best land cover classification (Figures 28-31).

Figure 28. Supported Vector Machines (SVM) from 60 samples per class.
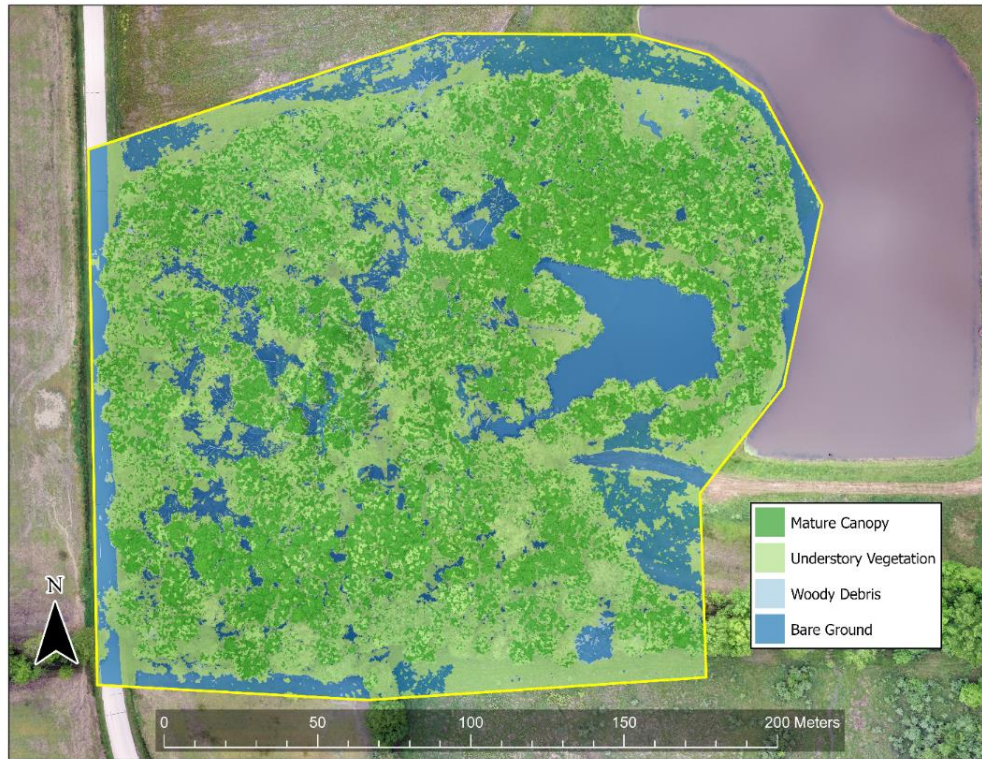
Figure 29. Maximum Likelihood (ML) from 60 samples per class.

Figure 30. Random Forests (RF) from 60 samples per class.
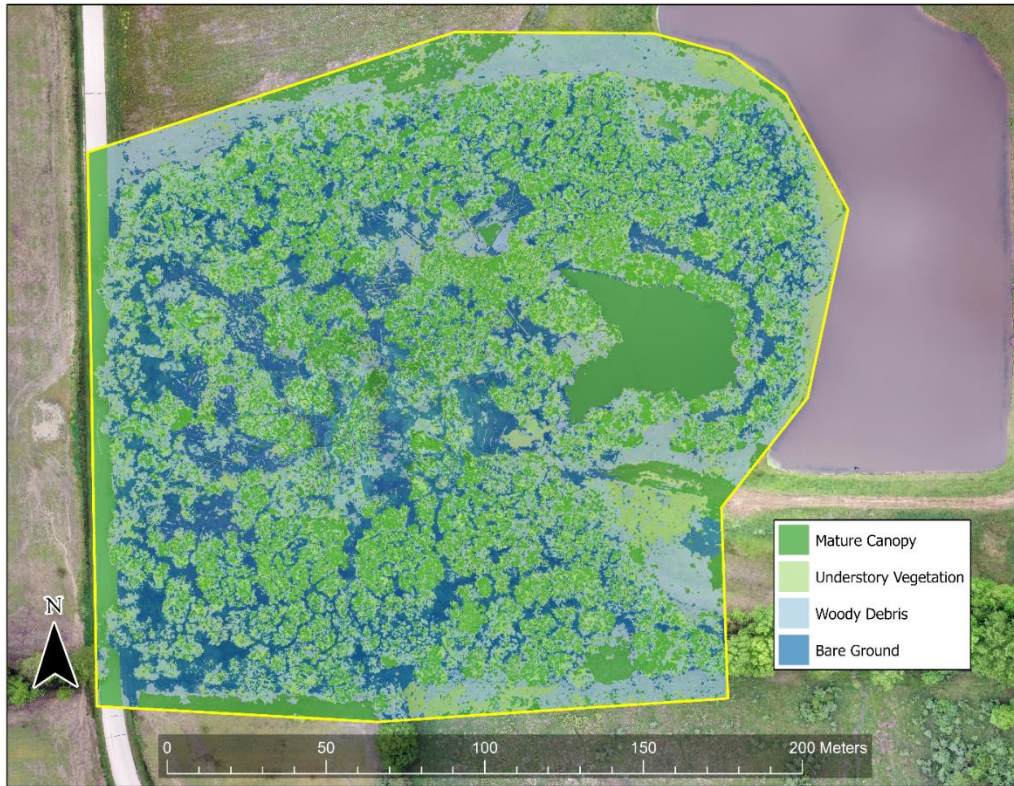
Figure 31. ISO clusters (ISO) from 60 samples per class.

4.2.2.1 Volz with RF and SVM from 80 Samples per Class (Mid-Cut)

RF and SVM produced the best land cover classifications with 60 samples per class, so these OBC algorithms were tested again with 80 samples per class and confusion matrices were produced to objectively determine the performance of each OBC algorithm (Figures 32-33 and Tables 33-34).
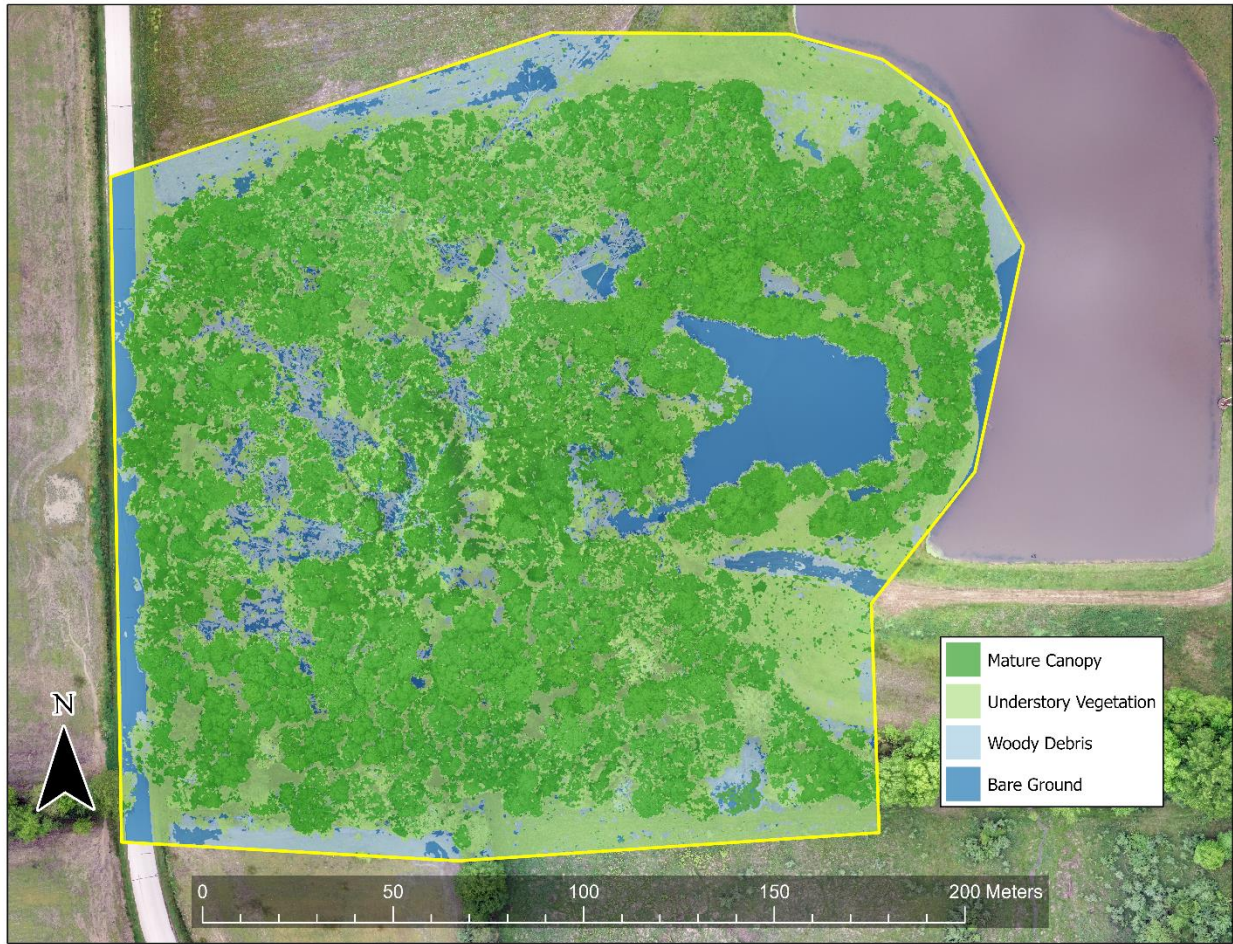
Figure 32. SVM from 80 samples per class.

Table 33. Volz mid-cut confusion matrix for SVM with 80 samples per class.

Volz Mid-Cut (SVM -80)	Mature Canopy	Understory Vegetation	Woody Debris	Bare Ground	Total	User's Accuracy
Canopy	**48**	2	0	0	50	96%
Understory	3	**28**	0	0	31	90.3%
Woody Debris	1	4	**2**	3	10	20%
Bare Ground	0	0	0	**10**	10	100%
Total	52	34	2	13	**101**	
Producer's Accuracy	92.3%	82.4%	100%	76.9%	**OA=**	**87.1%**

Figure 33. RF from 80 samples per class.

Table 34. Volz mid-cut confusion matrix for RF with 80 samples per class.

Volz Mid-Cut (RF - 80)	Mature Canopy	Understory Vegetation	Woody Debris	Bare Ground	Total	User's Accuracy
Canopy	**48**	4	0	0	52	92.3%
Understory	5	**26**	0	1	32	81.3%
Woody Debris	0	2	**2**	6	10	20.0%
Bare Ground	0	0	0	**10**	10	100.0%
Total	53	32	2	17	**104**	
Producer's Accuracy	90.6%	81.3%	100%	58.8%	**OA=**	**82.7%**

101

4.2.3 Resulting Land Cover Classifications Surrounding Volz Selective Timber Harvest

   The four georeferenced orthomosaics surrounding the selective timber harvest at Volz were used for producing three-class land cover maps with SVM and 80 samples per class (Figures 34-37 and Tables 35-38).

Figure 34. Volz pre-cut land cover classification.

Table 35. Volz pre-harvest land cover quantification.

Pre Harvest - (05/07/20)	Square Meters	Percentage
Mature Canopy	18,814.22	42.82%
Understory Vegetation	15,907.28	36%
Bare or Woody Debris	9,216.65	21%
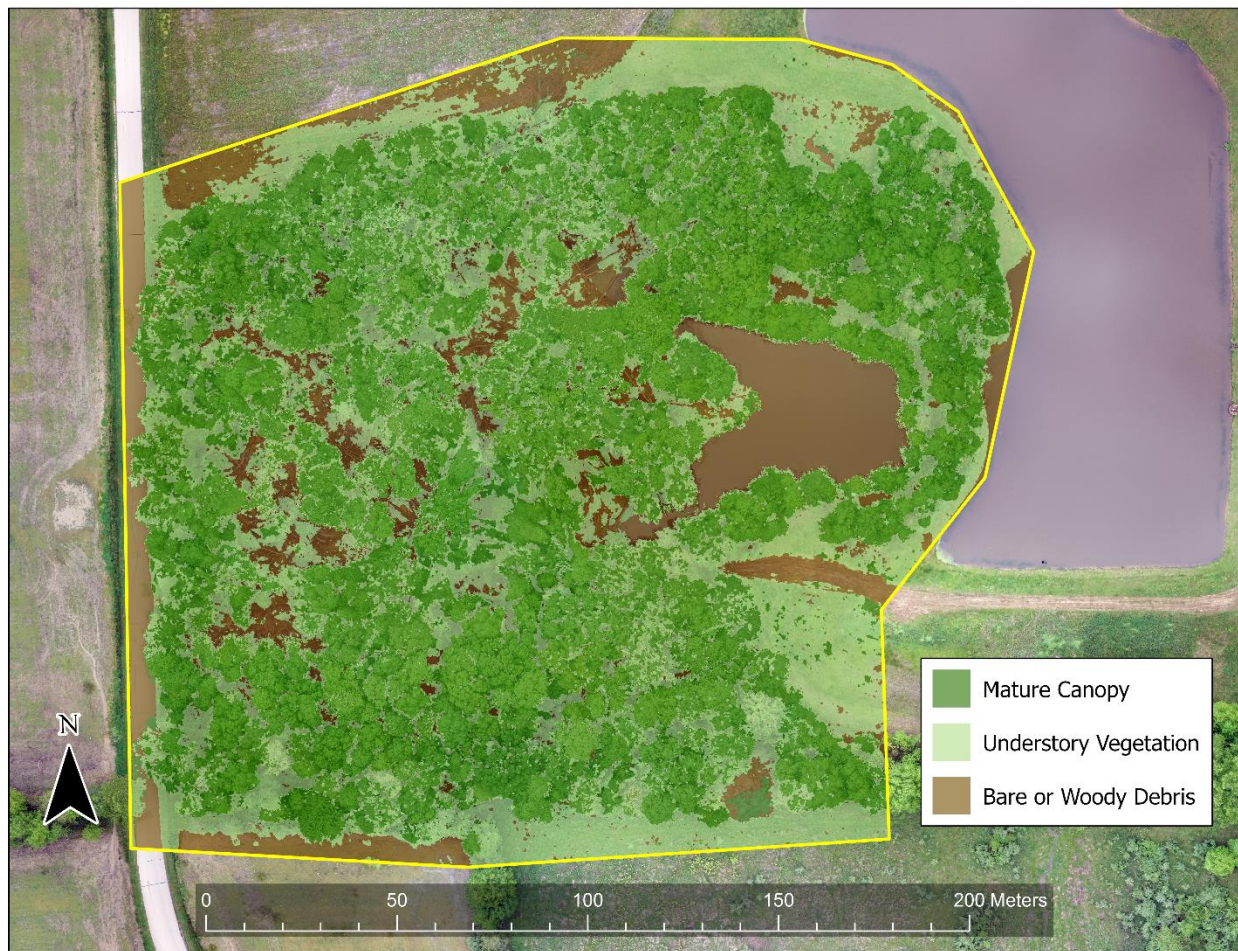
Figure 35. Volz mid-cut land cover classification.

Table 36. Volz mid-harvest land cover quantification.

Mid Harvest - (05/21/20)	Square Meters	Percentage
Mature Canopy	21,940.22	49.88%
Understory Vegetation	15,633.69	35.54%
Bare or Woody Debris	6,411.74	14.58%

Figure 36. Volz post-harvest land cover classification.

Table 37. Volz post-harvest land cover quantification.

Post Harvest - (07/02/20)	Square Meters	Percentage
Mature Canopy	24,072.75	54.77%
Understory Vegetation	12,301.35	28%
Bare or Woody Debris	7,576.53	17.24%

Figure 37. Volz post-harvest 2 land cover classification.

Table 38. Volz post-harvest 2 land cover quantification.

Post Harvest 2 - (08/26/20)	Square Meters	Percentage
Mature Canopy	22,391.45	51%
Understory Vegetation	11,415.43	26%
Bare or Woody Debris	10,135.84	23%

4.2.3.1 Resulting Volz Selective Timber Harvest Confusion Matrices

The four selected georeferenced orthomosaics surrounding the prescribed prairie burn at PWA were used for producing land cover classifications (Figures 24-27 and Tables 25-28).

Table 39. Volz three-class pre-harvest confusion matrix.

Pre-Cut (SVM -80)	Mature Canopy	Understory Vegetation	Bare or Woody Debris	Total	*User's Accuracy*
Canopy	**62**	20	1	83	74.7%
Understory	13	**69**	1	83	83.1%
Bare or Woody Debris	4	4	**75**	83	90.4%
Total	79	93	77	**249**	
Producer's Accuracy	78.5%	74.2%	97.4%	**OA=**	**82.7%**

Table 40. Volz three-class mid-cut confusion matrix.

Mid-Cut (SVM -80)	Mature Canopy	Understory Vegetation	Bare or Woody Debris	Total	*User's Accuracy*
Canopy	**77**	6	0	83	92.8%
Understory	10	**72**	1	83	86.7%
Bare or Woody Debris	0	3	**80**	83	96.4%
Total	87	81	81	**249**	
Producer's Accuracy	88.5%	88.9%	98.8%	**OA=**	**92.0%**

Table 41. Volz three-class post-cut confusion matrix.

Post-Cut (SVM -80)	Mature Canopy	Understory Vegetation	Bare or Woody Debris	Total	*User's Accuracy*
Canopy	**75**	7	1	83	90.4%
Understory	6	**74**	3	83	89.2%
Bare or Woody Debris	0	4	**79**	83	95.2%
Total	81	85	83	**249**	
Producer's Accuracy	92.6%	87.1%	95.2%	**OA=**	**91.6%**

Table 42. Volz three-class post-cut 2 confusion matrix.

Post-Cut 2 (SVM -80)	Mature Canopy	Understory Vegetation	Bare or Woody Debris	Total	*User's Accuracy*
Canopy	**63**	18	2	83	75.9%
Understory	14	**67**	2	83	80.7%
Bare or Woody Debris	2	5	**76**	83	91.6%
Total	79	90	80	**249**	
Producer's Accuracy	79.7%	74.4%	95.0%	**OA=**	**82.7%**

4.3 Objective 3

Objective three was to determine if there was a significant difference between land cover classifications for each type of disturbance.

4.3.1 Significance Testing

A two-tailed t-test assuming equal variances was conducted between the average overall accuracies of each disturbance type in order to determine whether the difference in overall accuracy between disturbance types/vegetation cover was significant at a 95% confidence interval

(0.05) (Table 43). Because the GEOBIA processed used in this study was mostly the same between the two types of disturbances and land covers, the variances were assumed to be equal. Furthermore, by conducting this particular type of t-Test, the objective effectiveness of this method could be tested for the two types of NDBM treatments commonly employed in the CHF region.

Table 43. Two-tailed t-Test Results.

t-Test: Two-Sample Assuming Equal Variances	PWA Burn	Volz Harvest
Mean	0.8728	0.8725
Variance	0.0013	0.0026
Observations	4	4
Pooled Variance	0.0020	
Hypothesized Mean Difference	0	at 0.05 CI
df	6	
t Stat	0.0086	
P(T<=t) two-tail	0.9933	
t Critical two-tail	2.4468	

In order to have a statistically significant difference between the two types of disturbances and land covers, the P-value (0.9933) would need to be less than the confidence interval (0.05). In this case, the P-value is *not* less than the confidence interval, and therefore, there is *not* a statistically significant difference between the overall accuracies of PWA prescribed prairie burn and Volz selective timber harvest land cover classifications. This means that, while PWA did have higher overall and individual class accuracies, they were not significantly better than Volz, so both the collection and classification methods employed in this study were effective for either disturbance and land cover type.

CHAPTER 5 – DISCUSSION & CONCLUSION

This chapter discusses the findings of this study—what was done, what was left out, and what could have been done differently, as well as what can be done in the future.

5.1 Discussion

This section elaborates on the findings of this study and how the results were achieved.

5.1.1 Objective 1 - Part I: Optimal Data Collection Parameters

Before collecting any data, the various parameters affecting quality image collection with UAS were defined by reviewing similar studies within the literature and recalling UAS survey experience prior to engaging in this research study. Unfortunately, as Buters, et al. (2019) points out, each study contained a unique set of parameters for various parts of the collection, processing, or classification steps—thus, standards for this UAS application were non-existent. This led to the iterative testing of atmospheric, sensor, and mission planning parameters, in conjunction with diligent note-taking, to infer how these variables affected the quality of imagery collected by the UAS. Fortunately, a number of suitable prairie burn and timber harvest sites were identified, which allowed for this type of iterative testing without compromising the production of final land cover classifications for either type of disturbance.

The results show that prairie burn sites were less sensitive to atmospheric conditions, such as sun angle, brightness/cloud cover, and wind (Tables 19 and 22). This was likely due to the low height and visual simplicity of the vegetation being imaged. Conversely, timber harvest sites were more sensitive to all three atmospheric conditions, likely due in part to the tall height and visual complexity of mature forest canopies. Therefore, the best resulting images were collected as close to solar noon as possible, with overcast skies and diffuse lighting, and low wind (Table 22 and Figure 20). Furthermore, the sensor settings were mostly the same, with the exception of shutter speed. However, this was mostly dependent on lighting and wind (Tables 19 and 22). Finally, the flight altitude and number of images collected outside the study area differed between the two land covers. Ensuring sufficient distance between the sensor and vegetation was easily done at 121m above ground level (AGL) for prairie sites, but given the height of mature trees at timber harvest

sites (often between 24 – 30 meters), the flight altitude was increased to 121m *above forest canopy* (AFC). Additionally, while prairie burn sites required just 1 image outside the study area to reduce outer image distortion in resulting orthomosaics, timber harvest sites required 2 or more, depending on the adjacent vegetation. This was likely due to the presence of ground within the datasets, where prairies had ample visible ground within and/or surrounding the study area, timber harvest sites only had visible ground present along plot perimeters, if at all.

Overall, quality images were gathered with the respective data collection parameters, despite logistical challenges that prevented ideal data collection scenarios, especially for timber harvest sites.

5.1.2 Objective 1 – Part II: Optimal Data Processing Parameters

After gathering quality images for each site, the next step was to engage in data processing. This involved correcting image coordinates collected by the post-processing kinematic (PPK) sensor during flight, before synchronizing those coordinates with their associated image in a photogrammetric processing software to produce georeferenced orthomosaics. Because all of the datasets fell within the state of Indiana, or just across the border into Michigan or Ohio, the sites fell within the 16th zone of the universal transverse Mercator (UTM) projected coordinate system. This allowed each site to be corrected to the WGS 84 UTM Zone 16 North spatial reference which has an estimated error of just 2cm (GISGeography, 2021d). Fortunately, the world geodetic system (WGS) datum was also what was referenced by the connected satellite networks during data collection with the PPK. This made image coordinate correction both simple and precise for both types of land covers, which was especially important for the 3cm-resolution of images collected in this study (Tables 20 and 23).

At the orthomosaic generation stage, photogrammetric processing parameters diverged slightly. Prairie sites performed well with the default parameters, often achieving image calibration numbers of 99% or better (Table 16). On the other hand, timber harvest sites required more "salvaging" in order to produce quality orthomosaics, particularly when images were collected in the aforementioned adverse conditions (Table 16). Motion blur, overexposure, dark shadows, and/or too few images collected outside the study area proved problematic for orthomosaic generation of timber harvest sites. To "salvage" these datasets, the keypoint image scale (KPIS) was reduced from "1" to "1/2", thus reducing the number of tie points the software would look for

at one time and therefore performing better mosaicking than with the default KPIS (Pix4D, 2021b). Additionally, the calibration method was changed from "standard" to "alternative", for which the back-end procedure is not publicly available. However, this parameter likely reduced the number of images discarded if enough keypoints were not identified, thus increasing the number of images kept in the resulting orthomosaic.

Overall, many high-quality georeferenced orthomosaics were produced for both prescribed prairie burn and selective timber harvest sites, with some datasets requiring more adjustments to do so.

5.1.3 Objective 2: Optimal Data Classification Parameters

Using the high-quality georeferenced orthomosaics generated in the previous step, supervised data classification methods were used to produce a series of land cover classification maps surrounding both PWA prescribed prairie burn and Volz selective timber harvest sites (Figures 24 – 27 and 34 – 37). This was done by adjusting segmentation parameters that affect the spatial, spectral, and size details of output segmented objects. As Kucharczyk, et al. (2020) noted, "determining an optimal segmentation parameter is a heuristic, subjective, challenging, and time-intensive trial-and-error process" (p. 7). Looking at the resulting classifications, it appears that this process might be to blame for not achieving even higher overall and individual classification accuracies. While the "optimal" parameters for the cm-level resolution of images used in this study were assumed to be suitable for all datasets collected with the same sensor, this was decided after testing just one dataset (Doak post-burn). In hindsight, each iteration of segmentations tried should have been classified to determine which parameters led to the best initial classification accuracies before segmenting the rest of the datasets. Furthermore, timber harvest datasets would likely require different parameters, especially for spectral detail and minimum segment size, to better coagulate large tree crowns and distinguish felled timber stem colors from bare ground in canopy gaps.

Before collecting training samples, classification schemas were developed for both land covers, with specific and appropriate classes for each. When monitoring vegetation loss and recovery surrounding prescribed burns, it was important to know the proportions of no vegetation growth (bare ground), fuel (litter), healthy and/or unconsumed vegetation (green vegetation), and vegetation consumed by the fire (burned vegetation) (Miller & Brooke, 2019). By quantifying

111

these areas both *before* and *after* the disturbance, land managers have an objective determination of prescribed burn efficacy as it relates to native ecosystem vitality. For selective timber harvests, it was important to monitor the proportions of no visible growth (bare ground), regenerative growth (understory vegetation), and well-established growth (mature canopy), with woody debris being a function of wildlife habitat and forest structure (Nordén et al., 2019). While in some ways, quantifying the "volume" of these classes would be more desirable for forest managers, measuring the "area" of each land cover still provides a valuable insight into patterns and rate of regeneration as it relates to harvest techniques (Boardman, 2020; Goodbody et al., 2018; Husson et al., 2016; Knoth et al., 2013; Lister et al., 2020; Ruwaimana et al., 2018). Because the high-resolution of images used in this study were able to capture felled timber stems, woody debris was included in the initial classification schema for timber harvest sites. However, the space consumed by this type of land cover was too minimal to successfully classify, and caused omission and commission errors in resulting classifications. Therefore, this class was combined with "bare ground" in final land cover classifications for Volz.

Next, sample polygons were collected for each segmented image in order to train the machine-learning classification algorithm. Provided that the recommended sample size was equal across all classes with ≥50 per class (Kucharczyk et al., 2020), 60 samples were used for PWA and initial Volz classifications. While this worked well for PWA datasets, Volz required 80 samples per class to produce quality land cover classifications. This was likely due to the similar spectral profiles of mature canopy and understory vegetation, combined with less-than-optimal segmentation parameters for the given land cover. Furthermore, distinguishing between understory vegetation and mature canopy proved difficult from visual interpretation alone. As a result, each Volz classification displayed instances of a ring around some tree crowns that was misclassified as understory vegetation. Layering a 3D digital surface model (DSM), which was a generated output from photogrammetric processing anyway, could help differentiate the understory from canopy through height filtering (Gibril et al., 2020; Larrinaga & Brotons, 2019; Lehmann et al., 2017).

Despite the number of samples collected, the machine-learning algorithm that performed the best, and therefore was selected for final land cover classifications in this study, was supported vector machines (SVM). Although, when tested on the Volz four-class mid-cut dataset, random forests (RF) produced similar accuracies to SVM, but was slightly less successful in both overall

and individual class accuracies, and was less user-friendly, which aligned with findings of similar studies (Belgiu & Drăguţ, 2016; Boardman, 2020; Ghosh & Joshi, 2014; Gibril et al., 2020; Liu et al., 2018).

Finally, the results of the two-tailed t-Test assuming equal variances revealed no significant difference in resulting classification accuracies between the PWA burn and Volz harvest sites, thus, the data procurement and processing parameters applied were effective.

5.2 Conclusion

Quantifying planned disturbance is an important component of any ecosystem management plan that allows land managers to objectively determine the efficacy of their treatment and adjust the frequency and severity of NDBM treatments accordingly. To do this, inventories of land cover must be collected both *before* and repeatedly *after* the disturbance event. This way, vegetation recovery can be determined by knowing what land covers were present *before* the disturbance event, what was removed as a result of the disturbance treatment, and what grew back *after* the disturbance.

Traditionally, obtaining a pre-disturbance inventory has been challenging to do because disturbances have mainly been viewed as *un*planned events where the start time could not have been anticipated and therefore temporally precise image datasets would be unavailable. Additionally, traditional remote sensing methods, such as satellite, has a fixed return-rate that limits the temporal precision of pre-disturbance inventories, and commercially-available spatial resolutions are legally limited to 30cm that can be expensive to obtain.

Furthermore, manned aircraft surveys can be logistically challenging to conduct for remote areas, and/or too expensive to be worthwhile. With *planned* disturbances, which are typically conducted in discrete (10-60 acres) areas, especially within the CHF region, the start time of the event is known, and therefore, this presents an opportunity to obtain a pre-disturbance inventory.

UAS imagery presents an efficient and precise solution to obtaining both *pre*-disturbance *and* repeated *post*-disturbance inventories, but until now, has not been used much for this purpose. With PPK georeferencing, that both triggers the camera and collects coordinate information for each image, precise UAS image surveys are more efficient than ever before. Using a standard RGB digital camera that was connected to the PPK and attached to the UAS, a GSD of <3cm can be achieved with positional orientations of similar accuracies. With unmatched spatial and temporal

resolutions, land cover classifications at the centimeter-level surrounding planned disturbances can be produced through GEOBIA methods in a GIS.

Land cover surveys were conducted surrounding two different types of *planned* disturbances and land covers that are common within the CHF region—namely prescribed prairie burns and selective timber harvests. Four classified maps were produced for each disturbance type to objectively determine the change in land cover from *before* and *after* a prescribed burn and timber harvest treatment.

It was determined that prairie burn sites were less sensitive to atmospheric, sensor, and mission planning parameters than forested sites during data collection. However, forested sites were still able to be successfully surveyed with the UAS after increasing the flight altitude, the shutter speed, and the number of images collected outside the study area. This was likely due to the height and visual complexity of the vegetation present at the forested sites, causing more issues with motion blur and overexposure. Additionally, the prairie burn site was successfully processed with default photogrammetric parameters in Pix4D, while the forest site required reducing the scale of keypoint identification and an alternative calibration method to produce quality georeferenced orthomosaics. Again, this was likely a result of the visual complexity of the tree canopies in the imagery, making keypoint matching difficult for the software. Lastly, both land covers achieved similar overall accuracies (87.27% for prescribed prairie burn and 87.25% for selective timber harvest), the variance for each type differed slightly, with the prairie site outperforming the forested site. This difference was probably caused by improper training sample collection in the timber harvest site, where understory vegetation and mature canopy was more difficult to distinguish than land covers present in prairie burn sites. Overall, the methods of data collection, processing, and classification produced high-quality land cover assessments surrounding *planned* ecological disturbances within the CHF region.

In future studies, researchers should compound on this study by examining optimal temporal resolutions for post-disturbance inventories, verifying land covers through field sampling, using field samples to train classifier algorithms, and experimenting with different segmentation parameters. Although the temporal resolution of post-disturbance inventories was not a main focus in this study, determining the optimal frequency and duration of surveys following a planned disturbance treatment would enhance the usability of this method. Due to COVID protocols, ground-truthing through field sample collection was not conducted in this study. However, doing

so would have been helpful in determining the accuracy of resulting land cover classifications as well as projecting those field samples onto the imagery during classifier training sample collection. Furthermore, while the segmentation parameters used in this study worked well for the prairie burn datasets, the minimum segment size was too small relative to the size of tree crowns, which likely contributed to the ability of the classifier algorithm to distinguish between mature canopies and seedlings in the understory, as well as bare ground and coarse woody debris. By experimenting with minimum segment sizes for forested sites further, optimal segmentation parameters for ultra-high-resolution UAS imagery GEOBIA can be determined.

While these methods were effective for quantifying land cover change as a result of NDBM treatments, a plethora of other applications could benefit from this workflow. For example, land cover remediation following construction, mining, or landscaping projects could employ a similar workflow to objectively determine vegetation recovery. Other application examples include, but are not limited to: invasive species identification; preventative wildfire management; federal and private land use; pesticide and herbicide use in agriculture; water level monitoring (lakes, coastal, dams, etc.); excavation or landslide analysis; wildlife habitat development; and energy sector projects (solar, wind, conventional, etc.)—all of which present opportunities to examine *before* and *after* effects of *planned* disturbances.

Although the solutions provided in this study require further development, they do progress the use of UAS and GIS technology in environmental applications by presenting a strong potential for land managers to efficiently and objectively determine the efficacy of their actions. This will undoubtedly enhance the sustainable management of Earth's precious and finite natural resources.

APPENDIX A. SUPPLEMENTAL RESOURCES

Zach Miller's Professional Portfolio

Here you will find my personal website which acts as my professional portfolio and contains links to all of the resources below, as well as all pertinent undergraduate and graduate coursework, a research blog, and contact information.

Quick Reference Guide for DJI Matrice 600 Pro

View the quick reference guide my colleagues and I developed during my time at Purdue University. This QRF covers a lot of basic information for safely and efficiently using an M600 Pro for data collection.

Operators Checklist for DJI Matrice 600 Pro with PPK-Triggered Sony A6000

Click to view the Pilot-in-Command (PIC) checklist I developed with Kaleb Gould and William Weldon for operating the M600 Pro with GeoSnap PPK and Sony A6000 camera.

PPK Processing with EZSurv Workflow Document

Click to view the workflow I developed for using EZSurv to correct image geotags collected with a PPK-triggered UAS.

PPK Processing with EZSurv Workflow Video

Click to view my video which walks through the EZSurv workflow.

Photogrammetric Processing for PPK-Derived UAS Imagery with Pix4D Document

Click to view the workflow I developed for using Pix4D to produce quality georeferenced orthomosaic datasets from PPK-derived UAS imagery.

Photogrammetric Processing for PPK-Derived UAS Imagery with Pix4D Video

Click to view my video which walks through the Pix4D workflow.

Land Cover Classification Workflow Blog Post

Click to view my blog post on using SVM object-based classification to produce land cover maps.

REFERENCES

Accuracy Metrics. (2019). Retrieved on 12/8/2021:
http://gsp.humboldt.edu/olm_2019/courses/GSP_216_Online/lesson6-2/metrics.html

Al-Ali, Z. M., Abdullah, M. M., Asadalla, N. B., & Gholoum, M. (2020). A comparative study of remote sensing classification methods for monitoring and assessing desert vegetation using a UAV-based multispectral sensor. *Environmental Monitoring and Assessment*, *192*(6). http://dx.doi.org/10.1007/s10661-020-08330-1

Alberdi, I. (2021). Forest resources assessments: Mensuration, inventory and planning. *Forests*, *12*(3). https://doi.org/10.3390/f12030296

Alvarez-Taboada, F., Paredes, C., & Julian-Pelaz, J. (2017). Mapping of the invasive species *hakea sericea* using unmanned aerial vehicle (UAV) and WorldView 2 imagery and an object-oriented approach. *Remote Sensing*, *9*(9), 913. http://dx.doi.org/10.3390/rs9090913

Anderson, C. L. (2019). *Examining aspen expansion from before and after prescribed burning in a native fescue grassland through geospatial techniques* (Publication Number 13900181) [M.S., Michigan Technological University]. ProQuest Dissertations & Theses Global; Publicly Available Content Database. Ann Arbor. Retrieved on 12/8/2021: https://www.proquest.com/openview/c8586ad8a357d54a7de6b721b3444b4b/1?pq-origsite=gscholar&cbl=18750&diss=y

Anderson, J. R. (1976). *A land use and land cover classification system for use with remote sensor data* (Vol. 964). US Government Printing Office. Retrieved on 12/8/2021: https://pubs.usgs.gov/pp/0964/report.pdf

Anderson, K., & Gaston, K. J. (2013). Lightweight unmanned aerial vehicles will revolutionize spatial ecology. *Frontiers in Ecology and the Environment*, *11*(3), 138-146. https://doi.org/10.1890/120150

Aplet, G. H. (2006). Evolution of wilderness fire policy. *International Journal of Wilderness*, *12*(1), 9-13. Retrieved on 12/8/2021: https://www.researchgate.net/publication/237127088_Evolution_of_Wilderness_Fire_Policy

Asenova, M. (2018). GIS-based analysis of the tree health problems using UAV images and satellite data. *Surveying Geology & Mining Ecology Management (SGEM)*, *18*, 813-820. http://dx.doi.org/10.5593/sgem2018/3.2/S14.104

Bagaram, M. B., Giuliarelli, D., Chirici, G., Giannetti, F., & Barbati, A. (2018). UAV remote sensing for biodiversity monitoring: Are forest canopy gaps good covariates? *Remote Sensing*, *10*(9). http://dx.doi.org/10.3390/rs10091397

117

Bakuła, M., Oszczak, S., & Renata, P.-M. (2009). Performance of RTK positioning in forest conditions: Case study. *Journal of Surveying Engineering*, *135*, 125-130. https://doi.org/10.1061/(ASCE)0733-9453(2009)135:3(125)

Beheler, B. (2020). Martell forest manager's silvicultural goals for prescribed burn in oak plantation. In (Prescribed burns (Spring, 2020) in southeastern oak plot at Martell Forest (West Lafayette, IN) were conducted for purposes of oak regeneration, invasive species (autumn olive, bush honeysuckle, and Eastern burning bush) mitigation, and wildlife habitat (from course woody debris). *Personal Communication.*

Belgiu, M., & Drăguţ, L. (2016). Random forest in remote sensing: A review of applications and future directions. *ISPRS Journal of Photogrammetry and Remote Sensing*, *114*, 24-31. https://doi.org/10.1016/j.isprsjprs.2016.01.011

Berie, H. T., & Burud, I. (2018). Application of unmanned aerial vehicles in earth resources monitoring: Focus on evaluating potentials for forest monitoring in ethiopia. *European Journal of Remote Sensing*, *51*(1), 326-335. https://doi.org/10.1080/22797254.2018.1432993

Boardman, A. L. (2020). *Next generation of land system science: Integrating meso-scale analysis and UAS remote sensing in changing plant communities of the United States' Southern Great Plains.* [Masters thesis, Oklahoma State University]. Stillwater, OK, USA. Retrieved on 12/8/2021: https://hdl.handle.net/11244/325470

Boon, M. A., Drijfhout, A. P., & Tesfamichael, S. (2017). Comparison of a fixed-wing and multi-rotor UAV for environmental mapping applications: A case study. *The International Archives of Photogrammetry, Remote Sensing and Spatial Information Sciences*, *42*, 47. https://doi.org/10.5194/isprs-archives-XLII-2-W6-47-2017

Brooke, J. (2021). PWA Seed Mixtures. *Personal Communication.*

Brown, M. L., Canham, C. D., Murphy, L., & Donovan, T. M. (2018). Timber harvest as the predominant disturbance regime in northeastern U.S. forests: Effects of harvest intensification. *Ecosphere*, *9*(3). https://doi.org/10.1002/ecs2.2062

Buters, T. M., Bateman, P. W., Robinson, T., Belton, D., Dixon, K. W., & Cross, A. T. (2019). Methodological ambiguity and inconsistency constrain unmanned aerial vehicles as a silver bullet for monitoring ecological restoration. *Remote Sensing*, *11*(10). http://dx.doi.org/10.3390/rs11101180

CORS. (2021). National Geodetic Survey - The NOAA CORS Network (NCN). Retrieved on 12/8/2021: https://geodesy.noaa.gov/CORS/index.shtml

Cromwell, C., Giampaolo, J., Hupy, J., Miller, Z., & Chandrasekaran, A. (2021). A systematic review of best practices for UAS data collection in forestry-related applications. *Forests*, *12*(7). https://doi.org/10.3390/f12070957

CRS. (2020). *Wildfire Statistics*. Congressional Research Service. Retrieved on 12/8/2021: https://crsreports.congress.gov/product/pdf/IF/IF10244/45

CRS. (2021). *Wildfire Statistics*. Congressional Reseach Service. Retrieved on 12/8/2021: https://crsreports.congress.gov/product/pdf/IF/IF10244/56

Dainelli, R., Toscano, P., Di Gennaro, S. F., & Matese, A. (2021). Recent advances in unmanned aerial vehicles forest remote sensing—A systematic review. Part II: Research applications. *Forests*, *12*(4). https://doi.org/10.3390/f12040397

Dandois, J. P., Olano, M., & Ellis, E. C. (2015). Optimal altitude, overlap, and weather conditions for computer vision UAV estimates of forest structure. *Remote Sensing*, *7*(10). https://doi.org/10.3390/rs71013895

DJI. (2018). Zenmuse XT2 User Manual. Retrieved on 12/8/2021: https://dl.djicdn.com/downloads/Zenmuse%20XT%202/Zenmuse%20XT%202%20User%20Manual%20v1.0.pdf

DJI. (2021). *Matrice 600 Pro: Product Information: Specs*. Retrieved on 12/8/2021: https://www.dji.com/matrice600-pro/info#specs

Domadia, S. G., & Zaveri, T. (2011). *Comparative analysis of unsupervised and supervised image classification techniques*. Proceedings from the National Conference on Recent Trends in Engineering & Technology, Nagar, Gujarat, India. Retrieved on 12/8/2021: https://www.bvmengineering.ac.in/misc/docs/published-20papers/etel/etel/401043.pdf

Díaz-Varela, R. A., De la Rosa, R., León, L., & Zarco-Tejada, P. J. (2015). High-resolution airborne UAV imagery to assess olive tree crown parameters using 3D photo reconstruction: Application in breeding trials. *Remote Sensing*, *7*(4), 4213-4232. https://doi.org/10.3390/rs70404213

ESRI. (2021). *Segmentation - ArcGIS Pro: Documentation*. Retrieved on 12/8/2021: https://pro.arcgis.com/en/pro-app/2.7/help/analysis/image-analyst/segmentation.htm

Evans, T. P., Green, G. M., & Carlson, L. A. (2001). Multi-scale analysis of landcover composition and landscape management of public and private lands in Indiana. *GIS and Remote Sensing Applications in Biogeography and Ecology, 626*, 271-287. https://doi.org/10.1007/978-1-4615-1523-4_16

FAA. (2021). *14 CFR - Part 107: Small Unmanned Aerial Systems*. Retrieved on 12/8/2021: https://www.ecfr.gov/current/title-14/chapter-I/subchapter-F/part-107

Fernandes, P. M., & Botelho, H. S. (2003). A review of prescribed burning effectiveness in fire hazard reduction. *International Journal of Wildland Fire*, *12*(2), 117-128. Retrieved on 12/8/2021: https://www.fs.fed.us/rm/pubs/rmrs_gtr292/2003_fernandes.pdf

Fernández-Guisuraga, J. M., Sanz-Ablanedo, E., Suárez-Seoane, S., & Calvo, L. (2018). Using unmanned aerial vehicles in postfire vegetation survey campaigns through large and heterogeneous areas: Opportunities and challenges. *Sensors*, *18*(2), 586. http://dx.doi.org/10.3390/s18020586

Field of View, LLC. (2019). *Processing GeoSnap PPK files using EZSurv*. YouTube. Retrieved on 12/8/2021: https://www.youtube.com/watch?v=7pYrxagCOVo&t=0s

Field of View, LLC. (2021). *GeoSnap PPK - Product Sheet*. Retrieved on 12/8/2021: https://static1.squarespace.com/static/5d0d06f497c0e80001c6ca18/t/5ebdab9213269e6b5b3a3fd9/1589488532053/GeoSnap_PPK_Product_Sheet_rev12_web.pdf

Forest Inventory and Analysis Strategic Plan, USDA Forest Service. (2016). Retrieved on 12/8/2021: https://www.fia.fs.fed.us/library/bus-org-documents/docs/strategic-plan-docs/FIA%20Strategic%20Plan%20FS-1079.pdf

Fralish, J. S. (2003). *The Central Hardwood Forest: Its Boundaries and Physiographic Provinces*. Retrieved on 12/8/2021: https://www.nrs.fs.fed.us/pubs/ch/ch13/CHvolume13page001.pdf

Fraser, B. T., & Congalton, R. G. (2018). Issues in Unmanned Aerial Systems (UAS) data collection of complex forest environments. *Remote Sensing*, *10*(6), 908. https://doi.org/10.3390/rs10060908

Fraser, B. T., & Congalton, R. G. (2019). Evaluating the effectiveness of Unmanned Aerial Systems (UAS) for collecting thematic map accuracy assessment reference data in New England forests. *Forests*, *10*(1), 24. https://doi.org/10.3390/f10010024

Frayer, W. E., & Furnival, G. M. (1999). History of forest survey sampling designs in the United States. *Journal of Forestry*, *97*(12), 4-10. Retrieved on 12/8/2021: https://www.nrs.fs.fed.us/pubs/gtr/gtr_nc212/gtr_nc212_042.pdf

Frey, J., Kovach, K., Stemmler, S., & Koch, B. (2018). UAV photogrammetry of forests as a vulnerable process: A sensitivity analysis for a structure from motion RGB-image pipeline. *Remote Sensing*, *10*(6). https://doi.org/10.3390/rs10060912

Garcia Millan, V. E., Rankine, C., & Sanchez-Azofeifa, G. A. (2020). Crop loss evaluation using digital surface models from unmanned aerial vehicles data. *Remote Sensing*, *12*(6), 981. http://dx.doi.org/10.3390/rs12060981

Getzin, S., Nuske, R. S., & Wiegand, K. (2014). Using unmanned aerial vehicles (UAV) to quantify spatial gap patterns in forests. *Remote Sensing*, *6*(8). https://doi.org/10.3390/rs6086988

Getzin, S., Wiegand, K., & Schöning, I. (2012). Assessing biodiversity in forests using very high-resolution images and unmanned aerial vehicles. *Methods in Ecology and Evolution*, *3*(2), 397-404. https://doi.org/10.1111/j.2041-210X.2011.00158.x

Ghosh, A., & Joshi, P. K. (2014). A comparison of selected classification algorithms for mapping bamboo patches in lower Gangetic plains using very high resolution WorldView 2 imagery. *International Journal of Applied Earth Observation and Geoinformation*, *26*, 298-311. https://doi.org/10.1016/j.jag.2013.08.011

Gibril, M. B. A., Kalantar, B., Al-Ruzouq, R., Ueda, N., Saeidi, V., Shanableh, A., . . . Shafri, H. Z. M. (2020). Mapping heterogeneous urban landscapes from the fusion of digital surface model and unmanned aerial vehicle-based images using adaptive multiscale image segmentation and classification. *Remote Sensing*, *12*(7), 1081. https://doi.org/10.3390/rs12071081

GISGeography. (2021a). *How Universal Transverse Mercator (UTM) Works*. Retrieved on 12/8/2021: https://gisgeography.com/utm-universal-transverse-mercator-projection/

GISGeography. (2021b). *What is Geographic Information Systems (GIS)?* Retrieved on 12/8/2021: https://gisgeography.com/what-gis-geographic-information-systems/

GISGeography. (2021c). *What is georeferencing? How to georeference anything*. Retrieved on 12/8/2021: https://gisgeography.com/georeferencing/

GISGeography. (2021d). *World Geodetic System (WGS84)*. Retrieved on 12/8/2021: https://gisgeography.com/wgs84-world-geodetic-system/

Goodbody, T. R. H., Coops, N. C., Hermosilla, T., Tompalski, P., & Crawford, P. (2018). Assessing the status of forest regeneration using digital aerial photogrammetry and unmanned aerial systems. *International Journal of Remote Sensing*, *39*(15-16), 5246-5264. https://doi.org/10.1080/01431161.2017.1402387

GPS.gov. (2021a). *Other Global Navigation Satellite Systems (GNSS)*. Retrieved on 12/8/2021: https://www.gps.gov/systems/gnss/

GPS.gov. (2021b). *The Global Positioning System (What is GPS?)*. Retrieved on 12/8/2021: https://www.gps.gov/systems/gps/

Grimm, O. (2017). Volz Management Plan. *Personal Communication*.

Guerra-Hernández, J., González-Ferreiro, E., Monleón, V., Faias, S., Tomé, M., & Díaz-Varela, R. (2017). Use of multi-temporal UAV-derived imagery for estimating individual tree growth in *pinus pinea* stands. *Forests*, *8*(8), 300. https://doi.org/10.3390/f8080300

Guimarães, N., Pádua, L., Marques, P., Silva, N., Peres, E., & Sousa, J. J. (2020). Forestry remote sensing from unmanned aerial vehicles: A review focusing on the data, processing and potentialities. *Remote Sensing*, *12*(6), 1046. http://dx.doi.org/10.3390/rs12061046

Halpern, C. B., Halaj, J., Evans, S. A., & Dovčiak, M. (2012). Level and pattern of overstory retention interact to shape long-term responses of understories to timber harvest. *Ecological Applications*, *22*(8), 2049-2064. https://doi.org/10.1890/12-0299.1

Harwin, S., & Lucieer, A. (2012). Assessing the accuracy of georeferenced point clouds produced via multi-view stereopsis from unmanned aerial vehicle (UAV) imagery. *Remote Sensing*, *4*(6), 1573-1599. https://doi.org/10.3390/rs4061573

Hassler, S. C., & Baysal-Gurel, F. (2019). Unmanned aircraft system (UAS) technology and applications in agriculture. *Agronomy*, *9*(10), 618. https://doi.org/10.3390/agronomy9100618

Hesseln, H. (2000). The economics of prescribed burning: A research review. *Forest Science*, *46*, 322-334. https://doi.org/10.3390/agronomy9100618

Hobbs, R. J., Arico, S., Aronson, J., Baron, J. S., Bridgewater, P., Cramer, V. A., Epstein, P. R., Ewel, J. J., Klink, C. A., Lugo, A. E., Norton, D., Ojima, D., Richardson, D. M., Sanderson, E. W., Valladares, F., Vilà, M., Zamora, R., & Zobel, M. (2006). Novel ecosystems: Theoretical and management aspects of the new ecological world order. *Global Ecology and Biogeography*, *15*(1), 1-7. http://www.jstor.org/stable/3697651

Hoff, V., Queen, L., Seielstad, C., Moran, C., Wallace, T., Cunningham, M., & Jimenez, D. (2017). *Using Unmanned Aerial Systems for Monitoring Prescribed Fire*. Proceedings of the 7th International Fire Ecology and Management Congress, Orlando, FL, USA. Retrieved on 12/8/2021: https://static1.squarespace.com/static/5ea4a2778a22135afc733499/t/5eba1db10c8cd57a5366c9de/1589255602639/Research+Highlight_Hoff.pdf

HTIRC. (2017). *HTIRC Strategic Plan: 2017-2021*. Hardwood Tree Improvement and Regeneration Center. Retrieved on 12/8/2021: https://htirc.org//wp-content/uploads/2018/08/HTIRC-Strategic-Plan-2017-2021.pdf

Hubbard, S., Pak, A., Gu, Y., & Jin, Y. (2017). UAS to support airport safety and operations: Opportunities and challenges. *Journal of Unmanned Vehicle Systems*, *6*(1), 1-17. Retrieved on 12/8/2021: https://cdnsciencepub.com/doi/10.1139/juvs-2016-0020

Hupy, J. P., & Kroening, A. (2018). *Determining Ideal Parameters in Object Based Classification for Multiband UAS Imagery*. Proceedings from the University of Wisconsin – Madison: Student Research Day, Madison, WI, USA. Retrieved on 12/8/2021: https://minds.wisconsin.edu/handle/1793/78940

Husson, E., Ecke, F., & Reese, H. (2016). Comparison of manual mapping and automated object-based image analysis of non-submerged aquatic vegetation from very-high-resolution UAS images. *Remote Sensing*, *8*(9), 724. https://doi.org/10.3390/rs8090724

ICAO. (2011). *Unmanned Aerial Systems (UAS)*. International Civil Aviation Organization. Retrieved on 12/8/2021: https://www.icao.int/meetings/uas/documents/circular%20328_en.pdf

Jurjević, L., Gašparović, M., Milas, A. S., & Balenović, I. (2020). Impact of UAS image orientation on accuracy of forest inventory attributes. *Remote Sensing*, *12*(3). https://doi.org/10.3390/rs12030404

King, D. J. (2000). Airborne remote sensing in forestry: Sensors, analysis and applications. *The Forestry Chronicle*, *76*(6), 859-876. https://doi.org/10.5558/tfc76859-6

Knoth, C., Klein, B., Prinz, T., & Kleinebecker, T. (2013). Unmanned aerial vehicles as innovative remote sensing platforms for high-resolution infrared imagery to support restoration monitoring in cut-over bogs. *Applied Vegetation Science*, *16*(3), 509-517. https://doi.org/10.1111/avsc.12024

Kucharczyk, M., Hay, G. J., Ghaffarian, S., & Hugenholtz, C. H. (2020). Geographic object-based image analysis: A primer and future directions. *Remote Sensing*, *12*(12), 2012. http://dx.doi.org/10.3390/rs12122012

Kuppinger, D. M., Jenkins, M. A., & White, P. S. (2010). Predicting the post-fire establishment and persistence of an invasive tree species across a complex landscape. *Biological Invasions*, *12*(10), 3473-3484. http://doi.org/10.1007/s10530-010-9745-4

LaGro Jr, J. A. (2005). Land-use classification. 321-328.

Larrinaga, A. R., & Brotons, L. (2019). Greenness Indices from a Low-Cost UAV Imagery as Tools for Monitoring Post-Fire Forest Recovery. *Drones*, *3*(1), 6. https://doi.org/10.3390/drones3010006

Latifi, H., Schumann, B., Kautz, M., & Dech, S. (2014). Spatial characterization of bark beetle infestations by a multidate synergy of SPOT and Landsat imagery. *Environmental Monitoring and Assessment*, *186*(1), 441-456. http://dx.doi.org/10.1007/s10661-013-3389-7

Lehmann, J. R. K., Prinz, T., Ziller, S. R., Thiele, J., Heringer, G., Meira-Neto, J. A. A., & Buttschardt, T. K. (2017). Open-source processing and analysis of aerial imagery acquired with a low-cost unmanned aerial system to support invasive plant management. *Frontiers in Environmental Science*, *5*, 44. https://doi.org/10.3389/fenvs.2017.00044

Li, C., & Shao, G. (2012). Object-oriented classification of land use/cover using digital aerial orthophotography. *International Journal of Remote Sensing*, *33*(4), 922-938. https://doi.org/10.1080/01431161.2010.536183

Li, H., Chen, L., Wang, Z., & Yu, Z. (2019). Mapping of river terraces with low-cost UAS based structure-from-motion photogrammetry in a complex terrain setting. *Remote Sensing*, *11*(4), 464. https://doi.org/10.3390/rs11040464

Lister, A. J., Andersen, H., Frescino, T., Gatziolis, D., Healey, S., Heath, L. S., . . . Wilson, B. T. (2020). Use of Remote Sensing Data to Improve the Efficiency of National Forest Inventories: A Case Study from the United States National Forest Inventory. *Forests*, *11*(12). https://doi.org/10.3390/f11121364

Liu, T., Abd-Elrahman, A., Morton, J., & Wilhelm, V. L. (2018). Comparing fully convolutional networks, random forest, support vector machine, and patch-based deep convolutional neural networks for object-based wetland mapping using images from small unmanned aircraft system. *GIScience & Remote Sensing*, *55*(2), 243-264. https://doi.org/10.1080/15481603.2018.1426091

Manfreda, S., McCabe, M. F., Miller, P. E., Lucas, R., Victor Pajuelo, M., Mallinis, G., . . . Toth, B. (2018). On the Use of unmanned aerial systems for environmental monitoring. *Remote Sensing*, *10*(4), 641. http://dx.doi.org/10.3390/rs10040641

Mao, X., Deng, Y., Zhu, L., & Yao, Y. (2020). Hierarchical geographic object-based vegetation type extraction based on multi-source remote sensing data. *Forests*, *11*(12). https://doi.org/10.3390/f11121271

Martin, F.-M., Müllerová, J., Borgniet, L., Dommanget, F., Breton, V., & Evette, A. (2018). Using Single- and Multi-Date UAV and Satellite Imagery to Accurately Monitor Invasive Knotweed Species. *Remote Sensing*, *10*(10). http://dx.doi.org/10.3390/rs10101662

Matasci, G., Hermosilla, T., Wulder, M. A., White, J. C., Coops, N. C., Hobart, G. W., & Zald, H. S. J. (2018). Large-Area Mapping of Canadian Boreal Forest Cover, Height, Biomass and Other Structural Attributes Using Landsat Composites and Lidar Plots. *Remote Sensing of Environment*, *209*, 90-106. https://doi.org/10.1016/j.rse.2017.12.020

Matese, A., Toscano, P., Di Gennaro, S., Genesio, L., Vaccari, F., Primicerio, J., . . . Gioli, B. (2015). Intercomparison of UAV, Aircraft and Satellite Remote Sensing Platforms for Precision Viticulture. *Remote Sensing*, *7*(3), 2971-2990. https://doi.org/10.3390/rs70302971

Mayes, M. T., Estes, L. D., Gago, X., Debats, S. R., Caylor, K. K., Manfreda, S., . . . Nadal, M. (2016). Using Small Drone (UAS) Imagery to Bridge the Gap Between Field- and Satellite-Based Measurements of Vegetation Structure and Change. *AGUFM*, *2016*, B53J-05.

Merkert, R., & Bushell, J. (2020). Managing the drone revolution: A systematic literature review into the current use of airborne drones and future strategic directions for their effective control. *Journal of Air Transport Management*, *89*, 101929. https://doi.org/10.1016/j.jairtraman.2020.101929

Miller, Z. M., & Brooke, J. (2019). *Monitoring Efficacy and Impacts of Differing Prescribed Fire Seasonality with UAS*. Proceedings of the Indiana Chapter of the Wildlife Society Annual Conference, Morgan Monroe State Forest, IN, USA, Septmember 23-24, 2019.

Miller, Z. M., Hupy, J., Chandrasekaran, A., Shao, G., & Fei, S. (2021). Application of postprocessing kinematic methods with UAS remote sensing in forest ecosystems. *Journal of Forestry*. https://doi.org/10.1093/jofore/fvab021

Mountrakis, G., Im, J., & Ogole, C. (2011). Support vector machines in remote sensing: A review. *ISPRS Journal of Photogrammetry and Remote Sensing*, *66*(3), 247-259. https://doi.org/10.1016/j.isprsjprs.2010.11.001

NASA. (2021). *Temperate Deciduous Forest - Earth Observatory*. Retrieved on 12/8/2021: https://earthobservatory.nasa.gov/biome/biotemperate.php

NCRS. (2021). *Indiana Forestry Facts*. USDA. Retrieved on 12/8/2021: https://www.nrcs.usda.gov/Internet/FSE_DOCUMENTS/nrcs144p2_030050.pdf

Newman, E. A. (2019). Disturbance ecology in the Anthropocene. *Frontiers in Ecology and Evolution*, *7*, 147. https://doi.org/10.3389/fevo.2019.00147

Nordén, B., Rørstad, P. K., Magnér, J., Götmark, F., & Löf, M. (2019). The economy of selective cutting in recent mixed stands during restoration of temperate deciduous forest. *Scandinavian Journal of Forest Research*, *34*(8), 709-717. http://doi.org/10.1080/02827581.2019.1679876

Nuijten, R. J., Kooistra, L., & De Deyn, G. B. (2019). Using unmanned aerial systems (UAS) and object-based image analysis (OBIA) for measuring plant-soil feedback effects on crop productivity. *Drones*, *3*(3), 54. https://doi.org/10.3390/drones3030054

O'Hara, K. L. (2016). What is close-to-nature silviculture in a changing world? *Forestry: An International Journal of Forest Research*, *89*(1), 1-6. https://doi.org/10.1093/forestry/cpv043

Ollero, A., Martínez-de-Dios, J. R., & Merino, L. (2006). Unmanned aerial vehicles as tools for forest-fire fighting. *Forest Ecology and Management*, *234*, S263. https://doi.org/10.1016/j.foreco.2006.08.292

Pande-Chhetri, R., Abd-Elrahman, A., Liu, T., Morton, J., & Wilhelm, V. L. (2017). Object-Based Classification of Wetland Vegetation Using Very High-Resolution Unmanned Air System Imagery. *European Journal of Remote Sensing*, *50*(1), 564-576. https://doi.org/10.1080/22797254.2017.1373602

Pike Lumber, LLC. (2017). *Volz Tract #125 - Forest Stewardship Management Plan*. (Personal Communication).

Pix4D. (2021a). *Photo stitching vs orthmosaic generation*. Retrieved on 12/8/2021: https://support.pix4d.com/hc/en-us/articles/202558869-Photo-stitching-vs-orthomosaic-generation

Pix4D. (2021b). *Support - Initial Processing - Calibrate (Image Scale and Keypoints)*. Retrieved on 12/8/2021: https://support.pix4d.com/hc/en-us/articles/360043442151-Calibrate

Pix4D. (2021c). *Support - Initial Processing - Calibration*. Retrieved on 12/8/2021: https://support.pix4d.com/hc/en-us/articles/205327965-Menu-Process-Processing-Options-1-Initial-Processing-Calibration

Powell, D. C. (1996). White Paper F14-SO-WP-Silv-10 November 2012 *A Stage Is A Stage Is A Stage… Or Is It? Successional Stages, Structural Stages, Seral Stages*. Retrieved on 12/8/2021: https://www.fs.usda.gov/Internet/FSE_DOCUMENTS/stelprdb5413728.pdf

Pádua, L., Adão, T., Guimarães, N., Sousa, A., Peres, E., & Sousa, J. J. (2019). Post-fire forestry recovery monitoring using high-resolution multispectral imagery from unmanned aerial vehicles. *International Archives of the Photogrammetry, Remote Sensing & Spatial Information Sciences*. *42*, 301-305. https://doi.org/10.5194/isprs-archives-XLII-3-W8-301-2019

Pádua, L., Guimarães, N., Adão, T., Sousa, A., Peres, E., & Sousa, J. J. (2020). Effectiveness of Sentinel-2 in Multi-Temporal Post-Fire Monitoring When Compared with UAV Imagery. *ISPRS International Journal of Geo-Information*, *9*(4), 225. http://dx.doi.org/10.3390/ijgi9040225

Pérez-Rodríguez, L. A., Quintano, C., Marcos, E., Suarez-Seoane, S., Calvo, L., & Fernández-Manso, A. (2020). Evaluation of prescribed fires from unmanned aerial vehicles (UAVs) imagery and machine learning algorithms. *Remote Sensing*, *12*(8), 1295. https://doi.org/10.3390/rs12081295

Restas, A. (2006). *Forest Fire Management at Aggtelek National Park Integrated Vegetation Fire Management Program from Hungary*. Proceedings of the 2006 First International Symposium on Environment Identities and Mediterranean Area, Corte-Ajaccio, France, July 9-12, 2006. https://doi.org/10.1109/ISEIMA.2006.345051

Ristorto, G., Mazzetto, F., Guglieri, G., & Quagliotti, F. (2015). *Monitoring Performances and Cost Estimation of Multirotor Unmanned Aerial Systems in Precision Farming*. Proceedings of the 2015 International Conference on Unmanned Aircraft Systems (ICUAS), Denver, CO, USA, June 9-12, 2015. https://doi.org/10.1109/ICUAS.2015.7152329

Rousselet, G. (2019). *Classification of post-wildfire aerial imagery using convolutional neural networks: A study of machine learning and resampling techniques to assist post-wildfire efforts*. B.S., KTH Royal Institute of Technology, Stockholm, Sweden. Retrieved on 12/8/2021: https://www.diva-portal.org/smash/get/diva2:1353041/FULLTEXT01.pdf

Ruwaimana, M., Behara, S., Otero, V., Muslim, A. M., Muhammad, S. A., Sulong, I., Raymaekers, D., Koedam, N., Dahdouh-Guebas, F. (2018). The advantages of using drones over space-borne imagery in the mapping of mangrove forests. *PLoS One*, *13*(7). http://dx.doi.org/10.1371/journal.pone.0200288

Sakumara, C. (2019). *Seeing a Better World from Space*. Proceedings of the Purdue GIS Day Annual Conference, West Lafayette, IN, USA, November 7, 2019.

Samiappan, S., Hathcock, L., Turnage, G., McCraine, C., Pitchford, J., & Moorhead, R. (2019). Remote sensing of wildfire using a small unmanned aerial system: Post-fire mapping, vegetation recovery and damage analysis in Grand Bay, Mississippi/Alabama, USA. *Drones*, *3*(2), 43. https://doi.org/10.3390/drones3020043

Sandino, J., Gonzalez, F., Mengersen, K., & Gaston, K. J. (2018). UAVs and machine learning revolutionising invasive grass and vegetation surveys in remote arid lands. *Sensors*, *18*(2), 605. http://dx.doi.org/10.3390/s18020605

Seifert, E., Seifert, S., Vogt, H., Drew, D., Jan van, A., Kunneke, A., & Seifert, T. (2019). Influence of drone altitude, image overlap, and optical sensor resolution on multi-view reconstruction of forest images. *Remote Sensing*, *11*(10). http://dx.doi.org/10.3390/rs11101252

Shahbazi, M., Théau, J., & Ménard, P. (2014). Recent applications of unmanned aerial imagery in natural resource management. *GIScience & Remote Sensing*, *51*(4), 339-365. https://doi.org/10.1080/15481603.2014.926650

Sill, K. (2020). *Use of GIS Spatial Analysis, Remote Sensing, and Unmanned Aerial Systems in Determining the Susceptibility to Wildfires in Barber County, Kansas*. M.S., Fort Hays State University, Hays, KS, USA. Retrieved on 12/8/2021: https://scholars.fhsu.edu/cgi/viewcontent.cgi?article=4166&context=theses

Simpson, J. E., Wooster, M. J., Smith, T. E. L., Trivedi, M., Vernimmen, R. R. E., Dedi, R., . . . Dinata, Y. (2016). Tropical peatland burn depth and combustion heterogeneity assessed using UAV photogrammetry and airborne LiDAR. *Remote Sensing*, *8*(12), 1000. https://doi.org/10.3390/rs8121000

Singh, K. K., & Frazier, A. E. (2018). A meta-analysis and review of unmanned aircraft system (UAS) imagery for terrestrial applications. *International Journal of Remote Sensing*, *39*(15-16), 5078-5098. https://doi.org/10.1080/01431161.2017.1420941

Sony. (2018). *Sony A6000 Specifications*. Retrieved on 12/8/2021: https://www.bhphotovideo.com/c/product/1029860-REG/sony_ilce6000l_b_alpha_a6000_mirrorless_digital.html

Souliman, S. (2021). *RINEX files and differential corrections in post-processing*. Retrieved on 12/8/2021: https://support.oxts.com/hc/en-us/articles/115003212489-RINEX-files-and-differential-corrections-in-post-processing

Tang, L., & Shao, G. (2015). Drone remote sensing for forestry research and practices. *Journal of Forestry Research*, *26*(4), 791-797. https://doi.org/10.1007/s11676-015-0088-y

Tomaštík, J., Mokroš, M., Saloň, Š., Chudý, F., & Tunák, D. (2017). Accuracy of photogrammetric UAV-based point clouds under conditions of partially-open forest canopy. *Forests*, *8*(5), 151. https://doi.org/10.3390/f8050151

Tomaštík, J., Mokroš, M., Surový, P., Grznárová, A., & Merganič, J. (2019). UAV RTK/PPK method—An optimal solution for mapping inaccessible forested areas? *Remote Sensing*, *11*(6), 721. https://doi.org/10.3390/rs11060721

Walford, A. (2017). *Photogrammetry*. Retrieved on 12/8/2021: http://www.photogrammetry.com/

White, R. A., Bomber, M., Hupy, J. P., & Shortridge, A. (2018). UAS-GEOBIA approach to sapling identification in jack pine barrens after fire. *Drones*, *2*(4), 40. https://doi.org/10.3390/drones2040040

Zhang, H., Aldana Jague, E., Clapuyt, F., Wilken, F., Vanacker, V., & Van Oost, K. (2019). Evaluating the potential of PPK direct georeferencing for UAV-SfM photogrammetry and precise topographic mapping. *Earth Surface Dynamics Discussions*, 1-34. https://doi.org/10.5194/esurf-2019-2

Zhang, H., Aldana-Jague, E., Clapuyt, F., Wilken, F., Vanacker, V., & Van Oost, K. (2019). Evaluating the potential of post-processing kinematic (PPK) georeferencing for UAV-based structure-from-motion (SfM) photogrammetry and surface change detection. *Earth Surface Dynamics*, *7*(3), 807-827. https://doi.org/10.5194/esurf-7-807-2019

PUBLICATIONS

Miller, Z. M., Hupy, J., Chandrasekaran, A., Shao, G., & Fei, S. (2021). Application of postprocessing kinematic methods with UAS remote sensing in forest ecosystems. *Journal of Forestry*. https://doi.org/10.1093/jofore/fvab021

Cromwell, C., Giampaolo, J., Hupy, J., Miller, Z., & Chandrasekaran, A. (2021). A systematic review of best practices for UAS data collection in forestry-related applications. *Forests*, *12*(7). https://doi.org/10.3390/f12070957

In progress:

Miller, Z. M., Hupy, J., Hubbard, S., Shao, G. Utilization of UAS for precise land cover quantification surrounding planned disturbance (Pending submission)

Miller, Z. M., Wingren, C., Hupy, J. GIS technology in forest ecology: A review. (Pending sumbission)